CHIARA LOMBARDI

Strigolactones: plant hormones as versatile new players in the pitch

Università degli Studi di Torino
Dipartimento di Chimica

Scuola di Dottorato in Scienze della Natura e Tecnologie Innovative

Dottorato di Ricerca in Scienze Biologiche e Biotecnologie Applicate

Strigolactones: plant hormones as versatile new players in the pitch

Chiara Lombardi

Coordinatore del Dottorato: Prof. Silvia Perotto

Anni Accademici: 2014 - 2017

Settore Scientifico-disciplinare di afferenza: CHIM/06

Università degli Studi di Torino
Scuola di Dottorato in Scienze della Natura e
Tecnologie Innovative

Tesi di Dottorato in Scienze Biologiche e Biotecnologie Applicate
XXX° Ciclo: 2014 – 2017

Strigolactones:
Plant hormones as versatile new players in the pitch

Chiara Lombardi

Tutor accademico: Prof. Cristina Prandi

Coordinatore del dottorato: Prof. Silvia Perotto

Index

Acronims

ABA	Abscisic acid
ACN	Acetonitrile
AIBN	Azobisisobutyronitrile
AMF	Arburscolar mycorrhizal fungi
4-BD	4-Br debranone; 5-[4-bromophenoxy]-3-methylfuran-2[5H]-one
BFs	Branching factors
Boc	tert-Butyloxycarbonyl
BP o BODIPY	4,4-difluoro-4-bora-3a,4a-diaza-s-indacene
Bu	Butyl
Cbz	Carboxybenzyl
CCD	carotenoid cleavage deoxygenase
CD	Circular dichroism or Cyclodextrin
CDI	1,1'-carbonyldiimidazole
CDMT	2-Chloro-4,6-dimethoxy-1,3,5-triazine
CD-NS	Cyclodextrin-nanosponges
CISA-1	Cyano-Isoindole Strigolactone Analogue
CGT	Cyclodextrin glucosyl transferase
CNRS	Centre national de la recherche scientifique
CIP	Cahn-Ingold-Prelog
D27	Dwarf27
DCM	Dichloromethane
DHES	2-hydroxyethyl disulfide
DIEA	N,N-Diisopropylethylamine
DiFMU	6,8-difluoro-7-hydroxy-4-methylcoumarin
DMAP	4-(Dimethylamino)pyridine
DME	Dimethoxyethane
DMEM	Dulbecco's Modified Eagle Medium
DMF	Dimethylformamide
DMSO	Dimethyl sulfoxide
DSC	Differential scanning calorimetry
ECD	Electronic circular dichroism
ESI	Electrospray ionization
Et	Ethyl
EtOAc	Ethyl acetate
FBS	Fetal bovine serum
FCS	Fetal bovine serum
FTIR	Fourier transformed infrared
GSH	Glutathione
HPLC	High-performance liquid chromatography
HRMS	High-resolution mass spectra

IARC	International Agency for Research on Cancer
ICSN	Institute de Chimie des Substances Naturelles
LC	Liquid chromatography
LUC	Luciferin
MFs	Mcy factors
MTT	2,3- bis [2- methoxy -4- nitro -5sulphophenyl] -2H- tetrazolium-5carboxanilide
NBS	N-Bromosuccinimide
NMM	N-Methylmorpholine
NS	Nanosponge
Nu	Nucleophile
Me	Methyl
MS	Mass spectra
MFs	Mcy factors
PCS	Photon correlation spectroscopy
PBS	Phosphate buffered saline
PE	Petroleum ether
PYRO	Pyromellitic
PP	Parasitic plant
RCM	Ring closing methatesis
RMS3	Ramosus3
SAR	Structure-activity relationship
SB	Shoot branching
SDS	Dodecyl sulphate
SMXL7	Suppressor of MAX2 7
SL	Strigolactone
TBABr	Tetrabutylammonium bromide
TFA	Trifluoroacetic acid
THF	Tetrahydrofuran
TLC	Thin-layer chromatography
UV	Ultraviolet
Vis	Visible

Abstract

Strigolactones (SLs) are carotenoid-derived plant hormones recently identified as responsible of various developmental functions. Biosynthesized by plant roots and released in the rizhosphere in very small amounts, this class of molecules controls plant architecture and is a key player in establishing beneficial symbiotic interactions with mycorrhizal fungi.

They also act as soil signaling chemicals in promoting seed germination of parasitic plants, therefore posing a threat to food security.

Being multifunctional hormones engaged in a complex interkingdom communication, biologists and chemists are currently struggling to elucidate the perception mechanisms and the molecular events associated to the high profile of activity of these phytohormones.

The aim of this thesis was to investigate the strigolactone perception through the chemical synthesis of structural analogues and the evaluation of their biological activity.

To this purpose, different survey methods were used, from the synthesis of analogues to the use of fluorescence to dig into the activity and the distribution of the receptor, to the use of delivery systems to enhance and target their activity.

For the sake of clarity, this thesis has been organized in chapters, one for each of the topic addressed and each of them comprehensive of its “Results and Discussion” and “Experimental” module.

The work done during these three years is the result of the collaboration between Professor Prandi’s group and other scientific research laboratories. Personally, I have designed and realized the synthesis of all the strigolactone derivatives that will be herein presented, and coordinated the interdisciplinary collaborations established to test my compounds. Additional experimental details will be described for a comprehensive understanding of the impact of my work.

The first two chapters are dedicated to introduce the topic and the state of art of the literature. The first is a Strigolactone overview (Chapter 1 – Telling the Strigolactone story), while the second is an outline of the delivery systems used as SL analogues carriers during my PhD (Chapter 2 – Medical field: improved delivery systems in a new SL frontier). Then the different PhD projects follow:

SYNTHESIS OF STRIGO D-LACTAMS – CHAPTER 3

Natural strigolactones are composed by a tricyclic lactone ABC framework linked by an enol ether bridge to a butenolide D-ring. SARs data highlighted the importance of the lactone D-moiety to retain the biological activity. We investigated the effects on bioactivity applying a bioisosteric approach, and decided to replace the butenolide ring with a γ-lactam mojety.

In this section the Strigo D-lactam family of analogues will be presented : several lactam rings presenting different substituents have been designed, and successively bound to the ABC scaffold of SL analogues which had previously shown a remarkable biological activity.

To investigate the bioactivity of these new analogues we proposed a novel bioassay based on *Arabidopsis* transgenic lines, where the AtD14 SL receptor was fused to the luciferin fluorescent protein. Furthermore, the synthesized compounds were subjected to docking simulations to figure out their binding modes to the D14 SL receptor and better correlate the structure to their activity.

SYNTHESIS OF FLUORESCENT DERIVATIVES – CHAPTER 4

Fluorescence is becoming an attractive tool to investigate and monitor the distribution of bioactive molecules.

To decipher the molecular events involving Strigolactones, three different approaches have been undertaken.

- Synthesis of fluorescent analogues, focused on traceability of tagged SL-analogues through an extension of their basic ABC-D scaffold. This study was implemented correlating the absolute configuration of the synthesized compounds with their biological activity.

- Synthesis of a fluorescent SL mimic, developed as a fluorescent non-hydrolysable agonist and as a marker to label the receptor site.

-Synthesis of profluorescent probes. In this case the activity of the analogue is revealed by the use of profluorescent probes in a “switch on/off” system based on fluorescence. This project was realized during my period abroad at the Institute de Chimie des Substances Naturelles (Gif sur Yvette, France), under the supervision of Dr. Francois-Didier Boyer.

SLs AND DRUG DELIVERY SYSTEMS– CHAPTER 5

The last part of my thesis is dedicated to the incapsulation of SLs into new generation delivery systems in view of applications either in agriculture and in medicine as anticancer agents.

With the aim of improving the SL therapeutic potential, cyclodextrin-based nanosponges, polymeric and biodegradable systems, were evaluated as promising analogues carriers.

CHAPTER 1

Telling the strigolactone story

1.0 - INTRODUCTION

Strigolactones (SLs) are a novel class of plant hormones which only recently has gained relevance in biology and agronomy. Belonging to a group of biologically active molecules called "semiochemicals", their function is the regulation of the interactions between living organisms.[1]

In the semiochemical class, two groups are distinguished: pheromones, involved in the communication between organisms of the same species, and allelochemicals, involved in the interaction of organisms belonging to different species.[2]

SLs, vegetal hormones and signaling molecules involved in plan-plant and plant-fungi interactions, act both as endogenous and exogenous factors, and for this reason they are classified as allelochemicals.

In 1992 it was discovered that parasitic plants as *Orobanche* and *Striga* were able to germinate when in close proximity to the roots of a suitable host plant in response to specific germination inducers (i.e. SLs), causing the consequent host plant decease. Acting as parasites, they could plague food crops with an high negative impact on food production.[3]

Given the fact that they have been isolated from the *Striga* parasitic plant and as a tribute to their peculiar chemical structure, in 1995 Butler coined the name "Strigo-lactone".[4]

Only later it was discovered that SLs were essential to the establishment of a symbiotic interaction between plants and arbuscular mycorrhizal fungi (AMF), heterotrophic organisms which require this aforementioned symbiosis for living.[5]

But plants do not synthesize SLs simply to give benefit to parasitic plants or to symbiotic organisms. Indeed, they have been recently recognized as authentic

plant hormones involved in the inhibition of shoot branching, in root architecture development,[6] and in many other plant functions, some of them yet to be discovered.

1.1 - NATURAL STRIGOLACTONES

Even though it is actually well established that plants produce and release chemicals into the soil, over the years the demanding challenge in the study of plant communication was related to the tricky isolation of molecules released in very small amounts into the soil, to their attitude to decompose rapidly both in the rhizosphere and during the purification processes. All these factors contribute to an intricate isolation and structure analysis of these multifunctional molecules.[1, 7]

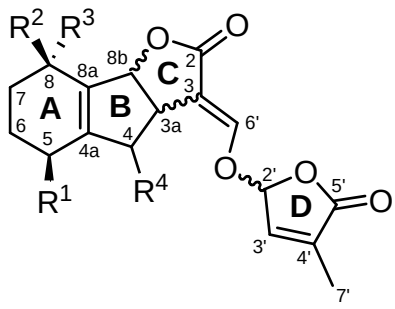

Figure 1. Framework of natural strigolactones.

Thanks to the development of highly sensitive analytical methods, it was possible to determine molecular structures of stereochemically complex compounds as strigol. Isolated in 1966 from root exudates of cotton (*Gossypium hirsutum*),[8] its backbone was clarified in 1972, and only twenty years after the discovery its configuration was totally disclosed by means of X-ray diffraction.[9,10]

Nowadays is common knowledge that strigolactones are characterized by a tricyclic system, the *ABC unit*, connected through an enol ether bridge to a butenolidic ring, called *D ring*. In addition they may present different substituents on the A and B rings (Figure 1). With a fixed *R* configuration at the C2' position, natural SLs are differentiated for the different stereochemistry at the BC junction, and divided in two classes: the (+)-strigol and the (-)-orobanchol class (Figure 2).

Essentially, the difference between the two classes is the stereochemistry on the B-C ring junction, with a β orientation (8bS) for the strigol family, and an α orientation for the orobanchol one (8bR).[11]

Moreover, the stereochemistry of almost all natural Strigolactones can be described as relative to that of parent compounds. As a consequence, considering strigol as the reference compound, the *ent*- prefix identifies enantiomers, while the prefix *epi*- identifies epimers.[12]

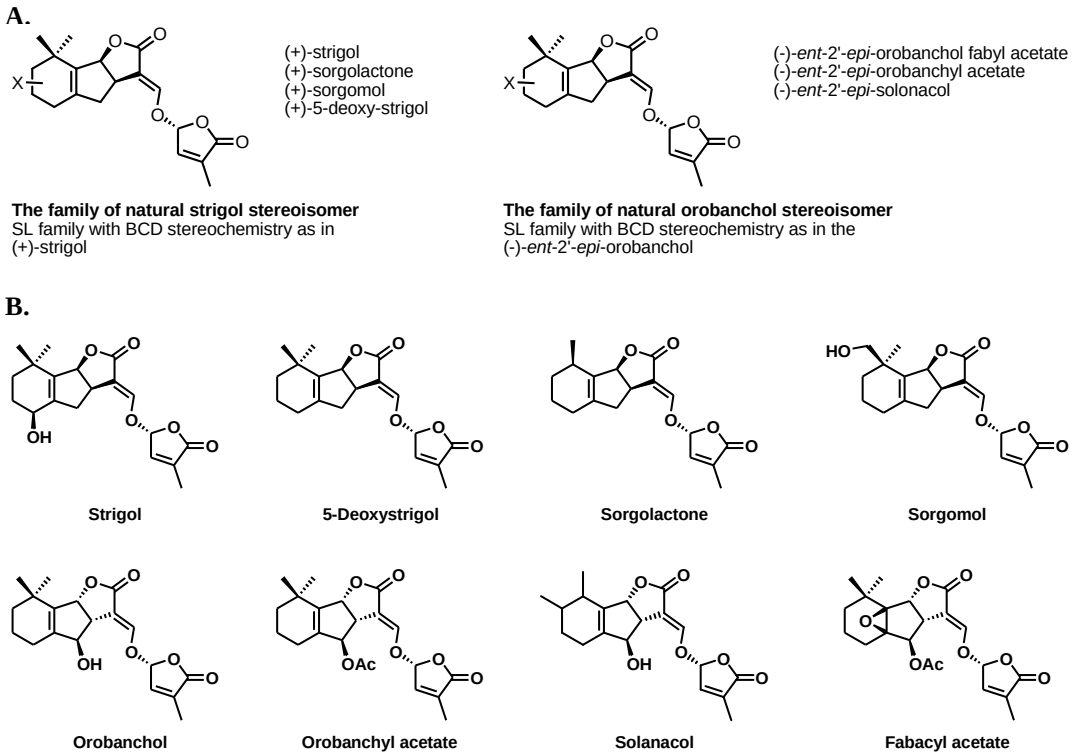

Figure 2. A. Stereochemistry of the two family of SLs; B. Some examples of natural Strigolactones.

1.2 - STRIGOLACTONES ROLES: from the detrimental effect to the healthful function.

Assemble the strigolactone story took half a century. As a matter of fact, at the beginning it wasn't clear the reason why plants should produce molecules able to induce the germination of parasitic plants (PP) and that are detrimental for the plant itself. Only later the connection among the SL exudation, their function as plant hormones and the symbiosis with AM fungi was identified.

1.2.1 - SLs as germination stimulants

The parasitic plant crop infestation prompted the investigation of this deleterious phenomenon. Parasitic plants belonging to the Orobanchaceae family (*Striga*, *Orobanche* and *Pelipanche*) are widespread all over the world and are responsible for the decreasing in food production.[3a] In particular *Striga* is widespread in Africa, Middle East and Asia, while *Orobanche* in central Europe, Australia, United States and some regions in Africa.[13]

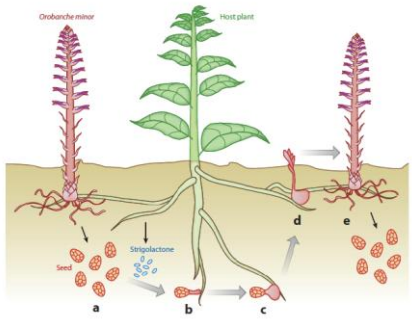

Figure 3. The life cycle of parasitic plants: (a) seed germination is promoted by germination stimulants (i.e. SLs); (b) host roots are attached by haustorium; (c-d) parasite tubercles deveop underground for weeks; (e) parasitic plant grows and release seeds into the soil. [14]

As reported in Figure 3, after an incubation period, PP seeds germination is induced by the release of specific chemical compounds (i.e. SLs) from the host plant. As a consequence, PP develop a specialized structure connecting the parasite with its host, called haustorium, able to penetrate in the host plant root and adsorb water and nutrients from it.[14]

To combact PP infestation two different approaches have been evaluated so far, one based on the stimulation of PP germination in the absence of the host plant (so called suicidal germination approach), while the second one aims at reducing the exudation of germination stimulants by the roots plants.

In the "suicidal germination" approach, as above mentioned, the PP germination is induced in the absence of the host plant.[15] Essentially, the soil is treated with a potent germination stimulant, thus triggering the parasitic plants germination. PP, being in absence of a host plant and being unable to independently provide nutrients for their own survival, very quickly go towards death. To this purpose, synthetic SLs analogues as GR24 and GR7 (Figure 4) have been used with decent results. However, the use of these compounds on a large scale is prohibiting, since they are prone to hydrolysis in alkaline medium: they rapidly decompose forming products without any activity. For this reason, derivatives having higher stability as Nijmegen-1, have been designed and synthesized (Figure 4).

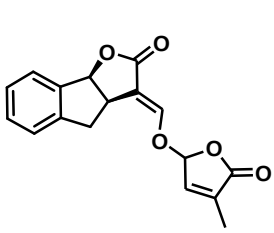

GR24

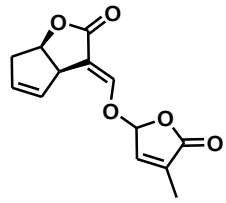

GR7

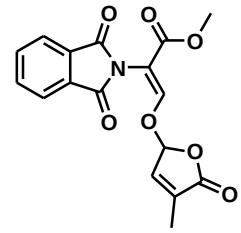

Nijmegen-1

Figure 4. Structure of synthetic strigolactones.

The recently published results suggest a potential employment of synthetic analogues in the field.[16]

The second approach consists in reducing the PP seeds germination by means of decreasing the strigolactone production and release by the host plant. At this

regard the elucidation of the biochemical pathway leading to SLs biosynthesis paved the way to the identification of inhibitors which hamper the SLs production.

1.2.2 - SLs as branching inducers in AM fungi

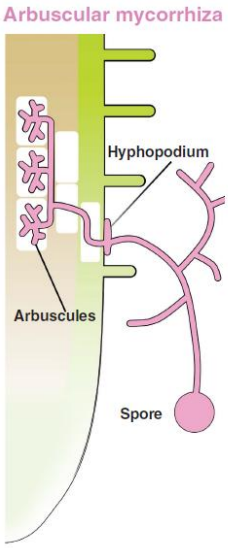

Figure 5. Illustration of AM interactions: hyphae develop from a spore and produce a hyphopodium on root epidermis. Then an intra and intercellular colonization occur, with the final formation of little fungal trees called arbuscules, positioned in the inner cortical cells. [19]

Arbuscular mycorrhizal fungi (AMF) are the most common and widespread symbiont on the earth.[17] Because of their inability to complete their lifecycle, they are defined as "obligate symbionts". They penetrate and colonize plant roots developing highly differentiated structures, called arbuscules, responsible of the nutrients exchange between the two organisms.[18] Meanwhile plant roots develop hyphal branches, and the symbiotic interaction is therefore established: carbohydrates deriving from host plant photosynthesis are taken to AMF, while nutrients as phosphates and nitrates are received from the symbiotic partner in a mutual beneficial exchange.

In addition this beneficial association confers resistance to the plant against biotic and abiotic stresses.[19]

But the only way for the association to occur is through the release from the host of signal molecules, called "branching factors" (BFs), essential for the interaction between the two organisms. At the same time fungi release the so called "mcy factors" (MFs), responsible of inducing a response at molecular and cellular level.[20]

In 2005 Akiyama *et al.* reported the first evidence of a branching factor, 5-deoxystrigol, isolated from root exudates of the leguminous plant *Lotus japonicus*, proving the BF role played by strigolactones.[5] The attention was focused on SAR

of 5-deoxystrigol, sorgolactone, strigol and synthetic GR24 in regard to their ability to induce hyphal branching in the AM fungus *Gigaspora margarita*, while further investigations have been performed to complete the whole picture.[21]

1.2.3 - SLs as plant hormones

- Shoot branching inhibitors -

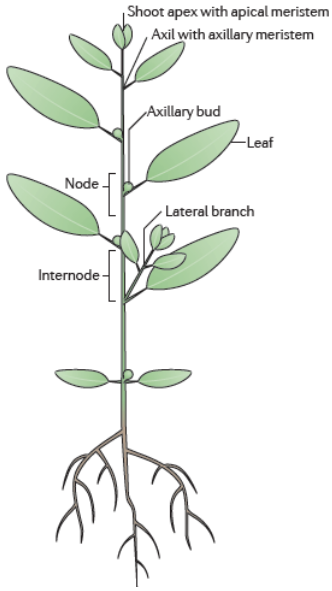

Figure 6. Schematic representation of plant shoot architecture. [23]

Strigolactones play a crucial role in regulating plant architecture as phytohormones, but the mechanisms by which they are able to control plant shoot branching (SB) is still not completely clear.

The first evidence regarding the SLs shoot branching inhibition effect was reported by Gomez-Roldan *et al*. in 2008.[6] By the use of mutants, they have been able to demonstrate the correlation between SLs and their effect on bud growth. With SLs deficient mutants the phenotype was typically "bushy", while the normal phenotype could be restored by the exogenous application of the synthetic analogue GR24.

Nowadays, the overall picture is more complete and SLs are presumably involved in a complicate network of synergic effects with other plant hormones as auxin, abscisic acid (ABA), giberelline, cytokinin, brassinosteroids and jasmonates.[22,23]

Among them, auxin is one of the most important. Indeed, studies on SLs production accomplished on *Arabidopsis* mutants revealed a strong SL-auxin interaction,[23] with an SB enhancement due to the increase in the auxin transport. It

has even been suggested that several SLs functions are still probably to be identified because presumably obscured by the auxin effect.[6]

- **SLs in root hair elongation –**

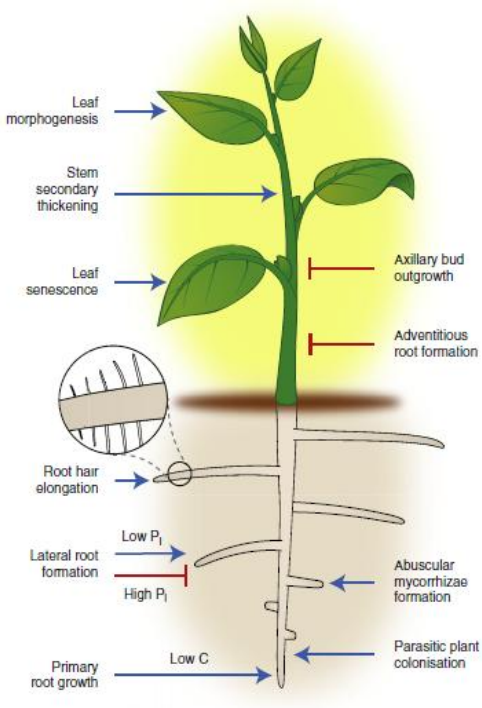

Figure 7. Hormonal roles of strigolactones.[26]

Plant roots contain a considerable amount of SLs respect to other plant regions as stem and leafs. This suggests that they play a key role at root level, especially for root development.

It could be envisaged that various mechanisms and other hormones are involved in root elongation, however the SL-auxin interaction is thought to be crucial: as a matter of fact by controlling the auxin efflux, SLs control primary root growth and lateral root formation.

Studies on rice and on *Arabidopsis* mutants revealed the influence on plant root architecture. More in detail, Arite *et al.* in 2012 investigated rice *dwarf* SL-insensitive or SL–deficient mutants, and only in this second case peculiar short crown roots were observed, which were immediately dismissed after the application of exogenous GR24.[24]

Studies on the *Arabidopsis* system, instead, were accomplished by Kalpunik and coworkers in 2011. In their paper they demonstrated that the lacking of strigolactones led to an increase in the lateral roots number and to a decrease in the

root-hair length. In this case also the effect was reversed after the GR24 subministration.[25]

The surrounding environment is also an important parameter to take into account. Indeed, the SL production is heavily influenced by the soil conditions. The presence of soil nutrients as phosphates and nitrates has a crucial role for the roots and shoots development. In conditions of nutrients deficiency, the generation of more-branched roots and less-branched shoots is triggered, with the addition of an increased tendence to the establishment of the AM fungi symbiotic interaction.

We may say that the whole picture fits with the general aim of improving the potential for acquiring further nutrients and reducing the shoot demand, so that everything is properly settled as a well-oiled machine and results in a modulated absorption.[26]

1.3 - STRIGOLACTONE'S STRUCTURE-ACTIVITY RELATIONSHIP (SAR)

Over the years, the growing interest in these fascinating molecules brought to highlighting their functions on different systems.

But what is has a consequence: it becomes difficult to make generalizations on the relation between some peculiar structural elements of SLs and their activity in plants, parasitic plants and fungi. In order to identify the biologically active parts on the SLs organic backbone, SAR studies have been addressed and developed.

As before mentioned, the SLs backbone can be described as an ABC trycyclic *core* of fused rings connected to a fourth butenolide D-ring. For parasitic plants, the CD fraction seems to be essential to stimulate their seeds germination,[11] and the same can be addressed in root-hair elongation. In this second case, however, substituents on the A ring drastically reduce the SLs bioactivity.

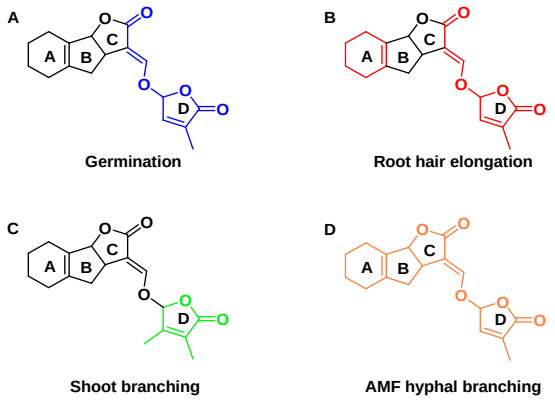

Figure 8. Evidence of relevant portions in the SL framework to obtain a specific activity on different systems.[27]

Concerning the AMF hyphal branching, the activity resulted totally compromised when an extra methyl group on the C4' of the D ring was introduced.[27] Furthermore analogues lacking the A, B or C rings have been tested and they resulted partially inactive. This revealed that all the different parts in the SL framework are essential for these molecules to have biological effects.[21b]

For shoot branching inhibition, contrary, Boyer *et al.* recognized the D ring as the only important feature of the backbone, at least on the pea system, with an increased activity in case of an extra methyl group on the C4' position.[28]

In addition, as plant hormones and as germination stimulants of parasitic plants, the so called "SLs mimics" proved to be good candidates, where for "mimics" we mean simpler molecules where the D ring is connected with a good leaving group at the C2'(see 1.6.2 section). Despite this, among the synthetized analogs, GR24 was the first to exhibit a good biological activity on all the three different biological systems. This is the reason why it is typically used as a positive control in biological assays (see 1.6.1 section).

1.4 - SL PERCEPTION MECHANISM

As for every hormone in the animal and plant kingdoms, strigolactones too have to interact with a receptor protein in order to perform their action.

In superior plants, several lines of evidence support a receptor function for D14, an α/β hydrolases whose hydrolytic activity is a key part of the perception process. After binding with SL, the substrate is hydrolysed and D14 undergoes a conformational change which enables the interaction between D14 and a target protein, as complex SCF-D3 or SCF-MAX2, triggering the signal transduction cascade.[29]

Therefore, an important aspect arises: depending on the species, differences in the component of SLs/D14/D3/SCF complex may confer specificity (Figure 9).[30]

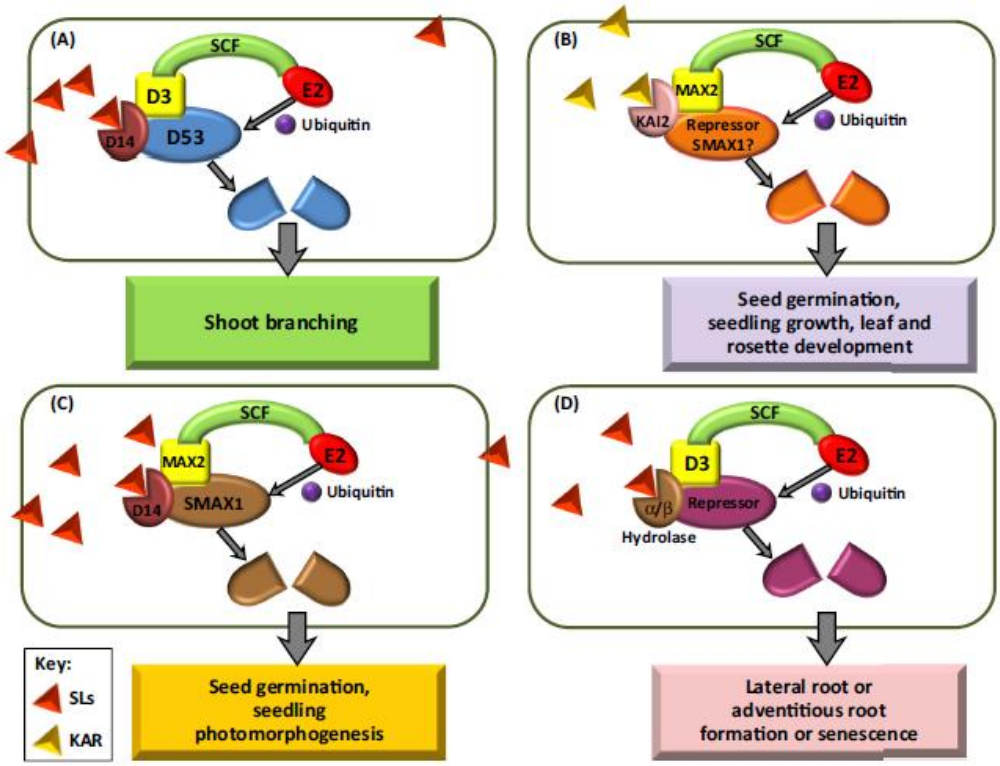

Figure 9. Strigolactone perception in different biological systems. As reported, once tagged the receptor, an immediate degradation occurs, with a consequent signal transduction cascade.[31]

To better understand the mechanism of action of strigolactones, the knowledge of the association partner structure becomes really important.

Thanks to the X-ray crystallography studies on D14 receptor, in 2013 Kagiyama *et al.* proved the existence of a nucleophilic catalytic triad responsible of the substrate hydrolysis. More in detail, the hydrophobic active site is characterized by three amino acid residues (Figure 10): serine (Ser147), histidine (His297) and aspartic acid (Asp268).[31]

Later on, it was clarified how the SL molecule accommodates inside the binding pocket, with the D ring deeper positioned in the active site and coordinated to the triad, and the ABC tricycle at its entrance, then not involved in the catalytic mechanism and in the biological activity.

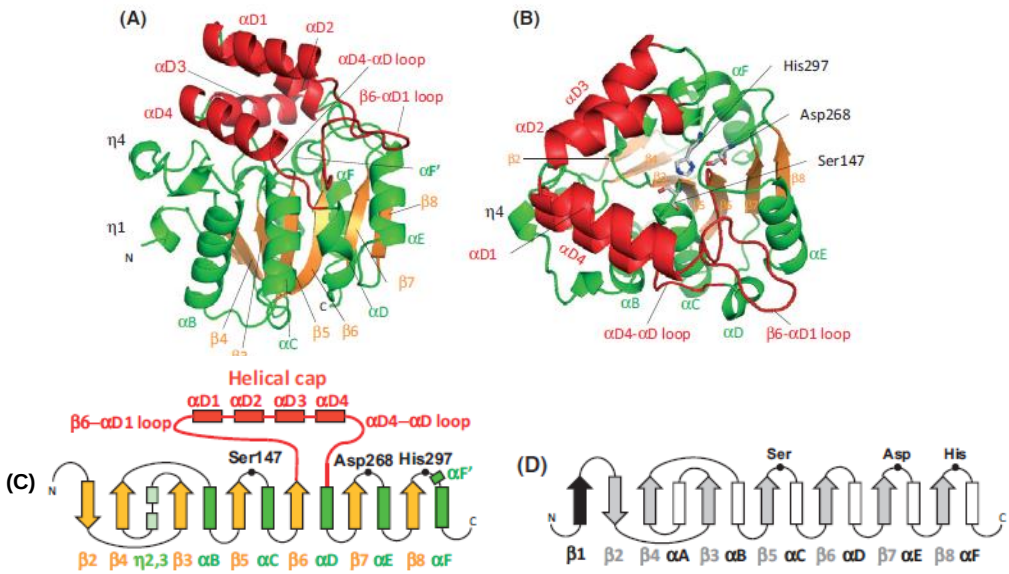

Figure 10. Structure of the rice D14 protein receptor. (A) Side view of D14, characterized by α helices in green and red (in red the four helices between the β strands), and β strands in orange; (B) Top view of D14; (C) Topology of D14; (D) Topology of a canonical α/ β hydrolase core domain. [32]

Only in 2013 it was possible to observe the results of the hydrolytic activity of the D14 α/β hydrolase (Figure 11). Indeed Nakamura *et al.* solved the crystalline structure of D14 complexed with the SLs hydrolysis product, D-OH, and proved

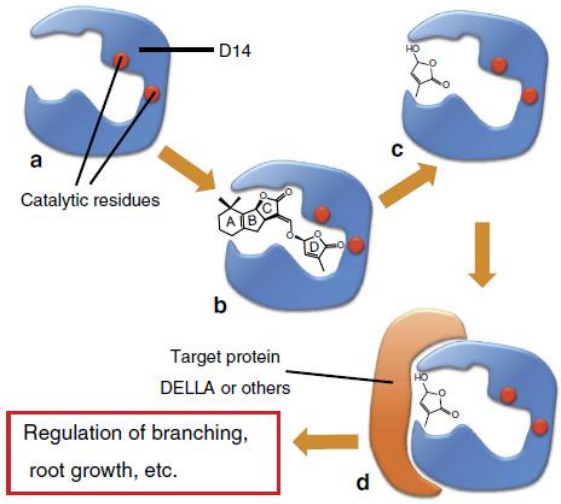

Figure 11. Model proposed by Nakamura in 2013 for the SL recognition and hydrolyzation.[33]

that, after the SLs-catalytic triad interaction, the hydroxybutenolide fragment remains inside the binding pocket.[32]

But even though some light has been shed on the receptor structure and on its hydrolytic activity, the mechanism of action which brings to the D-OH fragment formation is still under investigation.

Until now, several hypotheses have been made:

- The first was proposed by Zwanenburg in 1992, and it implies that a nucleophile, situated in the receptor site, attacks on the enol-ether bridge in a Michael addition fashion, and then the D ring is eliminated. At the end, only the ABC part is covalently bound to the receptor;[33]

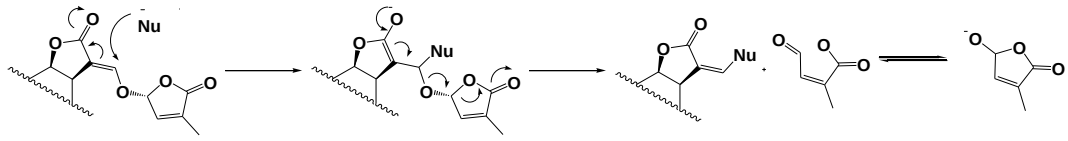

Figure 12. Zwanenburg mechanism proposal - 1992

- The second hypothesis was proposed by Scaffidi, and relies on an acyl nucleophilic substitution on the butenolidic D ring;[34]

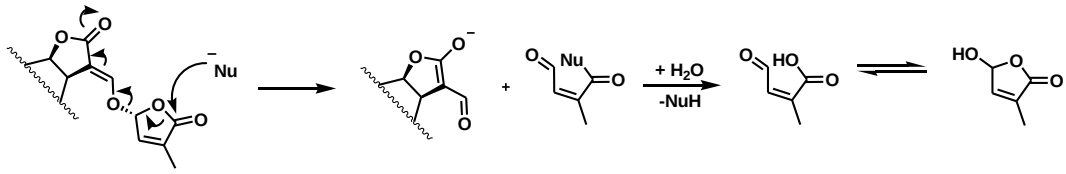

Figure 13. Scaffidi mechanism proposal - 2012

- In 2013 Zhao *et al.* suggested a four passages mechanism: an acyl nucleophilic substitution which involve the serine residue and brings to the D ring opening; a conformational change through the double bond rotation, difficult to occur for the high activation energy; then a water molecule takes action and an aldehydic intermediate is formed; and finally, the D-OH fragment is obtained after a lactonization and a water molecule loss;[35]

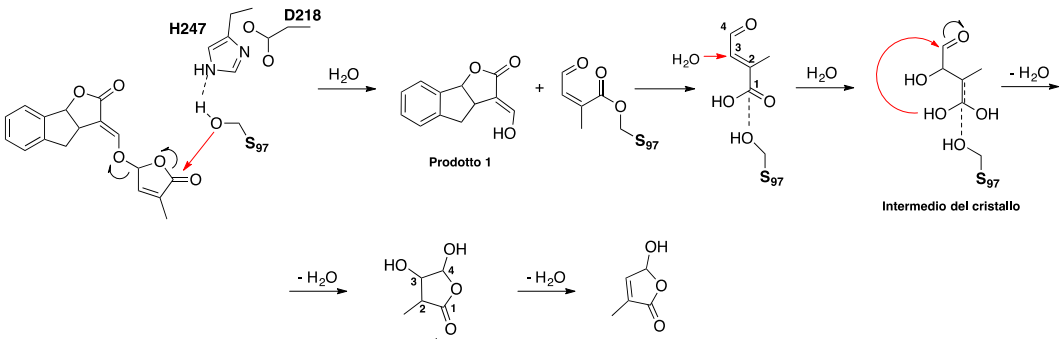

Figure 14. Zhao mechanism proposal - 2013

- Zwanenburg and Pospìsil, in 2016, proposed a more realistic mechanism by which a water molecule is coordinated to the substrate (i.e. strigolactone) and prevents the D ring rotation. The serine triggers a Michael addition of the water molecule on the C ring, with a consequent elimination of the D-OH and ABC=CHOH fragments;[1]

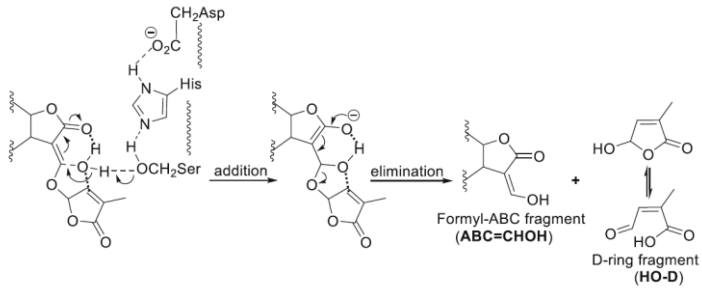

Figure 15. Zwanenburg mechanism proposal - 2016

- The most recent hypothesis has been put forward by De Saint Germain and co-workers in 2016. Studying the pea system, he proposed a serine nucleophilic attack on the C5', with the consequent formation of an aldehyde intermediate. Then the nitrogen atom of the histidine imidazole group performs a second nucleophilic attack at the C2' position, and a stable intermediate is obtained. Afterwards a water molecule steps in, and the D-OH fragment is finally released.[36]

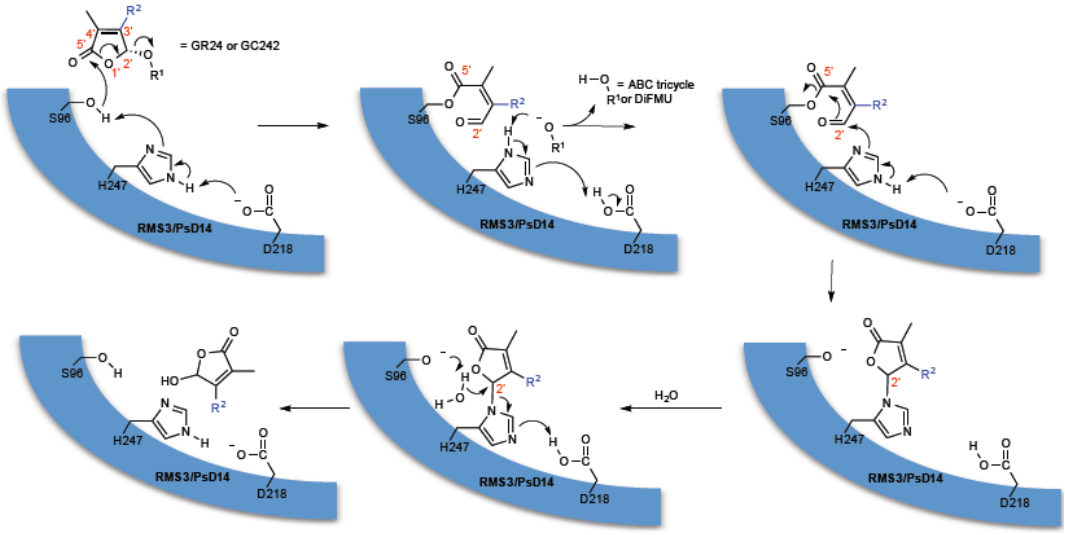

Figure 16. Boyer mechanism proposal - 2016

Superior plants have been extensively investigated, but considering the not yet conclusive version of the perception mechanism, is pretty clear that further studies have to be addressed.

Concerning parasitic plants and fungi, instead, we do not get far away from the truth saying that lots of data have still to be collected before having a clear picture of the perception mechanism. Worth of mention are Toh and co-workers,[37] which in 2015 obtained a crystal structure of *Striga hermontica* receptor and observed a larger binding pocket respect to that of *Arabidopsis*, assuming this peculiarity as the responsible of the remarkable parasitic plants sensitivity to strigolactones.

1.5 - STRIGOLACTONES BIOSYNTHESIS

The evidence that strigolactones derive from carotenoids comes from studies made on carotenoid-deficient mutants exhibiting a lower SL content.

In 2008, studies made on rice (*d7* and *d10*) and pea (*ccd8/rms1*) mutants lacking two CCD (carotenoid cleavage deoxygenase) enzymes, CCD7 and CCD8 respectively, disclose a reduction in the SL production.[6] Furthermore, a central role in their biosynthesis was discovered for the Dwarf27 (D27) enzyme[38] and the MAX1 cytochrome (in the *Arabidopsis* system).[39]

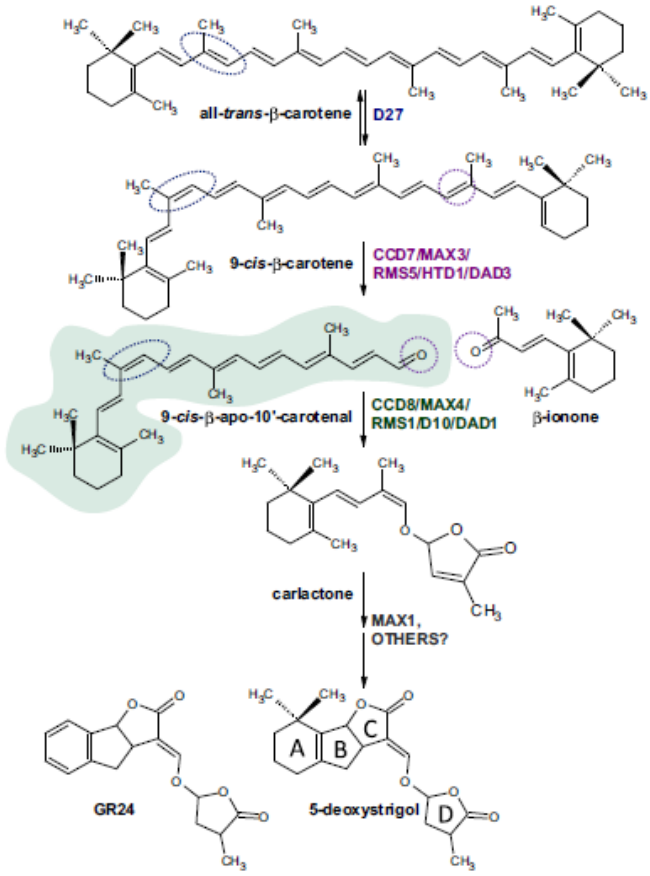

Figure 17. Proposed biosynthetic pathway for the SL production, from the all-trans-β-catotene to the 5-deoxystrigol. The molecular re-arrangements catalyzed by the enzymes D27, CCD7 and CCD8 are highlighted in blue, violet and green respectively.[41b]

Trans-β-carotene is the first substrate involved in the SL production.[40] This molecule, thanks to the D27 action, is catalitically isomerized at the C9 position to obtain 9-*cis*-β-carotene.

A better understanding of the biosynthetic route was possible once Alder et al. demonstrated the CCD7 stereospecificity, which preferentially breaks 9-*cis*-β-carotene with the consequent formation of 9- *cis*-β-apo-10'-carotenale. Then in *vitro* CCD8 incubations revealed its catalytic properties and stereoisomeric selectivity respect to 9-*cis*-β-apo-10'-carotenale, rapidly converted in a SL-like compound: the carlactone.[41] The discovery of this last compound is quite recent. Its biological activity and its structure are really similar to that of natural SLs: a C_{19} backbone with a C_{14} unit connected to a butenolidic group through an enol ether bridge, corresponding to the SL D ring.[42]

Actually, the most uncertain step is the one related to the conversion of carlactone in 5-deoxystrigol, the precursor of all strigolactones. A deoxygenation, followed by a dehydrogenation and two ring closures would be required. In this regard it has been proposed the involvement of MAX1 enzyme, the only one remained with an unknown function. Nevertheless, whether this final step is due to MAX1 or to other enzymes, is still an unsolved problem.[41]

1.6 - SYNTHETIC STRIGOLACTONES

Naturally occurring SLs are produced in very small amounts (10^{-7} – 10^{-8} M) and have a too complex structure for a proper synthesis on a multi-gram scale.

For this reason, synthetic SLs with a simpler structure and activity comparable to natural ones have been proposed. They can be divided in two main categories: analogues and mimics.

Once identified the bioactivity requirements, according to SAR studies, the design of lab-made strigolactones became an intriguing target for chemists.

1.6.1 - SLs analogues

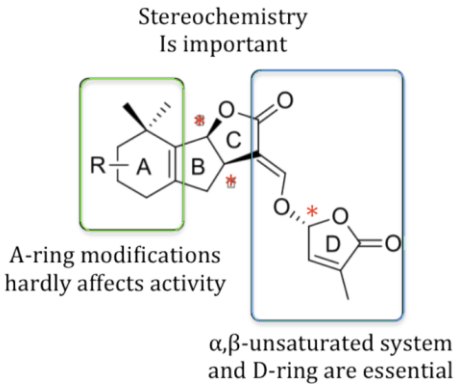

Figure 18. Model for designing synthetic SL analogues.[11]

The main feature of analogues is their strict similarity to the natural SL scaffold. To retain bioactivity, the strigolactone backbone needs to preserve some peculiarities, as represented in Figure 18 according to the model where structural requirements to induce germination in parasitic plants are highlighted.[11]

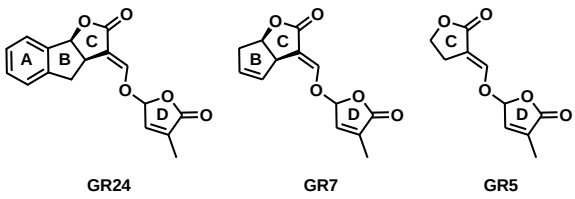

Figure 19. The GR family of synthetic strigolactones.

In the group of analogues, the main role is played by the GR series, whose name comes from Gerald Rosebery, the creator of the most known and widespread family of analogues: GR24, GR7 and GR5 (Figure 19).[16a] More in detail, GR24 was the first synthetic SL to exhibit a good biological activity on all the three different biological systems, and for this reason it is still used as a positive control in biological assays.[43] The three represented GR compounds share a common CD part, that can be considered the essential subunit for bioactivity. Indeed, this hypothesis is supported by the loss of activity in case the C ring is missing.

As a matter of fact, the first important aspect in designing analogues is the identification of the crucial biologically active framework portion.

In addition to GR24, a further well known synthetic SL is Nijmegen-1 (Figure 20A). Designed by Zwanenburg and coworkers, this analogue was obtained from readly available starting materials in few synthetic steps. Compared to GR24, Nijmegen presents a lower germination activity and a greater stability.[15]

Other typical examples of analogues are characterized by simple modifications of the ABC portion (Figure 20B) or isosteric substitutions of an oxygen with another etheroatom (Figure 20C and D).[44]

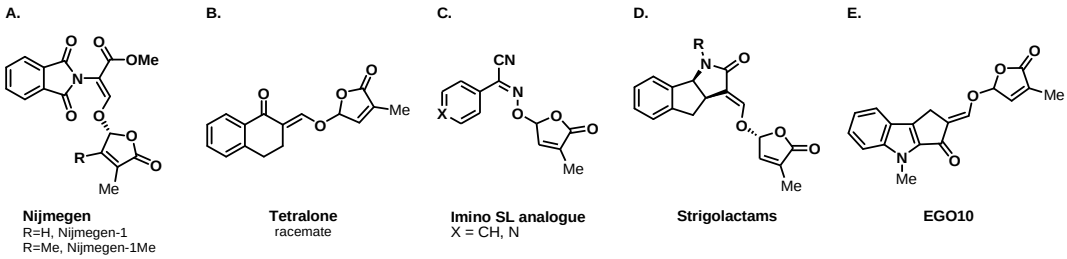

Figure 20. Synthetic strigolactones.

Finally, the EGO, PL and ST (EGO10, EGO5, EGO15, PLN65 e PLN655, ST23a e ST23b) series are mentioned as the indolyl-derived analogue families (Figure 21).[45,46] Revealed as active compounds in the parasitic plants germination, these molecules were found to possess an intrinsic fluorescence, which will be further discussed in the "Fluorescent SLs" section (1.6.3).

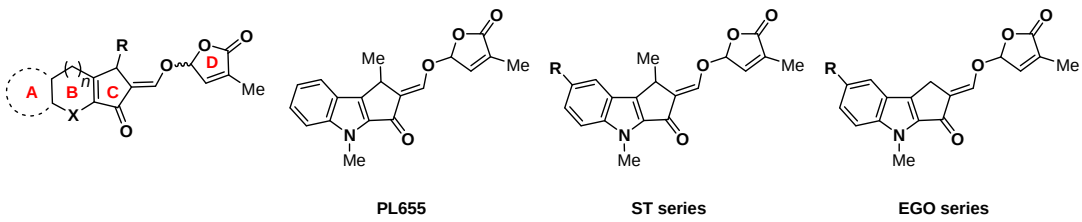

Figure 21. PL, ST and EGO series of strigolactone analogues.

1.6.2 - SLs mimics

The second synthetic SL category is known as mimics, whose structure is much simpler than natural Strigolactones as they simply present the D-ring with a good leaving group at the position C2'. In spite of their simplified structure and the lacking of the both ABC scaffold and enol ether bridge, they show a bioactivity similar to that of synthetic SLs and are still able to be active as germination stimulants and plant hormones.[1]

Mimics can be distinguished in Debranones and Aryloxy mimics:

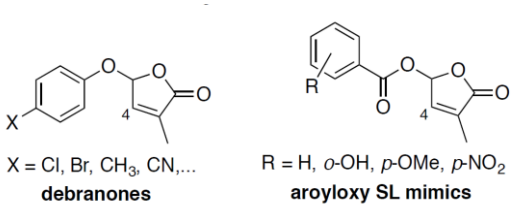

Figure 22. The two families of SL mimics.

- Debranones, which are phenoxy furanone derivatives also called "debranching factors". Their activity in *rice* and *Arabidopsis thaliana* mutants has been investigated, disclosing a remarkable shoot branching inhibition compared to GR24, especially for 4-Br debranone (4-BD). On the contrary, no 4-BD effect on *Striga hermontica* germination was observed, suggesting its possible employment as chemical able to control plant architecture avoiding the parasitic plant germination.[47]
- Aroyloxy mimics. The evaluation of their activity revealed them as considerably active on the *Orobanche cernua* parasitic plant, and mildly active on *Striga hermontica*.[48]

Nowadays, several assumptions on the way how mimics are perceived have been suggested.[49,28,11] A fluorescent approach has even been used for further elucidation,[50] but their mechanism of action is still under investigation. Anyway, the design of compounds having a lower germination activity in the soil still continues to be the chemists target in strigolactone field.

1.6.3 - Fluorescent SLs

The first proposition of fluorescent SLs came in 1997, when Thuring *et al.* suggested the use of photoreactive labelled analogues as promising tools for *in vivo* investigations.[51]

Since the biological activity resides in the CD portion, the labelling was targeted on the A ring, in accordance with the SAR studies previously mentioned.

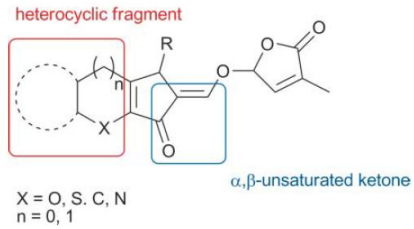

Figure 23. Heterocyclic SL analogues - ST, PL and EGO series.[47]

Interestingly, in 2009 Prandi and co-workers designed a new family of conjugated analogues having intrinsic fluorescent properties. Considering that modifications on the A ring are well tolerated, two other elements of innovation were introduced on the ABC framework: the B ring was converted into a heterocyclic and the C ring into a cyclic ketone (instead of a lactone).

On these bases the PL[45], ST and EGO[46] derivatives took shape, the first generation of SLs analogues possessing an innate fluorescence due to their conjugated tryciclic structure. Tested towards *Orobanche aegyptiaca* seeds, they were found to possess a remarkable activity compared to GR24. But even so, their photoactivity was not adequate for bioimaging studies by means of confocal microscopy, which requires a minimum excitation wavelength of 405 nm.

On this basis, to improve the spectroscopic properties of those molecules, studies have been addressed to the synthesis of highly conjugated SLs through the introduction of substituents on the A ring. Still unemployable, the research move towards the introduction of actual fluorophores as dansyl group, fluorescein and boranyl group.[52,53] Furthermore, a fluorescent open chain analogue has been studied by Rasmussen *et al.* and called CISA-1 (Cyano-Isoindole Strigolactone Analogue).[54]

For biological inactivity or inadequate spectroscopic properties, these derivatives have been side-lined a little, leaving the stage to a new class of fluorophores called BODIPY (difluoroBOron DIPYrromethene), which actually constitute the most promising probes for *in vivo* investigations.[52]

1.6.4 - Pro-fluorescent probes

The use of profluorescent probes in the strigolactone field was a pioneer approach introduced by De Saint Germain and co-workers.[36]

As previously shown different models have been proposed to identify the mode of action of the SL receptor enzymatic activity. Indeed, Nakamura *et al.*[32] suggested that once the SL interacts with the receptor, an hydrolysis reaction product is stocked inside the binding pocket and far away from the catalytic triad, while Zhao *et al.* postulated a D ring close to the triad.[35]

With the aim of highlighting an unclear and apparently slow enzymatic activity, a "switch off/on" system, based on fluorescence, was devised: namely, the profluorescent approach.

Profluorescent probes are essentially phenol fluorophores which are quenched when engaged in a covalent bond. When a hydrolysis reaction is performed, the fluorophore is released (i.e. DiFMU) , and the fluorescence is dramatically enhanced, thereby providing a readout of the SL receptor hydrolytic activity (Figure 24).

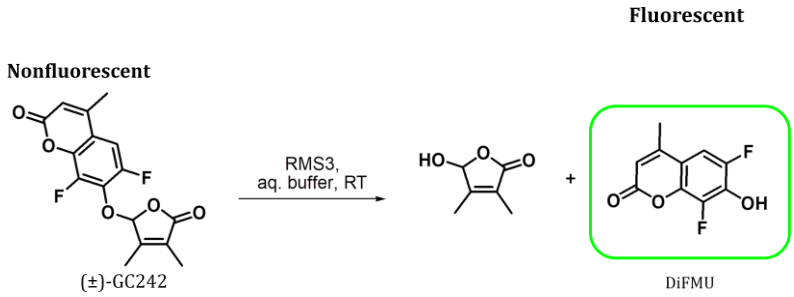

Figure 24. Principle of profluorescent probes.[37]

Pisum Sativum was chosen as lead candidate for the study. The SL receptor is called RMS3, and is the pea ortholog of rice D14. This scientific approach led to achieve important informations about the receptor hydrolysis kinetics.

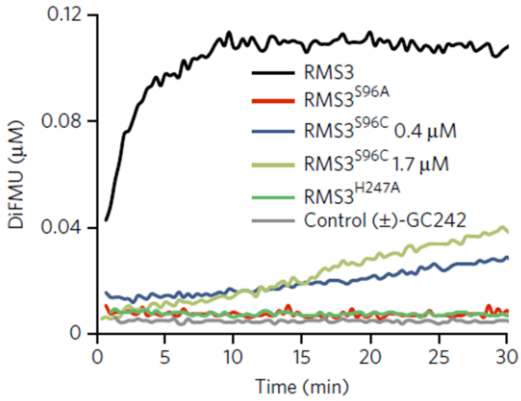

Figure 25. Progress curves deriving from the interaction of (±)-GC242 with RMS3 or RMS3 mutants.[37]

The fluorescence of the cumarine part of the probe (i.e. DiFMU) that is released upon hydrolysis of the compound allowed, not only to disclose the interaction with the RMS3 receptor, but also to underline the importance of the catalytic triad. Indeed, the activity of several RMS3 mutants having punctual modifications in the triad were analysed and resulted in a complete loss of activity (Figure 25). Additionally, the plateau phase reached after the interaction between GC242 and RMS3 suggested that the receptor acts as single-turnover enzyme, thus explaining its apparent low enzymatic rate. Therefore, a perception mechanism involving the catalytic triad was proposed (section 1.4 - SLs perception mechanism).[36]

A further implementation of this project was developed later and will be discussed in the following section (see 4.1.3 section), since belongs to my experience abroad during my PhD.

1.6.5 - SLs antagonist

I decided to introduce this paragraph in the synthetic strigolactone section, even if the molecules that will be pictured reside on the edge between an up-stream approach and a serendipitous target.

As a matter of fact, despite the importance of SLs as plant hormones and as chemicals responsible of symbiotic interactions, their heavy use could bring with it the great inconvenience of inducing germination in parasitic plants. Therefore, a simple and sharp approach would be the design of one single small molecule able to prevent or at least reduce the agonist-mediated response. The idea behind this plan is that a suitable non-hydrolysable molecule can enter inside the binding pocket and block the receptor cavity, and with it the cascade of events which brings to the PP germination.

Until now, the approaches proposed relied on molecules able to impact and to block the biosynthesis pathway. This is the reason why this can be defined as an up-stream approach: these molecules can not be properly defined as antagonist, since they do not compete for the same receptor site binded by strigolactones, but they hinder the enzymes involved in their biosynthesis.

Anyway, to design these molecules the nature of the enzymes involved in the SL production (i. e. CCD, carotenoid cleveage dioxygenases), which are iron dependent,[55] were considered.

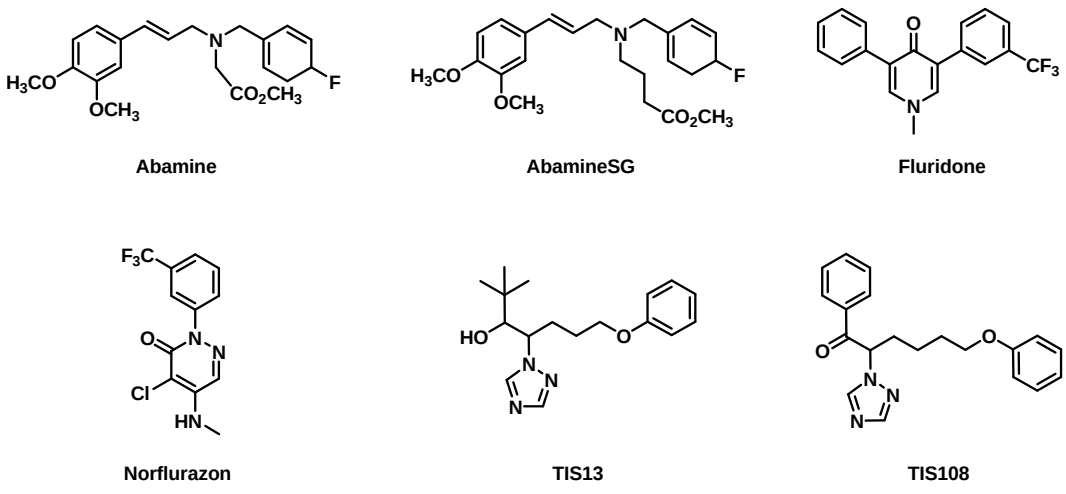

Figure 26. Strigolactone biosynthesis inhibitors.

Focusing on the chemical nature it was figured out that nitrogen, having a lone pair, would be able to form a coordinate bond with the free 3d orbital of the iron atom, meaning that compounds showing one or more heteroatoms could display a certain affinity for the binding site of this class of enzymes.

According to this hypothesis, abamine was found as one of the firsts molecule able to affect the strigolactone biosynthesis and thus inhibiting the function of the enzymes belonging to the CCD family.[56] Afterwards other inhibitors have been developed: fluridon and norflurazon, which were found to have side effects of lethal damages during plant growth,[57] and triazol derivatives as TIS13 and TIS108.[58]

However, the investigation for a strigolactone antagonist in the "truest sense of the word" is still on board.

CHAPTER 2

Medical field:
improved delivery systems in a new strigolactone frontier

2.0 - OUTLINE

Strigolactones have been recently found to have activity as anticancer agents.
Indeed, there is an urgent clinical need to discover new chemotherapic-like anti-neoplastic drugs with cytotoxic or cytostatic activities and with low toxicity. In this context, the use of natural compounds could be interesting because of their biological confirmed functions in the natural context and the possible biocompatibility also with the human being.
Nowadays a substantial percentage (~25%) of plant-derived compounds found an application as drugs.[59] Between them, worthy of mention as antineoplastic agents are jasmonates,[60] brassinosteroids[61,62] and, of course, taxol.[59]

2.1 - SLs AS ANTICANCER AGENTS

In 2008 Gomez-Roldan V.[6] and Umehara M.,[63] followed by Rameau C. in 2010,[64] thoroughly investigated this terpenoid class of plant hormones, demonstrating that the shoot branching inhibition was due to the control of axillary meristem cells growth. Afterwards, in 2011 Kalpunik Y. *et al.* discovered the SL capability to regulate the development of root meristems.[25]
The interaction between these plant hormones and the meristem cells was finally demonstrated, but an interesting result was obtained in 2010, when Koltai H. *et al.* showed that strigolactones can cause meristem cell cycle arrest.[65]
This result constituted the keystone which brought to direct the research to possible SLs application in the medical field. The connection between effects of SLs in plants and on cancer cell lines find an explanation in this simple definition:

*"The tissue from where the growth originates in plants is referred to as the **meristem**. The meristem contains unspecialized cells called **meristematic cells** that continually divide, allowing the plant to grow. […]*
Meristematic cells have often been compared to stem cells in humans."

Plant Meristem: Definition & Function, Lesson Transcript from Ryan Hultzman[66]

The similarity between meristematic cells in plants and stem cells in animals, combined with the problems connected with the existence of tumorigenic stem cells resistant to drug, brought to the first studies on strigolactones as anti-neoplastic agents.[67]

Breast cancer is probably one of the most studied form of tumor: despite this, it still has a high incidence in women and constitutes one of the most common causes of death. As reported by the International Agency for Research on Cancer (IARC), only in 2012 there were more than 1.6 millions of cases worldwide, with 500 thousands of deaths (Figure 27).[68]

Considering the significant number of people suffering from this disease, the activity of strigolactone analogues towards mammosphere cultures was evaluated, typically presenting enhanced values of cancer stem-like cells.

The cell lines tested were all breast cells: MCF-7, T47D (tumorigenic, non-metastatic), MDA-MB-231, MDA-MB-436 (tumorigenic, metastatic), BJ fibroblasts (normal, non-neoplastic line), and MCF10A (human breast epithelial cell line).

Figure 28 represents all the molecules that have been evaluated for the anticancer activity.[67] GR24 was used as reference compound for its widespread use in biological assays. In addition, indolyl-derived analogues belonging to the so called "EGO family" were considered.

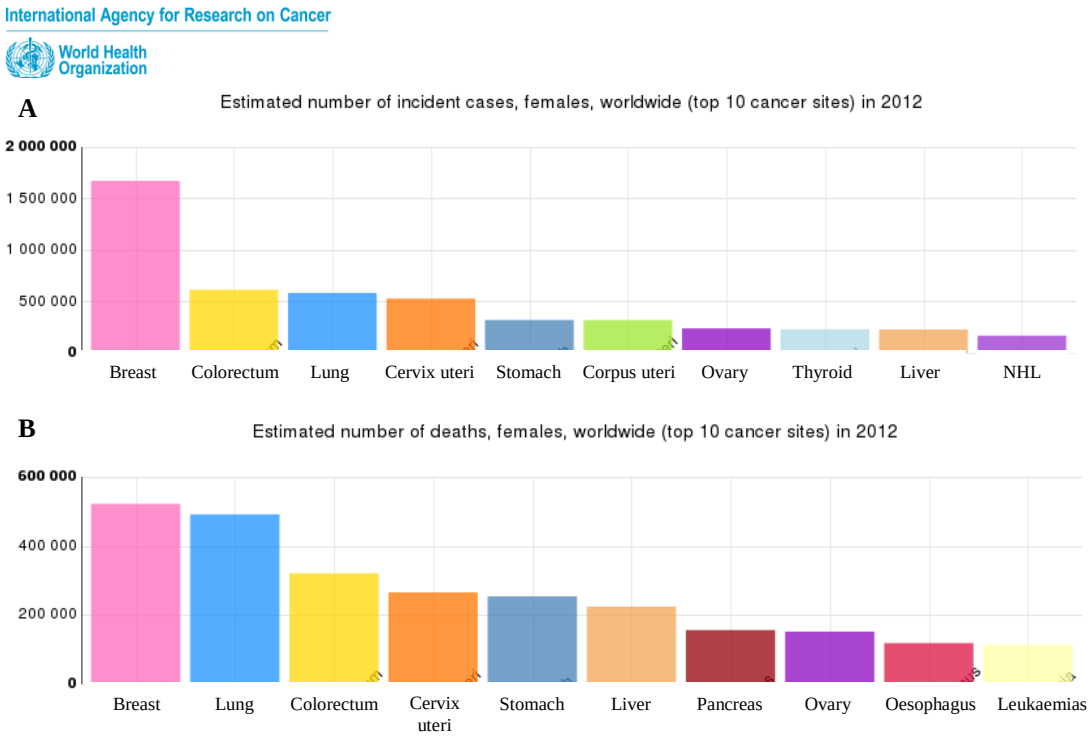

Figure 27. Estimated cancer cases (A) and deaths (B) between females worldwide in 2012.[69]

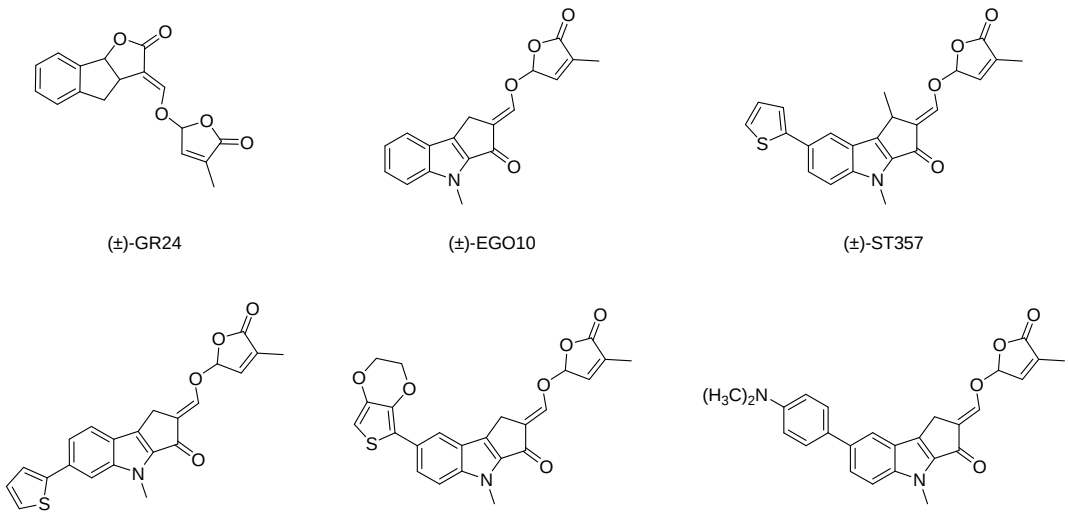

Figure 28. Strigolactone analogues tested towards breast cancer cell lines.

These last are nitrogen-containing analogues presenting different heterocyclic (ST357, MEB55, EDOT-EA) and aromatic substituents (EGO5) on the A ring.

Cell line	IC_{50}/7 days (ppm)
BJ fibroblast	>>10
MCF-7	5.7 ppm
MDA-MB-231	5.7 ppm
MDA-MB-436	5.2 ppm

Table 1. IC_{50} concentrations of GR24 in cancer cell lines.[68]

For GR24 the BJ fibroblast line was introduced as normal line, in order to see if there was a different response between tumorigenic and non-tumorigenic cells at the strigolactone treatment, and the same was done for the other analogues respect to the MCF-10A line.

GR24 efficacy was tested in a 0.5 -10 ppm (1.65 – 33 μM) range. The IC_{50} values disclose the effectiveness towards cancer cells, while for BJ fibroblast any significant reduction in growth was observed over this time of period (Table 1).

Tumor cell lines	IC_{50} (ppm) at 72 h				
	EGO5	**EGO10**	**ST357**	**EDOT-EA**	**MEB55**
MCF10A	>15	>15	>15	>15	>15
MCF-7	17.5	17.3	>20	8.1	>12.8
T47D	8.8	>10	>10	8.6	5.0
MDA-MB-231	7.5	>10	5.0	2.9	3.9
MDA-MB-436	ND	>10	ND	5.9	8.3

Table 2. IC_{50} concentrations of SL analogues in cancer cell lines.[68]

For the "EGO family" compounds the study was performed over 72 hours, not only revealing an almost total inactivity towards the MCF-10A non-tumorigenic line, but highlighting also a surprising activity for EDOT-EA and MEB55 in MDA-MB-231 cells (Table 2). Further experiments on strigolactones effect on cell cycle progression were performed (data not shown), confirming their ability to inhibit cancer cell proliferation and induce apoptosis.[67]

Following the exciting results obtained on breast, prostate, colon, leukemia, lung and osteosarcoma tumor lines were investigated. Different responses were obtained, also in these cases the EDOT-EA and MEB-55 proved to have a higher growth inhibition potential (Table 3).[69]

Tumor cell lines	IC_{50} (ppm) at 72 h				
	EGO5 1ppm = 2.3 μM	**EGO10** 1ppm = 3.2 μM	**ST357** 1ppm = 2.5 μM	**EDOT-EA** 1ppm = 2.0 μM	**MEB55** 1ppm = 3.1 μM
Prostate					
PC3	>15	>15	5.4	>15	8.8
DU145	>15	15	>15	7.5	12.8
LNCaP	13	>20	14.4	9.8	12
Colon					
HT-29	>15	>15	>15	7.3	8.2
HCT116	>15	>15	>15	6.0	12.8
SW480	>15	>15	>15	2.9	9.7
Leukemia					
K562	>15	>15	>15	4.3	8.1
Lung					
A549	18.3	13.5	10.6	6.7	6.9
Osteosarcoma					
U20S	3.9	4.5	4.5	2.8	2.7

Table 3. IC_{50} concentrations of SL analogues in prostate, colon, leukemia, lung and osteosarcoma cancer cell lines.[107]

2.2 - DRUG DELIVERY

The encouraging results obtained in the cancer treatment, especially for the EDOT-EA and MEB55 analogues, brought to step further and to the tentative of improving the strigolactones activity.

As a matter of fact, working in the medical field means that not only is important that a drug works, but it is also crucial that it can reach its target selectively. According to this, there is a specific research area focused on what is called the "drug delivery".

Drug delivery systems are devices that enable the introduction of therapeutic substances in the body and improve their efficacy and safety by controlling the rate, time, and place of release of drugs in the body.[70]

For this reason, we have undertaken the investigation on new anti-cancer formulations with improved delivery systems, named "cyclodextrin-nanosponges" (CD-NS).

2.3 - CD DISCOVERY

The CDs discovery has been attributed to A. Villiers, which in 1981 published the first article about "cellulosine", a crystalline substance isolated from bacterial digest of starch whose molecular formula was identified as $(C_6H_{10}O_5)_2 \cdot 3H_2O$.

In 1903, thanks to the research of the microbiologist Franz Schardinger, expert in scientific food, two compounds where isolated from bacterial digest of potato starch, and identified as the same of Villiers' molecules, respectively named α-dextrin and β-dextrin (i.e. α-cyclodextrin and β-cyclodextrin).

Further studies disclosed the possibility to obtain these crystalline substances by starch starting from different sources.

Finally, the γ-cyclodextrins were discovered by Freudenberg in 1935, which also suggested the existence of a larger size version of dextrins, later confirmed by French *et al.* in 1965.

But even though these bacterial digest starch derivatives were discovered, characterized and identified as oligosaccharides, plenty of informations were still unknown, such as the chemical structure, the molecular weight and other physicochemical properties. Starting from 1938 an in-depth study was addressed in order to better understand their chemistry.

Furthermore an improvement in cyclodextrins production by means of enzymes was evaluated. Cyclodextrin glucosyl transferase (CGTase), an amylase also produced by *Bacillus macerans*, was found to be able to recognize, cut and link the two ends of a starch fragment, giving in this way a mixture of cyclic structures: α- (~60%), β- (~20%), and γ-CDs (~20%). Over the years optimizations in the manufacturing process by means of genetic engineering were pinpointed, thereby enabling more active and more specific CGTases.[71]

2.4 - CD STRUCTURE AND APPLICATIONS

The CDs are characterized by glucopyranose units linked through α-1,4 glucosidic bonds and forming a truncated cone shaped structure. They are classified as α-, β- or γ-cyclodextrins depending on the number of units, six, seven or eight respectively. Table 4 reports some CD physical properties: as shown the cavity size increases with the unit number as well as the molecular weight, which is always a multiple of 162.1, the molecular weight of a glucose residue.[72]

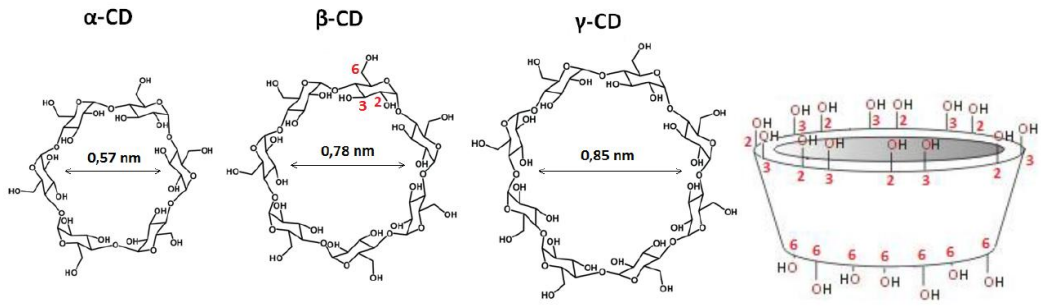

Figure 29. The three type of cyclodextrins: α-, β- and γ-CD. The most reactive hydroxyl groups (primary OH, in position 6) are oriented around the narrow edge of the truncated cone.

Cyclodextrins having less than six glucopyranose units do not exist, presumably as a consequence of steric reasons. On the other hand, CDs with 9, 10, 11, 12 and 13 units have been identified and respectively named δ-, ε-, ζ-, η-, and θ-CD, even though they tend to be rapidly transformed in smaller products.

Cyclodextrin	N° glucose residues	Molecular weight	Water solubility (g/100 mL)	Internal diameter (Å)	Depth (Å)
α-Cyclodextrin	6	972	14.5	4.5	6.7
β-Cyclodextrin	7	1135	1.85	~7.0	~7.0
γ-Cyclodextrin	8	1297	23.2	~8.5	~7.0
δ-Cyclodextrin	9	1459	Very soluble	-	-

Table 4. Physical properties of cyclodextrins.[73]

Furthermore, the spatial arrangement of CDs functional groups provides them with interesting features. Indeed, each glucopyranose unit presents two primary –OH groups on the C_2 and C_3 atoms, and a secondary –OH on the C_6.

All of them are oriented towards the outer part of the ring, providing in this way a hydrophilic feature at the external side.

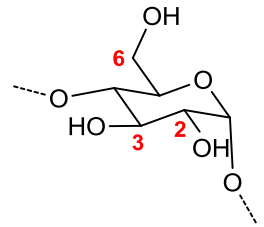

Figure 30. Glucopyranose fragment of a CD structure.

Conversely, the aliphatic hydrogen atoms and the glucosidic oxygen are responsible of the hydrophobicity resulting inside the cyclodextrin structure.

Due to the strong interactions between the CDs units, their solubility is much lower especially if compared to that of linear maltodextrins. In addition, β-cyclodextrins, characterized by an odd number of glucopyranose units, are less soluble than the α- and γ- ones, this because of the intra-molecular hydrogen bonds formed between the hydroxyl groups: this hamper the formation of other hydrogen bonds with the surrounding water molecules.

Considering that their solubility goes hand in hand with the presence of hydroxyl groups, to overcome the problem CDs derivatives having an –OH replacement with other type of moieties have been pinpointed.

Anyway, the main added value of these compounds remains their ability to form inclusion complexes. In aqueous solution, the replacement of water molecules and consequent accommodation of a guest compound inside their cavity can occur.[73]

It is precisely the discovery of cyclodextrin complexation ability which laid the grounds for their industrial application.

Drug/cyclodextrin	Trade name	Formulation	Country
α-Cyclodextrin			
Alprostadil	Prostavastin, Rigidur	I.V. solution	Japan, Europe, USA
OP-1206	Opalmon	Tablet	Japan
Cefotiam hexetil HCl	Pansporin T	Tablet	Japan
β-Cyclodextrin			
Benexate HCl	Ulgut, Lonmiel	Capsule	Japan
Cephalosporin	Meiact	Tablet	Japan
Chlordiazepoxide	Transillium	Tablet	Argentina
Dexamethasone	Glymesason	Ointment	Japan
Diphenhydramin HCl	Stada-Travel	Chewing tablet	Europe
Iodine	Mena-Gargle	Solution	Japan
Nicotine	Nicorette, Nicogum	Sublingual tablet, chewing	Europe
Nimesulide	Nimedex	Tablet	Europe
Nitroglycerin	Nitropen	Sublingual tablet	Japan
Omeprazol	Omebeta	Tablet	Europe
PGE_2	Prostarmon E	Sublingual tablet	Japan
Piroxicam	Brexin, Flogene, Cicladon	Tablet, Suppository, Liquid	Europe, Brazil
Tiaprofenic acid	Surgamyl	Tablet	Europe

Drug/cyclodextrin	Trade name	Formulation	Country
2-Hydroxypropyl- β-Cyclodextrin			
Cisapride	Propulsid	Suppository	Europe
Itraconazole	Sporanox	Oral and I.V. solutions	Europe, USA
Mitomycin	Mitozytrex	I.V. infusion	Europe, USA
Methylated β-Cyclodextrin			
Chloramphenicol	Clorocil	Eye drop solution	Europe
17β-estradiol	Aerodiol	Nasal spray	Europe
Sulfobutylether β-Cyclodextrin			
Voriconazole	Vfend	I.V. solution	Europe, USA
Ziprasidone mesylate	Geodon, Zeldox	IM solution	Europe, USA
2-Hydroxypropyl-γ-cyclodextrin			
Diclofenac sodium	Voltaren	Eye drop solution	Europe
Tc-99 Teoboroxime	Cardiotec	I.V. solution	USA

Table 5. Cyclodextrin-containing pharmaceutical products. [72]

Firstly, in food and cosmetic industry, and later in medicine, they started spreading from the early 1970s. The main employments were the increasing of the stability of the included compound, odour and taste suppression, and molecular activity prolongation. Nowadays they are commonly used for pharmaceutical formulations, with approximately 30-40 drugs (Table 5) commercialized as cyclodextrin complexes.[71]

2.5 - TOXICOLOGICAL EVALUATIONS

The use of cyclodextrins and CD derivatives took long before to be introduced in the pharmaceutical industry because of a misinterpretation of toxicological results. In 1957 French and coworkers referred to unpublished results disclosing a marked toxicity, which brought to the rats decease within a week from the oral subministration of β-CD. Only later it was shown that these results were probably due to the presence of impurities, and not to the cyclodextrin itself.

Studies have been addressed revealing that, when administered orally, the CD uptake from the gastrointestinal tract doesn't occur, thus preventing a possible toxic effect.[71]

2.6 - NANOSPONGES

Even though cyclodextrins are worldwide used by lots of companies, their limitation resides in their incapability to form inclusion complexes with hydrophilic or high-molecular weight molecules. Furthermore, some of them present a very low aqueous solubility and toxicity when injected intravenously or in the parenteral treatment.

The efforts made in order to overcome these problems and improve their technological characteristics, led to the "cyclodextrin nanosponges" (CD-NS) appearance on the scientific scenario.

These are polymeric derivatives of cyclodextrins cross-linked with carbonate or ester bonds and connected one to the other in a three dimensional network. Starting from the same ciclodextrin, different nanosponges having different chemical behaviours can be obtained simply changing the type of cross-linker used.

More important is that, compared to CDs, nanosponges present a much larger number of active sites, both hydrophobic (inside the CD cavities) and hydrophilic (obtained as nanochannels connecting the CD monomers). Nowadays nanosponges find application in several fields, and one of them is the medical area. Drugs having different solubilities, activities and structures have been successfully complexed inside the NS structures, with a consequent solubility and activity improvement.[74]

2.6.1 - CD - polycarbonate nanosponges

Cyclodextrin-based polycarbonate nanosponges are synthesized using CDs and triphosgene, carbodiimidazole or diphenylcarbonate as active carbonyl compound. The resulting nanosponge presents carbonate bonds between the CD units. The purification from the unreacted cross-linking agent is performed washing with water and ethanol and through Soxhlet extraction.

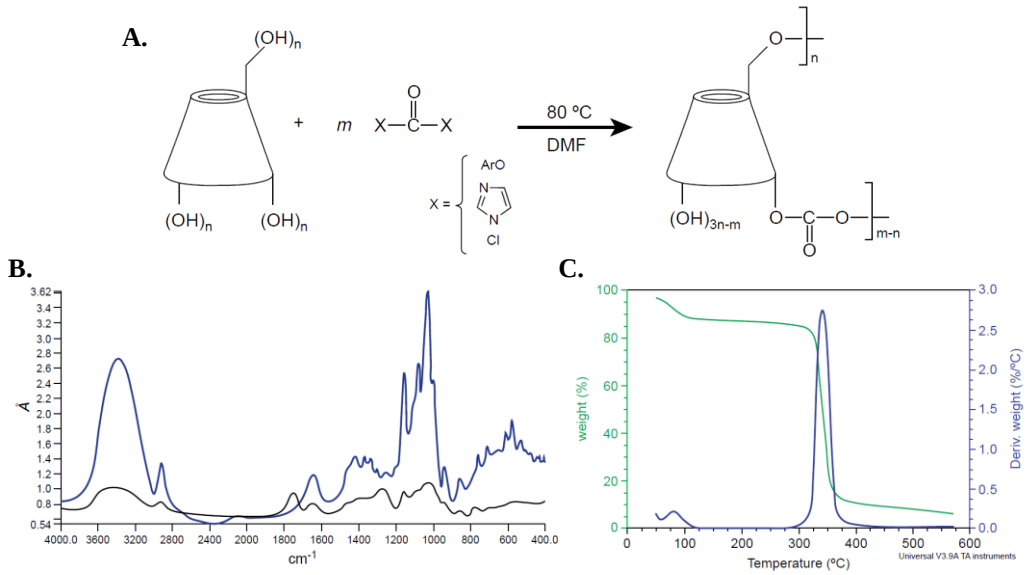

Figure 31. (A) Synthesis of CD carbonate nanosponges; (B) FTIR spectra of β-CD (blue line) and β-CD-carbonate nanosponges (black line); (C) thermogravimetric analysis of β-CD-NS. [75]

The product formation can be confirmed by means of FTIR analysis (Figure 31B). Indeed, the carbonyl group connecting the CD monomers in the nanosponge structure gives a 1750 cm^{-1} peak, which is absent from the CD infrared spectrum.

This class of nanospoges are characterized by a thermal stability until 340°C, confirmed by thermogravimetric analysis, low water solubility, nontoxicity, porousity and poor swelling capability.

In addition, their mechanical features can be tuned simply changing the molar ratio CD:cross-linker from 1:2 to 1:8. The higher cross-linker content and the higher will be the cross-linking degree. On the contrary, the type of cyclodextrin used seems to have no effect on the mechanical properties.[74]

2.6.2 - CD - polyester nanosponges

Also for pyro-NS the synthesis consists in stirring together CDs and a cross-linker of choice, which in this case is a dianhydride or a di/polycarboxylic acid (Figure 32). FTIR analysis confirms the nanosponge formation through the appearance of a band at 1727 cm^{-1}, due to the ester group connecting the monomers.

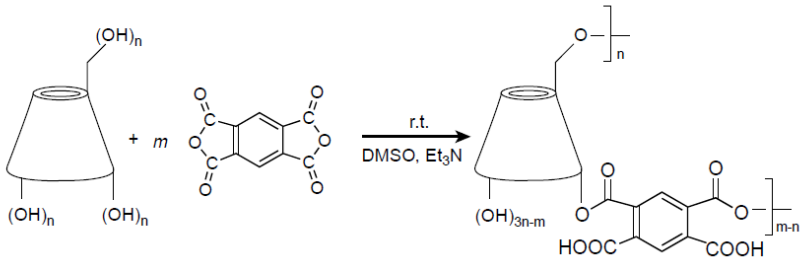

Figure 32. Synthesis of CD-polyester nanosponges. [75]

Opposite to polycarbonate nanosponges, they tend to swell appreciably and retaining a water amount up to 25 times their own weight. This, of course, depends on the molar ratio between the cyclodextrin and the cross-linker: the higher is the ratio less is the water uptake.

The flipside of the coin of their solubility resides in the chemical stability, they tend to be hydrolyzed easier than carbonate-NS.[74]

2.6.3 - Glutathione-responsive NS

A further improvement of the nanosponge application has been the development of delivery systems able to response and recognize selectively the site of interest.
In particular, the glutathione (GSH) concentration was found to be a trigger for the target release of active drugs. The GSH has a concentration of 2-20 μM in plasma, 2-20 mM in cells, and even higher in tumor cells. Exploiting this feature it was possible to target specific delivery apparatus.[75,76]

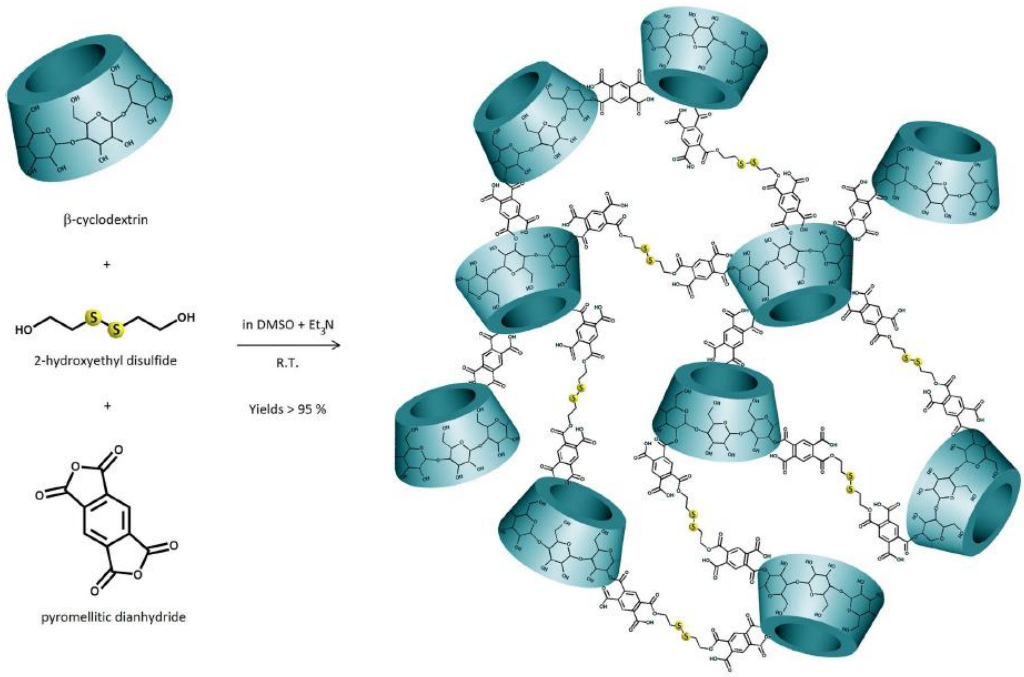

Figure 33. Synthesis of glutathione responsive nanosponges.[78]

This class of NS is characterized by the presence of disulfide bridges (Figure 33).[77] When the nanosponge comes in contact with the gluthathione, the GSH thiol group is oxidixed to disulfide bridge, while the NS disulfide bridges are reduced to thiol groups. As a consequence, the drug complexed inside the NS backbone is released during this break-and-formation bond process.

CHAPTER 3

- SYNTHESIS OF STRIGO D- LACTAMS -

3.1 – Results and discussion

This section is focused on the synthesis of a new class of strigolactone analogues, the Strigo D-lactams,[78] whose design has been realized by means of a bioisosteric approach.

Even though several hypothesis about the SL-D14 interaction have been proposed, the issue is still under debate. Up to date, the importance of the stereochemistry at the BC junction and at the C2' position have been assessed and considered crucial to induce selective biological responses. Once the SL ligand reaches the binding pocket, a hydrolysis reaction occurs and leads to the D-ring release, consequently trapped inside the receptor site.

The D-lactam family of analogues was devised in line with the bioisosterism principle, according to which the chemical similarities between groups or substituents impart similar biological properties to a chemical compound.

The idea was to replace the oxygen atom of the D-ring with a nitrogen, then changing functional group and switching from a lactone to a lactam.

Part of the work of my PhD thesis consisted in finding an efficient strategy for the synthesis of several 5-membered lactam rings. The key step of this strategy is a ring-closing metathesis (RCM). The following section will be focused on the synthesis, biological investigations, stability tests, luminometer assays and docking simulations of several analogues labelled to the modified D-rings.

Synthesis

The first step in the synthetic sequence was the synthesis of the appropriate amides. This was realized by condensation of primary amines, as allyl amine, 2-methylprop-2-en-1-amine and *N*,2-dimethylprop-2-en-1-amine with *meta* acryloyl chloride, under basic conditions.

The nitrogen atom was then protected either with Boc- or Cbz- group.

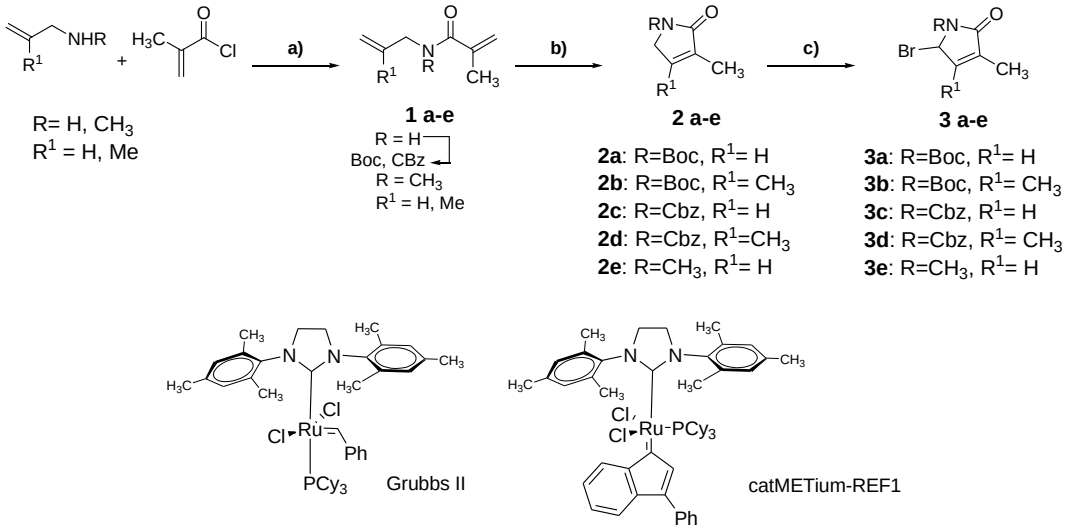

Figure 34. Synthetic procedure for the synthesis of D-lactams. a) K_2CO_3, DCM, 0°C to r.t., 16h; b) Hveyeda-Grubbs II (5-10%) or catMetium (1%), PhMe, 80°C, 14-32 h; c) NBS, AIBN, CCl_4, 90°C, o.n.

The protected amides were then subjected to a ring-closing metathesis (RCM) procedure, were two different catalysts have been evaluated: Grubbs II and catMETium-RF1. Different times, temperatures and catalyst amounts were evaluated, revealing the catMETium-RF1 as more appropriate, since an amount of 1% at 110° C required just 1.5 h for a complete conversion.

Entry	R	R^1	Grubbs catalyst	Catalyst load	Time, h	Temp. (°C)	Obtained lactam	Yield[a]
1a	Boc	H	Grubbs II	8 %	18	80	**2a**	83
1a	Boc	H	catMETium	1 %	1.5	110	**2a**	95
1e	Cbz	H	Grubbs II	8 %	16	80	**2c**	76
1e	Cbz	H	catMETium	1 %	1.5	110	**2c**	78
1g	Me	H	catMETium	1 %	1.5	110	**2e**	82
1b	Boc	Me	Grubbs II	8 %	16	80	**2b**	11
1b	Boc	Me	catMETium	1 %	1.5	110	**2b**	48
1f	Cbz	Me	Grubbs II	8 %	16	80	**2d**	15
1f	Cbz	Me	catMETium	1 %	1.5	110	**2d**	58

Table . All the reactions have been performed under an inert atmosphere in anhydrous toluene. CatMETium denotes catMETium-RF1. [a]Yield of pure compound.

The obtained *N*-protected lactams were then brominated, giving compounds **3a-d** in good yields. The only exception was represented by the **3e** molecule, obtained in tiny amounts (5% yield) because of the absence of an electron-withdrawing group on the nitrogen atom, which would lead to the allylic radical formation and to the consequent reaction with bromine.

From this point forward compounds **3a-d** were labelled to different strigolactone analogues following the general synthetic scheme reported below.

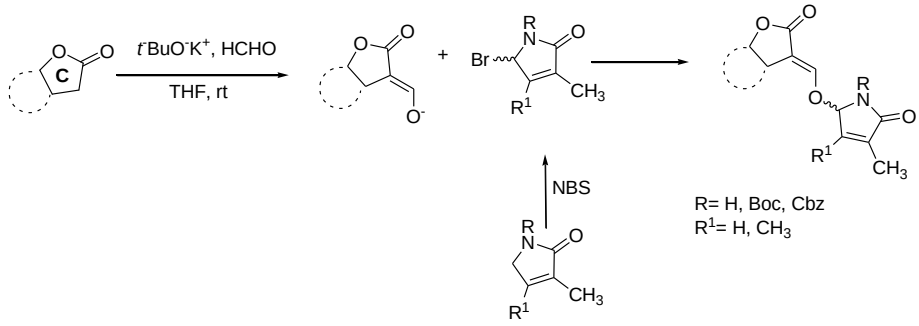

Figure 46. General synthetic pathway for the synthesis of strigo-D-lactams.

The first substrate was the GR24 tricycle (**4**). Coupled with the brominated lactams **3a** or **3b**, two racemic diastereoisomers were obtained and separated by column chromatography, giving **5a**, **5a'** and **5b**, **5b'** respectively.

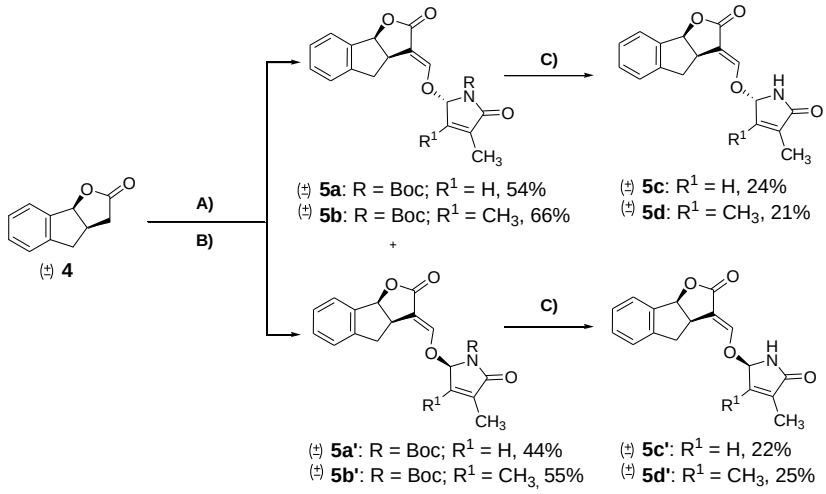

Figure 35. Synthetic procedure for the synthesis of GR24 D-lactams. A) t-BuOK, HCOOEt, DME, from 0°C to r.t., 1h; B) **3a**, **3b**, DME, from 0°C to r.t., 16h; C) TFA, DCM, 0°C, 10 min

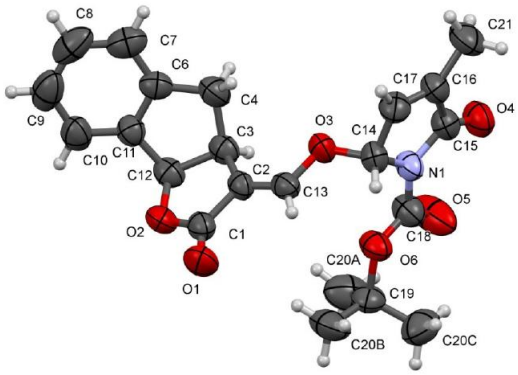

Figure 36. X-ray diffraction analysis of (+)-5a compound.

The absolute configuration was assessed by X-ray analysis of the **(+)-5a** compound (Figure 36).

Final deprotection step provided the final GR24 and *epi*-GR24 D-lactams **5c**, **5c'**, **5d** and **5d'**.

The second family of D-lactam compounds is represented by indolyl derived analogues (EGO family). As for the ABC tricycle **4**, the indole scaffold **6** was subjected to the D-ring attack with the **3a**,**c** and **d** lactams, giving respectively the **5e-g** products.

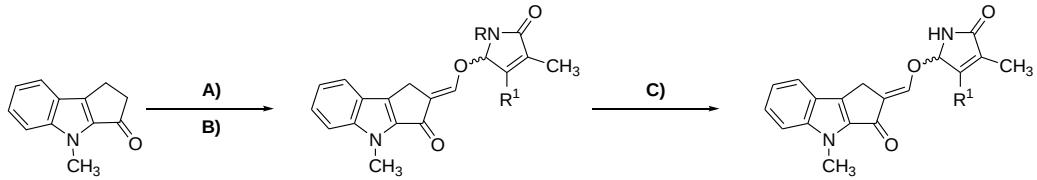

6

(±) **5e**: R = Boc; R^1 = H, 44%
(±) **5f**: R = Cbz; R^1 = H, 55%
(±) **5g**: R = Cbz; R^1 = CH_3, 55%

(±) **5h**: R^1 = H, 100%
(±) **5i**: R^1 = CH_3,100%

Figure 37. Synthetic procedure for EGO D-lactams. A) t-BuOK, HCOOEt, DME, from 0°C to r.t., 1h; B) **3a**, **3c**, **3d**, DME, from 0°C to r.t., 16h; C) H_2, Pd/C, r.t., 1h.

The removal of the Boc- protecting group only led to degradation products, therefore a different synthetic strategy involving the use of *N*-Cbz-lactam was exploited to obtain final compounds **5h-i** in excellent yields.

In addition, we designed also the D-lactam version of the debranone family of mimics, characterized by the presence of an aryloxy substituents at the C-5 position. Synthesized in two *N*-protected versions (**5j-k**), the deprotected **5l** was

obtained from the Boc-**5j**, by removal of the protecting group under conditions compatible with the substrate structure.

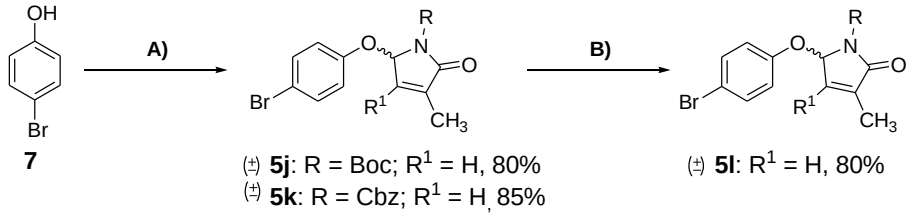

Figure 38. Synthetic procedure of mimic D-lactams. A) **3a**, **3c**, K_2CO_3, TBABr, DCE/H_2O r.t., 1h; B) TFA, DCM, from 0°C to r.t., 10 min.

Furthermore, with the aim to getting inside the mode of action of strigolactones, an EGO D-lactam version lacking of the enol ether bridge was proposed and synthesized.

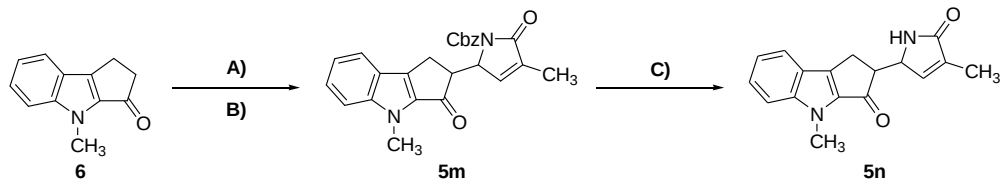

Figure 39. Synthetic procedure of EGO D-lactam lacking of the enol ether bridge. A) t-BuOK, DME, from 0°C to r.t., 1h; B) **3c**, DME, from 0°C to r.t., 16h; C) H_2, Pd/C, r.t., 1h.

Stability

The stability of racemic Boc protected and deprotected D-lactam analogues was evaluated in two different conditions: a 30% solution of MeOH in water, and an acetonitrile/water solution in 1:1 ratio. GR24 was used as reference compound. As predictable, the half-life time was lower in MeOH, especially for NH-lactams. By contrast *N*-Boc derivatives seemed to be much more stable compared to their unprotected versions. Best results in terms of stability were obtained for the **±5n** compound, which lacks the hydrolysable enol ether bridge and presents the lactone C-ring directly connected to the lactam-D ring.

Compounds	Half-life ($t_{1/2}$ in hours)	
	30% MeOH	ACN/H_2O 1/1
(+)-GR24	80	3375
±5a	110	720
±5a'	21	140
±5c	3	3.8
±5c'	3.3	4.4
±5h	2	24
±5e	190	528
±5l	11	17
±5j	230	1080
±5n	1100	2900

Table 7. Chemical stability of strigo D-lactams at 21 °C and pH 6.7. The $t_{1/2}$ values were extrapolated from the plots of peak area *vs* time.

Germination activity

The activity of the synthesized molecules was evaluated towards *Phelipanche aegyptiaca* seeds, comparing them with the well known (±)-GR24, used as standard, the EGO10 and EDOT analogues, for their reported good germination activity on the same biological system,[46] and Strigol, used as representative of natural SLs. As reported from the bar graph below (Figure 40), the activity of (±)-GR24, strigol, EGO10 and EDOT is in accordance with literature data,[46] while all the tested D-lactams compounds resulted active at concentration higher than GR24, thus indicating their lower bioactivity. The only exception was for **5a'** and **5c'**, revealed as the most active. Furthermore the comparable results obtained for the **5a'** and **5c'** compounds suggest that the Boc protecting group does not affect bioactivity. The same trend was detected for the other synthesized molecules, where D-lactams *N*-Boc derivatives and their corresponding deprotected NH versions exhibit analogous activity profiles.

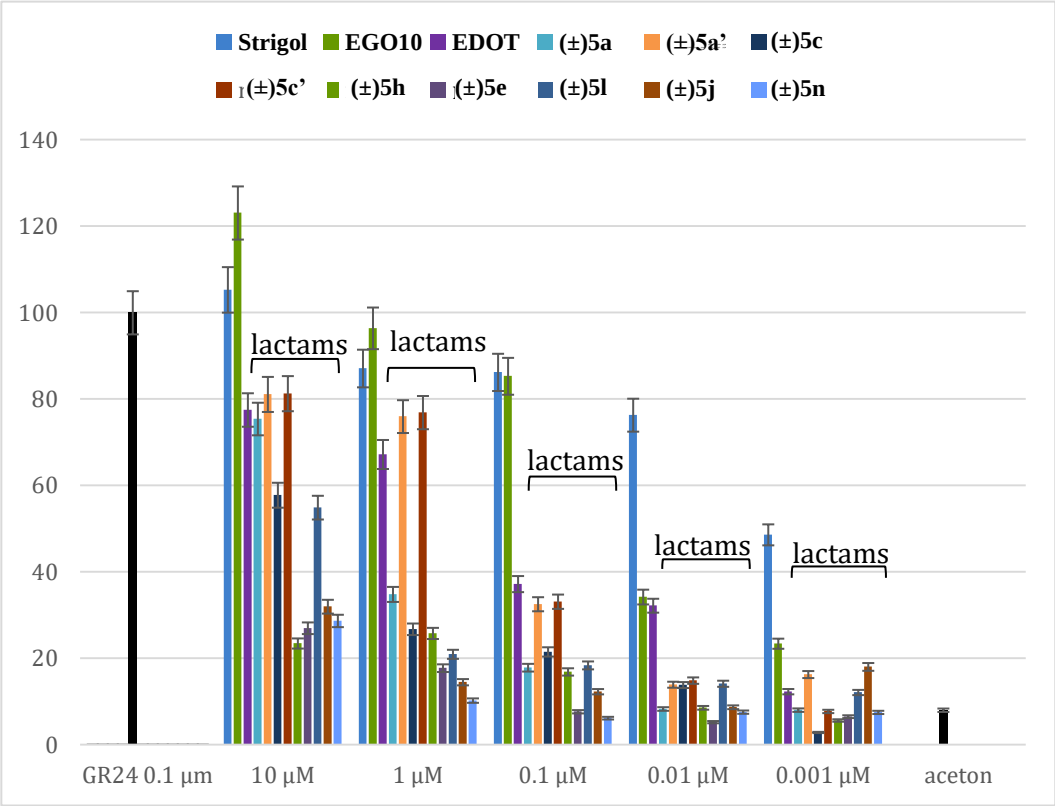

Figure 40. Percentages of germinated seeds (y axis) of *Peliphanche aegyptiaca* after exposure to the natural SL Strigol, EGO10 and EDOT analogues, and the strigo D-lactams series of analogues, at different concentrations. (±)-GR24 and acetone used as positive and negative control respectively.

Luminometer assays

D-lactams compounds were tested by an *in vivo* and quantitative assay, based on the decrease of luminescence caused by the degradation of D14 receptor fused to fluorescent luciferin protein in transgenic *Arabidopsis thaliana* lines. According to this analysis, the luminescence values read by a luminometer are inversely correlated to the SL-like activity of the molecule.

The assay, capable to detect bioactivity in the 0.01-100 µM wide dynamic range, was calibrated with (+)-GR24 and used to test the synthesized SL-D-lactam series in a concentration range.

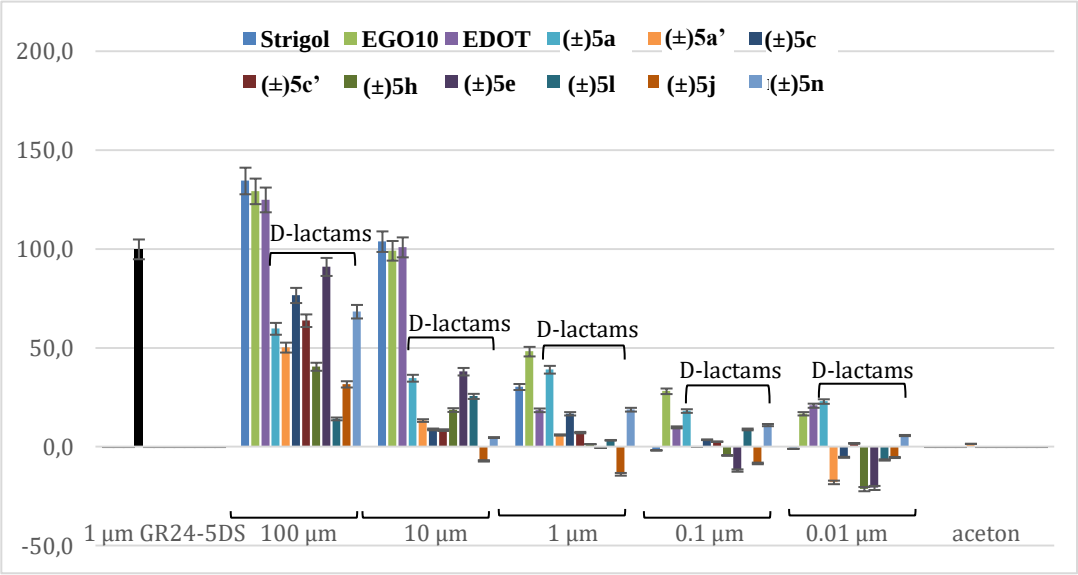

Figure 41. Luciferase assay, calibrated with (+)-GR24 in a range of concentrations of 0.01-100 µM.

As shown in Figure 41, natural SL strigol and synthetic EGO10 and EDOT analogues promote D14 degradation, even if were proved to be less effective than (+)-GR24. By contrast, all the tested D-lactams analogues proved to be inactive at concentrations equal to or lower than 10 µM, while some differences were detected at 100 µM.

Docking simulations

Docking simulations were performed in order to understand the accommodation and the interactions of the synthesized molecules in the receptor pocket. For this investigation we referred to the Zhao co-crystallized structure of GR24-D14,[35] according to which the compound is H-bonded to the Ser97 and Trp 155 residues (Figure 42A). We run superimposition experiments of **(±)-5c** referring to (+)-GR24 as shown in Figure 42B and identified the different areas responsible of interactions: hydrophobic regions are reported in yellow, while red is used for hydrogen bond acceptor and blue for hydrogen bond donor (Figure 42C).

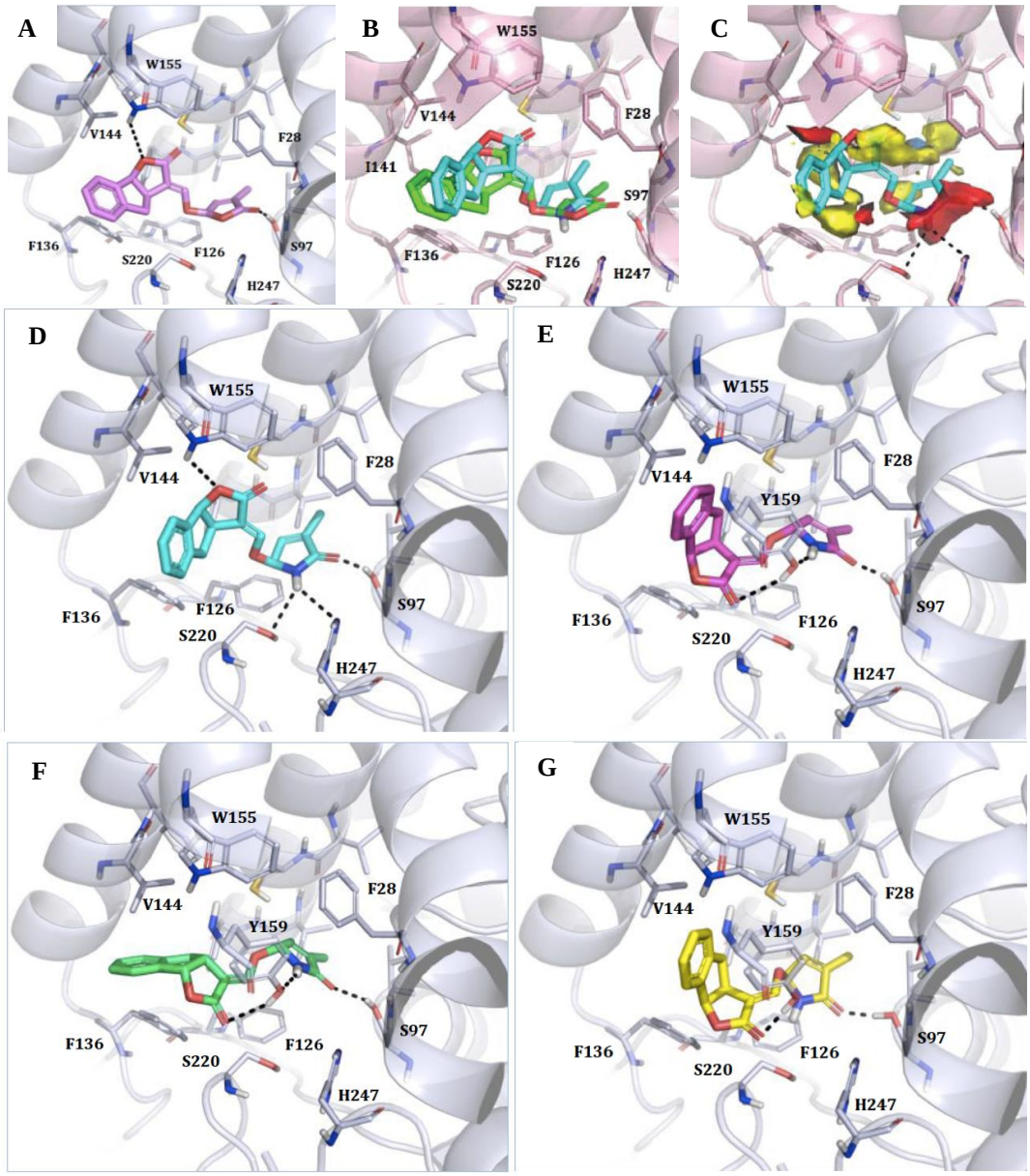

Figure 42. A) Crystallographic pose of (+)-GR24 within rice D14[35]; B) Superimposition of the docking model of compound (±)-**5c** (blue) and of the crystallographic pose of (+)-GR24 (green) in the binding site of rice D14; C) Hydrogen bonds made by compound (±)-**5c** within the pocket and calculated molecular interactions: red, blue and yellow contours identify the hydrogen bond acceptor, hydrogen bond donor and hydrophobic area, respectively;
Docking model of (±)-**5c** and (±)-**5c'** in the binding site of rice D14. Modelling was made for each enantiomer of the racemic mixtures: D) (±)-**5c**, (SSR, Strigol configuration); E) (±)-**5c** (RRS *ent*-Strigol configuration); F) (±)-**5c'** (RRR, Orobanchol configuration); G) (±)-**5c'** (SSS, *ent*-Orobanchol configuration). Hydrogen bonds are represented as black dashed lines.

Docking simulations were realized for each enantiomer of the GR24 D-lactam series of analogues (**(±)-5c** and **(±)-5c'**). As expected, a better accommodation was found for the enantiomer of the **(±)-5c** compound possessing the Strigol configuration SSR (i.e. (+)-GR24 stereochemistry). As a consequence of the similar orientation, interactions with Ser97, His 247, Ser220 and Trp155 were established (Figure 42D). The molecule, stabilized through electrostatic and hydrophobic interactions, appears susceptible to be hydrolyzed from the serine residue, thus proving to be a good candidate to mimick the SL activity. Nevertheless, the compound is quite inactive in the aforementioned bioassays. The reason for this discrepancy are currently under discussion but can be related to the change of functional group.

By contrast both **5c'** enantiomers exhibit a less reliable pose, in agreement with the luminometer assays, where a minor D14::LUC degradation is observed.

The respective Boc-protected versions **(±)-5a** and **(±)-5a'** were also investigated, but no reasonable orientation was found because of the presence of the bulky protecting group.

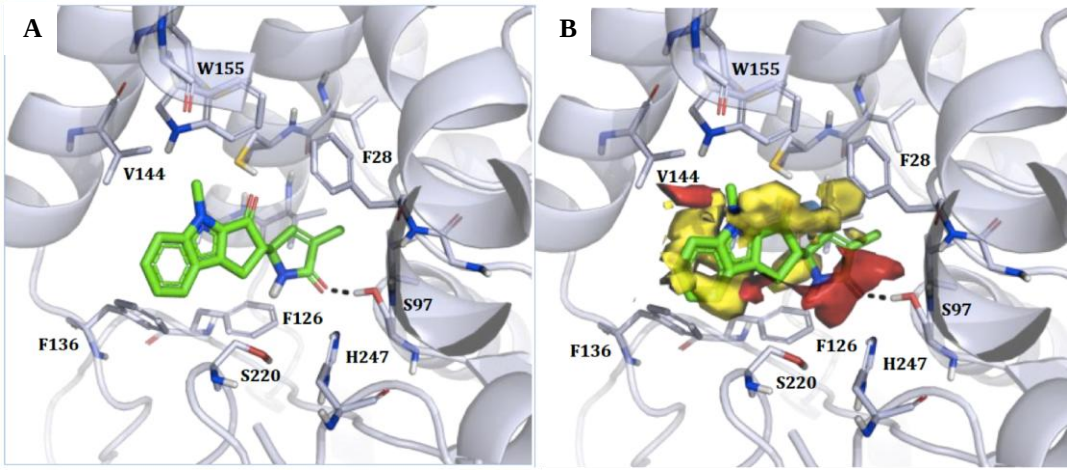

Figure 43. A) Docking model of (±)-**5n** in the binding site of rice D14. Only enantiomer SS is reported. Hydrogen bonds are represented as black dashed lines. B) Calculated Molecular Interactions of (±)-**5n** compound: red, blue and yellow contours identify the hydrogen bond acceptor , hydrogen bond donor and hydrophobic area, respectively.

Eventually, we tested **(±)-5n**, initially suspected as possible SL inhibitor due to its inactivity in both bioassays. Docking evaluations revealed that the molecule, once located in the binding pocket, interacts with the Ser97 residue forming an H bond. Since no other interaction occurs, the complex would be too unstable to act as inhibitor towards (+)-GR24. This was further supported by luciferase competition test. The aim was to compare the effects on bioactivity when (+)-GR24 was subministrated alone, or together with the **(±)-5n** molecule. The assay was performed on the *Arabidopsis* system, maintaining fixed the highest inactive **(±)-5n** concentration (10 μM) and varying the (+)-GR24 amount in the 0.01-100 μM range. Monitoring the decrease of fluorescence, the competition test revealed that the (+)-GR24 activity was not altered or affected by the **(±)-5n** presence (Figure 44), meaning that this last mentioned compound is only able to act as partial agonist at high concentrations (100 μM).

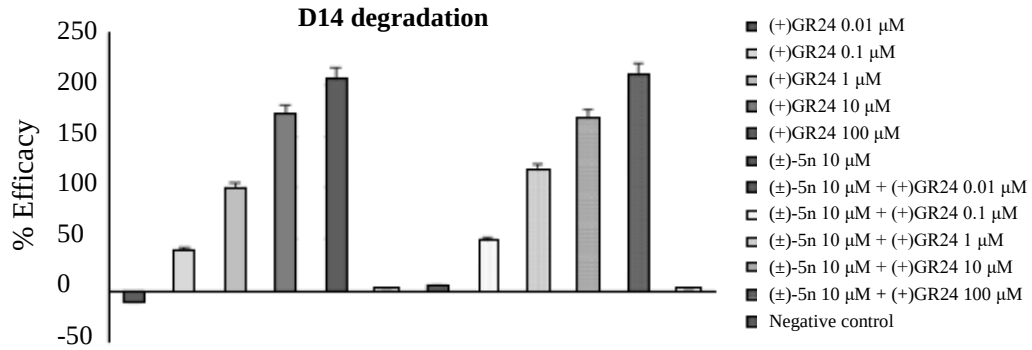

Figure 44. Luciferase competition test between (±)-5n and (+)-GR24.

3.2 - Experimental

The general synthetic approach to D-lactam ring and to Strigo-D-Lactams are respectively reported in Figure 45 and Figure 46.

D-Lactam synthesis : general procedure

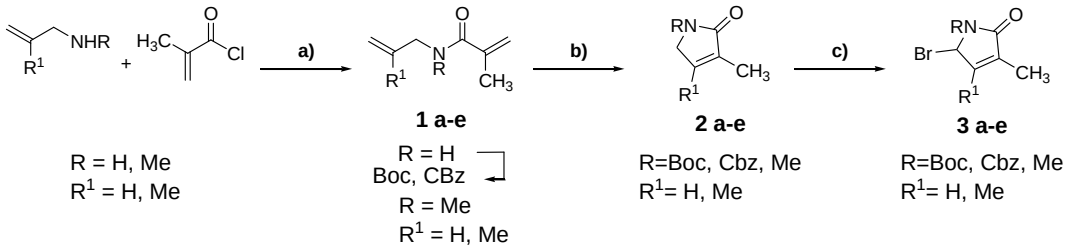

Figure 45. Synthetic pathway for the synthesis of D-lactams. a) K_2CO_3, DCM, 0°C to r.t., 16h; b) Hveyeda-Grubbs II (5-10%) or catMetium (1%), PhMe, 80°C, 14-32 h; c) NBS, AIBN, CCl_4, 90°C, o.n.

Strigo-D-Lactam synthesis : general procedure

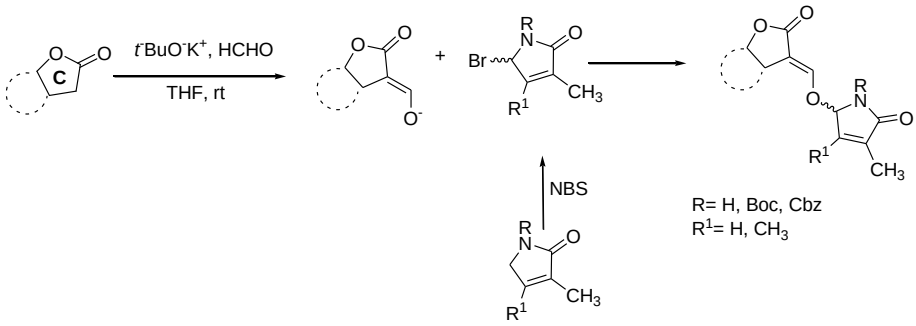

Figure 46. Synthetic pathway for the synthesis of strigo-D-lactams.

General procedure for the synthesis of *N*-allylmethacrylamides 1a, 1b, 1g.

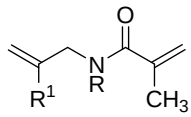

1a: R=H, R^1=H
1b: R=H R^1=CH_3
1c: R=Boc, R^1=H
1d: R=Boc, R^1=CH_3
1e: R=Cbz, R^1=H
1f: R=Cbz, R^1=CH_3
1g: R=CH_3, R^1=H

In an oven-dried round bottom flask, a solution of freshly distilled allylamine (1.00 eq) in anhydrous CH_2Cl_2 (57 mL) was cooled to 0°C. K_2CO_3 (3.00 eq) was added and the mixture was stirred at 0 °C for 2h. Then, methacryloyl chloride (1.20 eq) was added dropwise. The mixture was further stirred at 0°C for 3h, then raised to room temperature and stirred overnight (12h). The reaction mixture was poured into iced water and the aqueous phase was extracted with CH_2Cl_2 (3 x 20 mL). Then the combined organic layers were washed with brine, dried over Na_2SO_4 and filtered. Evaporation of the solvent gave a colourless liquid which was purified by silica gel chromatography.

***N*-allylmethacrylamide (1a)**.

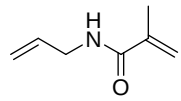

The crude was purified by flash chromatography (PE/EtOAc 4:1 v/v to PE/EtOAc 1:1 v/v) to obtain the final product as a colourless liquid in 91% yield. TLC Rf = 0.15 (PE/EtOAc 8:2 v/v). ^{1}H NMR (200 MHz, $CDCl_3$): δ 6.29 (br s, 1 H, NH), 5.80 (ddt, *J* = 17.1 Hz, *J* = 10.2 Hz, *J* = 5.6 Hz, 1H, CH_2=C*H*CH_2NH), 5.66 – 5.65 (m, 1H, (CH_3)C=CH_2), 5.28 - 5.26 (m, 1H, (CH_3)C=CH_2), 5.18 − 5.02 (m, 2H, CH_2=CHCH_2NH), 3.86 (tt, *J* = 5.7 Hz, *J* = 1.5 Hz, 2H, CH_2=CHCH_2NH), 1.91 –

1.90 (m, 3H, CH_3). Spectral data correspond to those previously reported in literature.[79]

***N*-(2-methyl)allylmethacrylamide (1b)**.

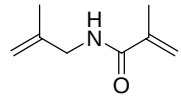

Starting from 2-methylallylamine (1.00 eq), compound **1b** was obtained after chromatography (PE/EtOAc 8:2 v/v, Rf = 0.37) as a colourless liquid in 89% yield. ^{1}H-NMR (600 MHz, $CDCl_3$): δ 6.32 (br s, 1H, NH), 5.64 (s, 1H, $CO(CH_3)C=CH_2$), 5.25 (s, 1H, $CO(CH_3)C=CH_2$), 4.74 (s, 2H, CH_2NH), 3.76 (s, 2H, $CH_2=C(CH_3)CH_2$), 1.89 (s, 3H, CH_3), 1.65 (s, 3H, CH_3); ^{13}C-NMR (150 MHz, $CDCl_3$): δ 168.55 (CO), 141.99 (Cq), 140.06 (Cq), 119.49 (=CH_2), 110.74 (=CH_2), 45.05 (CH_2), 20.38 (CH_3), 18.75 (CH_3). MS: (EI, 70 eV): m/z (%) = 41 (64), 69 (100), 96 (44), 124 (55), 139 (15) [M].

***N*-allyl-*N*-methylmethacrylamide (1g)**.

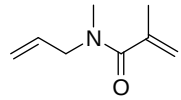

Starting from *N*-methylprop-2-en-1-amine (1.00 eq), compound **1g** was obtained after chromatography (PE/EtOAc/ Et_3N 1:1:0.03 v/v/v, Rf = 0.45) as a colourless liquid in 83% yield. ^{1}H-NMR (200 MHz, $CDCl_3$): δ 5.76 (ddt, *J* = 18.4 Hz, *J* = 10.6 Hz, *J* = 5.3 Hz, 1H, $CH_2=CHCH_2N(CH_3)$), 5.23 − 5.13 (m, 3H, 3 x CH_2=), 5.06 − 5.04 (m, 1H, CH_2=), 3.98 (br s, 2H, $CH_2=CHCH_2N(CH_3)$), 2.87 (s, 3H, CH_3), 1.96 − 1.95 (m, 3H, CH_3). Spectral data were in agreement with literature values.[80]

General procedure for the synthesis of compounds 1c and 1d.

To a solution of the corresponding *N*-allylmethacrylamide **1a** or **1b** (1.00 eq) in anhydrous THF (380 mL), (*t*-Boc)$_2$O (2.00 eq) and few milligrams of DMAP were added. The reaction mixture was stirred at 80°C overnight. Then, the reaction was quenched with water and extracted with CH_2Cl_2 (3 x 100 mL). The collected organic phases were dried over Na_2SO_4, filtered and concentrated under reduced pressure. The crude product was purified by silica gel chromatography.

***tert*-Butyl allyl(methacryloyl)carbamate (1c)**.

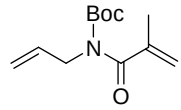

The crude product was purified by chromatography (PE/EtOAc 9:1 v/v, Rf = 0.88) to give the final product as a colourless liquid in 91% yield. ^{1}H-NMR (200 MHz, $CDCl_3$): δ 5.86 (ddt, *J* = 17.1 Hz, *J* = 10.2 Hz, *J* = 5.7 Hz, 1H, CH_2=C*H*CH_2NBoc), 5.18 – 5.05 (m, 4H, 2 x =CH_2), 4.18 (dt, *J* = 5.8 Hz, *J* = 1.4 Hz, 2H, CH_2=CHC*H*$_2$NBoc), 1.94 – 1.93 (m, 3H, CH_3), 1,41 (s, 9H, Boc); ^{13}C-NMR (50.2 MHz, $CDCl_3$): δ 173.82 (CON), 153.17 (COO Boc), 143.35 (*C*=CH_2), 133.06 (CH_2=C*H*CH_2NBoc), 117.08 (=CH_2), 116.11 (=CH_2), 83.30 (*C*(CH_3)$_3$), 47.03 (CH_2), 27.81 (3 x CH_3), 19.30 (CH_3); MS (EI): *m/z* (%) = 28 (45), 41 (73), 57 (100), 69 (96), 82 (20), 169 (62) . HRMS (ESI) for $C_{12}H_{19}NO_3$ Calcd 226.1443 $[M + H]^+$; Found 226.1501 $[M + H]^+$.

***tert*-Butyl methacryloyl(2-methylallyl)carbamate (1d)**.

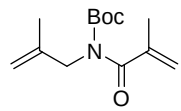

The crude product was purified by chromatography (PE/EtOAc 9:1, Rf = 0.60) to give the final product as a colourless liquid in 91% yield. ^{1}H-NMR (600 MHz, $CDCl_3$): δ 5.18 (br s, 1H, $(CH_3)C=CH_2$), 5.14 (br s, 1H, $(CH_3)C=CH_2$), 4.80 (br s, 1H, $CH_2=C(CH_3)CH_2N$), 4.73 (br s, 1H, $CH_2=C(CH_3)CH_2N$), 4.16 (s, 2H, CH_2), 1.98 (s, 3H, CH_3), 1.70 (s, 3H, CH_3), 1.42 (s, 9H, Boc); ^{13}C-NMR (150 MHz, $CDCl_3$): δ 173.85 (CON), 153.44 (CO Boc), 143.34 (Cq), 140.84 (Cq), 116.05 (CH_2), 110.67 (CH_2), 83.35 (Cq), 49.81 (CH_2), 27.78 (3 x CH_3), 20.42 (CH_3), 19.49 (CH_3); MS: (EI, 70 eV): *m/z* (%) = 41 (49), 57 (100), 69 (84), 183 (94) [M].

General procedure for the synthesis of compounds 1e and 1f.

A solution of the corresponding *N*-allylmethacrylamide (1.00 eq) in THF (20 mL) was cooled to -78 °C, then *n*-BuLi (1.20 eq) was added dropwise. The reaction mixture was stirred for 1h at the same temperature, then, CbzCl (1.00 eq) was added and the reaction mixture was slowly warmed to rt for 3h. The mixture was quenched with aqueous NH_4Cl and extracted CH_2Cl_2 (3 x 20 mL). Then the combined organic layers were dried over Na_2SO_4, filtered and concentrated in reduced pressure. The residue was purified by column chromatography.

Benzyl allyl(methacryloyl)carbamate (1e).

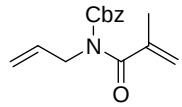

The crude product was purified by chromatography (PE/EtOAc 9:1 v/v, Rf = 0.65) to give the final product as a colourless liquid in 83 % yield. ^{1}H-NMR (600 MHz, $CDCl_3$): δ 7.39 − 7.34 (m, 5H, Ar*H*), 5.86 (ddt, *J* = 17.1 Hz, *J* = 10.3 Hz, *J* = 5.8 Hz, 1H, $CH_2=CHCH_2NCbz$), 5.21 – 5.13 (m, 6H, 2 x $=CH_2$ + CH_2Cbz), 4.31 (dt,

J = 5.8 Hz, *J* = 1.4 Hz, 2H, CH_2=CHC*H*$_2$NCbz), 1.93 – 1.92 (m, 3H, CH_3). ^{13}C-NMR (50.2 MHz, $CDCl_3$): δ 173.88 (CON), 154.58 (CO Cbz), 142.85 (ArC), 134.72 (*C*=CH_2), 132.72 (CH_2=*C*HCH_2NCbz), 128.78 (ArCH), 128.70 (2 x ArCH), 128.66 (2 x ArCH), 117.89 (=CH_2), 116.88 (=CH_2), 68.76 (CH_2Cbz), 47.37 (CH_2), 19.13 (CH_3). HRMS (ESI) for $C_{15}H_{17}NO_3$ Calcd 282.1106 [M + Na]$^+$; Found 282.1152 [M + Na]$^+$.

Benzyl methacryloyl(2-methylallyl)carbamate (1f).

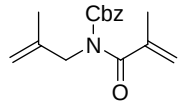

The crude product was purified by chromatography (PE/EtOAc 9:1, Rf = 0.55) to give the final product as colourless liquid in 85% yield. ^{1}H-NMR (200 MHz, $CDCl_3$): δ 7.36 (s, 5H, Ar*H*), 5.21–5.14 (m, 4H, C*H*$_2$Cbz + (CH_3)C=C*H*$_2$), 4.86 – 4.85 (m, 1H, C*H*$_2$=C(CH_3)CH_2NCbz), 4.78–4.77 (m, 1H, C*H*$_2$=C(CH_3)CH_2NCbz), 4.27 (s, 2H, CH_2=C(CH_3)C*H*$_2$NCbz), 1.95 (s, 3H, CH_3), 1.75 (s, 3H, CH_3); ^{13}C-NMR (50.2 MHz, $CDCl_3$): δ 173.63 (CON), 154.78 (CO Cbz), 142.90 (Cq), 140.48 (ArC), 134.78 (Cq), 128.68 (CH), 128.60 (2 x ArCH), 128.56 (2 x ArCH), 116.59 (CH_2), 111.11 (CH_2), 68.83 (CH_2Cbz), 49.89 (CH_2), 20.45 (CH_3), 19.30 (CH_3); MS: (EI, 70 eV): m/z (%) = 69 (12), 91 (100), 144 (8), 169 (4), 273 (1) [M].

Typical metathesis procedure.

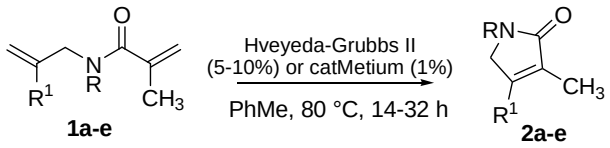

1a-e

R = H
Boc, CBz
R = CH_3
R^1 = H, Me

2a-e

2a: R=Boc, R^1= H
2b: R=Boc, R^1= CH_3
2c: R=Cbz, R^1= H
2d: R=Cbz, R^1= CH_3
2e: R=CH_3, R^1= H

A Schlenk three-neck round-bottom flask was evacuated and filled with N_2. A catalyst (Grubbs II 8% or catMETium-RF1 1%) was added under inert atmosphere; the flask was evacuated and filled again with N_2 (sequence repeated three times). Then a solution of alkyl allyl(methacryloyl)carbamate (1.00 eq.) in dry and degassed toluene (105 mL) was added. The reaction mixture was thoroughly degassed by bubbling N_2 and heated under the conditions described in Table . Then the reaction mixture was filtered through a Celite pad washing with CH_2Cl_2. The solvent was removed in vacuo and purification was carried out by column chromatography.

Entry	R	R^1	Grubbs catalyst	Catalyst load	Time, h	Temp. (°C)	Obtained lactam	Yield[a]
1a	Boc	H	Grubbs II	8 %	18	80	**2a**	83
1a	Boc	H	catMETium	1 %	1.5	110	**2a**	95
1e	Cbz	H	Grubbs II	8 %	16	80	**2c**	76
1e	Cbz	H	catMETium	1 %	1.5	110	**2c**	78
1g	Me	H	catMETium	1 %	1.5	110	**2e**	82
1b	Boc	Me	Grubbs II	8 %	16	80	**2b**	11
1b	Boc	Me	catMETium	1 %	1.5	110	**2b**	48
1f	Cbz	Me	Grubbs II	8 %	16	80	**2d**	15
1f	Cbz	Me	catMETium	1 %	1.5	110	**2d**	58

Table 6. All the reactions have been performed under an inert atmosphere in anhydrous toluene. CatMETium denotes catMETium-RF1. [a]Yield of pure compound.

***tert*-Butyl 3-methyl-2-oxo-2,5-dihydro-1*H*-pyrrole-1-carboxylate (2a).**

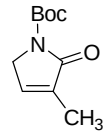

Following the reported procedure **1a** was treated with catMETium-RF1 (1%) at 110 °C for 1.5 h. The crude product was purified by column chromatography (PE/EtOAc 8:2, Rf = 0.07) to give **2a** as a white solid in 95% yield. ^{1}H-NMR (200 MHz, $CDCl_3$): δ 6.74 – 6.72 (m, 1H, vCH), 4.14 – 4.12 (m, 2H, CH_2), 1.82 (s, 3H, CH_3), 1.49 (s, 9H, Boc). Spectral data correspond to those previously reported in the literature.[81]

***tert*-Butyl 3,4-dimethyl-2-oxo-2,5-dihydro-1*H*-pyrrole-1-carboxylate (2b).**

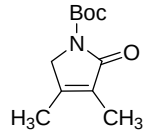

Following the reported procedure **1b** was treated with catMETium-RF1 (1%) at 110 °C for 1.5 h. The crude product was purified by column chromatography (PE/EtOAc 9:1, Rf = 0.66) to give **2b** as a white solid in 48% yield. ^{1}H-NMR (600 MHz, $CDCl_3$): δ 4.08 (s, 2H, CH_2), 1.98 (s, 3H, CH_3), 1.76 (s, 3H, CH_3), 1.53 (s, 9H, Boc); ^{13}C-NMR (150 MHz, $CDCl_3$): δ 170.42 (CON); 149.91 (CO Boc), 149.10 (Cq), 129.03 (Cq), 82.57 (Cq), 52.94 (CH_2), 28.23 (3 × CH_3), 13.41 (CH_3), 8.48 (CH_3); HRMS (ESI) for $C_{11}H_{17}NO_3$ calcd 212.1287 $[M + H]^+$; found 212.2199 $[M + H]^+$.

Benzyl 3-methyl-2-oxo-2,5-dihydro-1*H*-pyrrole-1-carboxylate (2c).

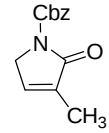

Following the reported procedure **1e** was treated with catMETium-RF1 (1%) at 110 °C for 1.5 h. The crude product was purified by column chromatography (PE/EtOAc 8:2, Rf = 0.21) to give **2c** as a white solid in 78% yield. ^{1}H-NMR (200 MHz, $CDCl_3$): δ 7.41 – 7.18 (m, 5H, Ar*H*), 6.78 – 6.77 (m, 1H, vCH), 5.25 (s, 2H, C*H*$_2$Cbz), 4.20–4.18 (m, 2H, CH_2), 1.83–1.82 (m, 3H, CH_3); ^{13}C-NMR (50.2 MHz, $CDCl_3$): δ 169.64 (CON), 151.16 (CO Cbz), 138.52 (CH), 135.46 (Cq + ArC), 128.67 (2 x ArCH), 128.42 (ArCH), 128.16 (2 x ArCH), 67.96 (CH_2Cbz), 49.39 (CH_2), 11.10 (CH_3); HRMS (ESI) for $C_{11}H_{17}NO_3$ calcd 254.0793 $[M + Na]^+$; found 254.0856 $[M + Na]^+$.

Benzyl 3,4-dimethyl-2-oxo-2,5-dihydro-1*H*-pyrrole-1-carboxylate (2d).

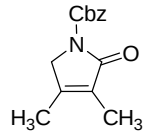

Following the reported procedure **1f** was treated with catMETium-RF1 (1%) at 110 °C for 1.5 h. The crude product was purified by column (PE/EtOAc 1:1, Rf = 0.48) to give **2d** as a white solid in 58 % yield. Mp 105.9 – 107.5 °C. ^{1}H-NMR (200 MHz, $CDCl_3$): δ 7.47 – 7.30 (m, 5H, Ar*H*), 5.31 (s, 2H, C*H*$_2$Cbz), 4.16 – 4.15 (m, 2H, CH_2), 1.99 (s, 3H, CH_3), 1.80–1.78 (m, 3H, CH_3); ^{13}C-NMR (50.2 MHz, $CDCl_3$): δ 169.98 (CON), 150.88 (CO Cbz), 149.85 (Cq), 135.53 (Cq), 128.68 (ArC), 128.54 (2 x ArCH), 128.25 (ArCH), 128.01 (2ArCH), 67.67 (CH_2Cbz), 52.72 (CH_2), 13.34 (CH_3), 8.34 (CH_3); HRMS (ESI) for $C_{14}H_{15}NO_3$ calcd 268.0950 $[M + Na]^+$; found 268.1002 $[M + Na]^+$.

1,3-Dimethyl-1,5-dihydro-2*H*-pyrrol-2-one (2e).

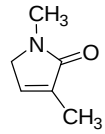

Following the typical procedure **1g** was treated with catMETium-RF1 (1%) at 110 °C for 1.5 h. The crude product was purified by column chromatography (PE/EtOAc 8:2, Rf = 0.13) to give **2e** as a pale yellow liquid in 82 % yield. ^{1}H-NMR (200 MHz, $CDCl_3$): δ 6.52 – 6.50 (m, 1H, CH), 3.69 – 3.67 (m, 2H, CH_2), 2.89 (s, 3H, NCH_3), 1.75 – 1.72 (m, 3H, CH_3). Spectral data were in agreement with literature values.[80]

Allylic bromination of lactams 2a-e: general method.

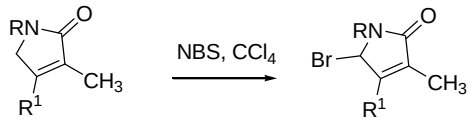

2a-e

2a: R=Boc, R^1= H
2b: R=Boc, R^1= CH_3
2c: R=Cbz, R^1= H
2d: R=Cbz, R^1= CH_3
2e: R=CH_3, R^1= H

3a-e

3a: R=Boc, R^1= H
3b: R=Boc, R^1= CH_3
3c: R=Cbz, R^1= H
3d: R=Cbz, R^1= CH_3
3e: R=CH_3, R^1= H

In a round bottom flask, a solution of lactam **2a-e** (1.00 eq.) in anhydrous CCl_4 (21 mL) was added under a N_2 atmosphere. Then NBS (1.00 eq.), previously recrystallized from water, and AIBN (2%) were added and the mixture was stirred at 90 °C overnight. When TLC analyses showed no further reaction, the mixture was quenched with water and the aqueous phase was extracted with CH_2Cl_2 (3 × 15 mL). Drying (Na_2SO_4) and concentration under low pressure gave a crude product which was purified by column chromatography.

***tert*-Butyl 5-bromo-3-methyl-2-oxo-2,5-dihydro-1*H*-pyrrole-1- carboxylate (3a).**

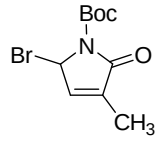

The crude product was purified by column chromatography (PE/EtOAc 7:3, Rf = 0.54) to give **3a** as a pale yellow solid in 82% yield. ^{1}H-NMR (200 MHz, $CDCl_3$): δ 6.83 – 6.82 (m, 1H, C*H*Br), 6.38 – 6.35 (m, 1H, C*H*vCH_2), 1.88 (s, 3H, CH_3), 1.51 (s, 9H, Boc). Spectral data were in agreement with literature values.[81]

***tert*-Butyl 2-bromo-3,4-dimethyl-5-oxo-2,5-dihydro-1*H*-pyrrole-1-carboxylate (3b).**

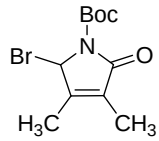

The crude product was purified by column chromatography (PE/EtOAc 7:3, Rf = 0.73) to give **3b** as a yellow solid in 71% yield. ^{1}H-NMR (600 MHz, $CDCl_3$): δ 6.26 (s, 1H, C*H*Br), 2.05 (s, 3H, CH_3), 1.77 (s, 3H, CH_3), 1.52 (s, 9H, Boc); ^{13}C-NMR (150 MHz, $CDCl_3$): δ 167.13 (CON), 150.42 (CO Boc), 147.38 (Cq), 129.47 (Cq), 83.78 (CqBr), 62.30 (CH), 27.78 (3 × CH_3), 12.51 (CH_3), 8.47 (CH_3). HRMS (ESI) for $C_{10}H_{14}BrNO_3$ calcd $[M + Na]^+$ 298.0055 (100.0%), 300.0034 (97.3%); found $[M + Na]^+$ 297.9975 (100%), 299.9954 (97.3%).

Benzyl 5-bromo-3-methyl-2-oxo-2,5-dihydro-1*H*-pyrrole-1-carboxylate (3c).

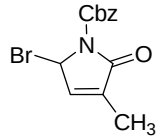

The crude product was purified by column chromatography (PE/EtOAc 8:2, Rf = 0.41) to give **3c** as a pale yellow oil in 58% yield. ^{1}H-NMR (200 MHz, $CDCl_3$): δ 7.51 – 7.33 (m, 5H, Ar*H*), 6.94 – 6.92 (m, 1H, C*H*Br), 6.50 – 6.48 (m, 1H, C*H*vCCH_3), 5.46 – 5.32 (m, 2H, CH_2Cbz), 1.97–1.96 (m, 3H, CH_3); ^{13}C-NMR (150 MHz, $CDCl_3$): δ 166.67 (CON), 149.31 (CO Cbz), 141.31 (*C*HvCCH_3), 134.84 (CHv*C*CH_3), 134.55 (ArC), 128.67 (2 x ArCH), 128.57 (ArCH), 128.22 (2 x ArCH), 68.75 (CH_2Cbz), 57.30 (CHBr), 10.79 (CH_3). HRMS (ESI) for $C_{13}H_{12}BrNO_3$ calcd $[M + Na]^+$ 331.9898 (100.0%), 333.9878 (97.3%); found $[M + Na]^+$ 332.0000 (100%), 333.9980 (97.3%).

Benzyl 2-bromo-3,4-dimethyl-5-oxo-2,5-dihydro-1*H*-pyrrole-1-carboxylate (3d).

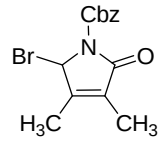

The crude product was purified by column chromatography (PE/EtOAc 7:3, Rf = 0.81) to give **3d** as a pale yellow oil in 54% yield. ^{1}H-NMR (600 MHz, $CDCl_3$): δ 7.36 – 7.34 (m, 2H, Ar*H*), 7.26 – 7.18 (m, 3H, Ar*H*), 6.25 – 6.24 (m, 1H, C*H*Br), 5.25 (d, *J* = 12.4 Hz, 1H, CH_2Cbz), 5.19 (d, *J* = 12.5 Hz, 1H, CH_2Cbz), 1.96 (s, 3H, CH_3), 1.70 (s, 3H, CH_3); ^{13}C-NMR (150 MHz, $CDCl_3$): δ 166.46 (CON), 151.25 (CO Cbz), 148.79 (BrCH*C*vCCH_3), 134.63 (ArC), 128.96 (ArCH), 128.18 (2 x ArCH), 128.00 (2 x ArCH), 127.65 (BrCHCv*C*CH_3), 67.98 (CH_2Cbz), 61.83 (CHBr), 12.39 (CH_3), 8.33 (CH_3). HRMS (ESI) for $C_{14}H_{14}BrNO_3$ calcd $[M + K]^+$ 361.9794 (100.0%), 363.9774 (97.3%); found $[M + K]^+$ 361.9892 (100%), 363.9872 (97.3%).

General procedure for the synthesis of 5a/5a′, 5b/5b′.

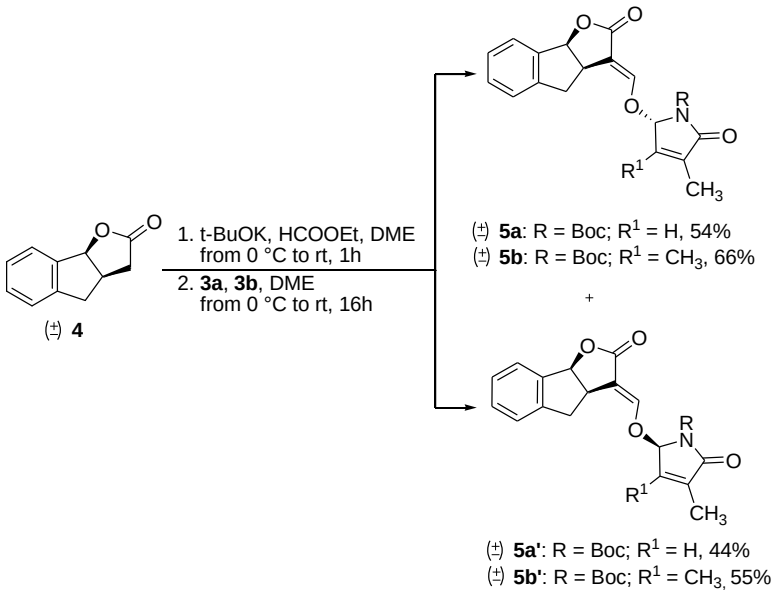

To a solution of the ABC-framework **±4** (1.00 eq, 0.470 mmol, 82 mg) in anhydrous DME (15 mL), cooled to 0 °C and under a nitrogen atmosphere anhydrous ethyl formate (10.0 eq, 4.70 mmol, 0.40 mL) and sublimated *t*-BuOK (2.00 eq, 0.94 mmol, 105.3 mg) were added. The reaction mixture was stirred at room temperature until a TLC control (PE/EtOAc 6 : 4) showed the disappearance of the starting material. After complete consumption of the substrate (2 h), the reaction mixture was cooled to 0 °C and a solution of the suitable brominated lactam **3a**/**3b** (1.70 eq) in anhydrous DME (10 mL) was added dropwise. The reaction mixture turned brown and was stirred at room temperature under a N_2 atmosphere overnight. Then the reaction was quenched by addition of water and the aqueous layer was extracted with CH_2Cl_2 (3 × 20 mL). The combined organic layers were dried over Na_2SO_4, filtered and concentrated under vacuum. The crude product was purified by flash chromatography (PE/EtOAc 3:2, 0.3% Et_3N) to give the two diastereomeric compounds GR24-N-Boc-D-lactams D1 **5a** or **5b** and GR24-N-Boc-D-lactams D2 **5a′**or **5b′**, all as white powders.

***tert*-Butyl-3-methyl-2-oxo-5-((*E*)-(2-oxo-4,8b-dihydro-2*H*-indeno [1,2-*b*]furan-3(3a*H*)-ylidene) methoxy)-2,5-dihydro-1*H*-pyrrole-1-carboxylate (±5a).**

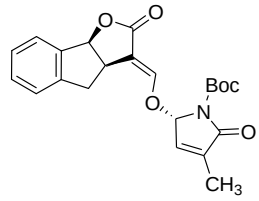

The product was obtained as a white solid in 54% yield. Mp 176.7 °C – 178.0 °C. TLC Rf = 0.62 (PE/EtOAc 1 : 1 v/v); ^{1}H-NMR (200 MHz, $CDCl_3$): δ 7.53 – 7.48 (m, 2H, Ar*H*), 7.37 – 7.20 (m, 4H, Ar*H* + $H_{6'}$), 6.66 – 6.64 (m, 1H, $H_{3'}$), 6.09 – 6.08 (m, 1H, $H_{2'}$), 5.96 (d, *J* = 7.9 Hz, 1H, H_{8b}), 3.97 – 3.86 (m, 1H, H_{3a}), 3.42 (dd, *J* = 16.9 Hz, *J* = 9.2 Hz, 1H, H_4), 3.08 (dd, *J* = 17.0 Hz, *J* = 3.0 Hz, 1H, H_4), 1.99 – 198 (m, 3H, CH_3), 1.56 (s, 9H, Boc); ^{13}C-NMR (50.2 MHz, $CDCl_3$): δ 172.47 (CON), 168.33 (COO), 153.3 (6′CH), 148.82 (CO Boc), 143.25 (ArC), 139.76 (ArC), 139.07 (4′Cq), 136.62 (3′CH), 130.68 (ArCH), 128.18 (ArCH), 127.15 (ArCH), 125.92 (ArCH), 110.60 (3Cq), 90.15 (2′CH), 86.45 (8bCH), 85.37 (Cq Boc), 39.61 (3aCH), 38.08 ($4CH_2$), 28.73 (3 × CH_3), 11.55 (CH_3). HRMS (ESI) for $C_{22}H_{23}NO_6$ calcd 436.1157 $[M + K]^+$; found 436.1170 $[M + K]^+$.

***tert*-Butyl 3-methyl-2-oxo-5-((*E*)-(2-oxo-4,8b-dihydro-2*H*-indeno[1,2-*b*]furan-3(3a*H*)-ylidene)methoxy)-2,5-dihydro-1*H*-pyrrole-1-carboxylate (±5a′).**

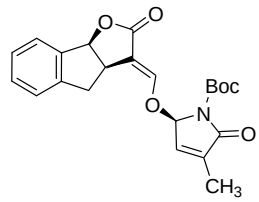

The product was obtained as a white solid in 44% yield. Mp 170.6 °C – 173.2 °C. TLC Rf = 0.40 (PE/EtOAc 1 : 1 v/v); ^{1}H-NMR (200 MHz, $CDCl_3$): δ 7.49 – 7.42 (m, 2H, ArH), 7.29 – 7.11 (m, 4H, Ar*H* + $H_{6'}$), 6.61 (br s, 1H, $H_{3'}$), 6.00 (br s, 1H,

$H_{2'}$), 5.88 (d, *J* = 7.9 Hz, 1H, H_{8b}), 3.89 – 3.78 (m, 1H, H_{3a}), 3.32 (dd, *J* = 16.9 Hz, *J* = 9.2 Hz, 1H, H_4), 2.97 (dd, *J* = 17.0 Hz, *J* = 3.0 Hz, 1H, H_4), 1.91 (s, 3H, CH_3), 1.39 (s, 9H, Boc); ^{13}C-NMR (50.2 MHz, $CDCl_3$): δ 171.83 (CON), 167.70 (COO), 154.24 (6′CH), 148.18 (CO Boc), 142.62 (ArC), 139.12 (ArC), 138.44 (4′Cq), 135.98 (3′CH), 130.04 (ArCH), 127.54 (ArCH), 126.51 (ArCH), 125.29 (ArCH), 110.09 (3Cq), 89.52 (2′CH), 85.82 (8bCH), 84.74 (Cq Boc), 38.97 (3aCH), 37.45 ($4CH_2$), 28.09 (3 × CH_3), 10.92 (CH_3). HRMS (ESI) for $C_{22}H_{23}NO_6$ calcd 436.1157 $[M + K]^+$; found 436.1169 $[M + K]^+$.

***tert*-Butyl 3,4-dimethyl-2-oxo-5-((*E*)-(2-oxo-4,8b-dihydro-2*H*indeno[1,2-*b*] furan -3(3a*H*) -ylidene) methoxy) -2,5- dihydro -1*H*pyrrole -1- carboxylate (±5b).**

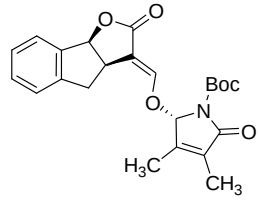

The product was obtained as a white solid in 48% yield. Mp 185.6 °C – 187.8 °C. TLC Rf 0.62 (PE/EtOAc 1 : 1 v/v); ^{1}H-NMR (600 MHz, $CDCl_3$): δ 7.53 – 7.52 (m, 1H, $H_{6'}$), 7.48 – 7.47 (m, 1H, Ar*H*), 7.31 – 7.19 (m, 3H, Ar*H*), 5.93 (d, *J* = 7.9 Hz, 1H, H_{8b}), 5.88 (br s, 1H, $H_{2'}$), 3.93 – 3.89 (m, 1H, H_{3a}), 3.42 (dd, *J* = 16.8Hz, *J* = 9.2 Hz, 1H, H_4), 3.05 (dd, *J* = 16.8 Hz, *J* = 2.9 Hz, 1H, H_4), 1.95 (s, 3H, CH_3), 1.85 (s, 3H, CH_3), 1.53 (s, 9H, Boc); ^{13}C-NMR (150 MHz, $CDCl_3$): δ 171.82 (CON), 167.88 (COO), 153.65 (6′CH), 148.35 (CO Boc), 146.54 (ArC), 142.63 (ArC), 139.12 (3′Cq), 131.78 (4′Cq), 130.01 (ArCH), 127.54 (ArCH), 126.55 (ArCH), 125.15 (ArCH), 110.38 (3Cq), 91.20 (2′CH), 85.79 (8bCH), 84.33 (Cq Boc), 38.93 (3aCH), 37.61 (CH_2), 28.17 (3 × CH_3), 11.72 (CH_3), 8.57 (CH_3).

HRMS (ESI) for $C_{23}H_{25}NO_6$ calcd 434.1580 $[M + Na]^+$; found 434.1689 $[M + Na]^+$.

tert-Butyl 3,4-dimethyl-2-oxo-5-((*E*)-(2-oxo-4,8b-dihydro-2*H*indeno[1,2-*b*] furan-3 (3a*H*) -ylidene) methoxy) -2,5-dihydro-1*H*pyrrole-1-carboxylate (±5b′).

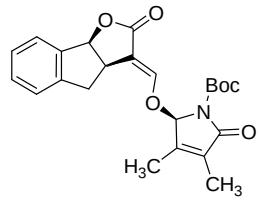

The product was obtained as a white solid in 42% yield. Mp 170.0 °C – 172.4 °C. TLC Rf = 0.55 (PE/EtOAc 1 : 1 v/v); ^{1}H-NMR (600 MHz, $CDCl_3$): δ 7.55 – 7.54 (m, 1H, $H_{6'}$), 7.48 – 7.47 (m, 1H, Ar*H*), 7.31 – 7.17 (m, 3H, Ar*H*), 5.94 (d, *J* = 7.9 Hz, 1H, H_{8b}), 5.83 (br s, 1H, $H_{2'}$), 3.92 – 3.88 (m, 1H, H_{3a}), 3.37 (dd, *J* = 16.8 Hz, *J* = 9.2 Hz, 1H, H_4), 3.02 (dd, *J* = 16.8 Hz, *J* = 2.9 Hz, 1H, H_4), 1.96 (s, 3H, CH_3), 1.85 (s, 3H, CH_3), 1.43 (s, 9H, Boc); ^{13}C-NMR (150 MHz, $CDCl_3$): δ 171.88 (CON), 167.05 (COO), 154.57 (6′CH), 148.23 (CO Boc), 146.70 (ArC), 142.59 (ArC), 139.09 (3′Cq), 131.54 (4′Cq), 130.05 (ArCH), 127.55 (ArCH), 126.51 (ArCH), 125.29 (ArCH), 110.04 (3Cq), 91.96 (2′CH), 85.83 (8bCH), 84.45 (Cq Boc), 38.96 (3a CH), 37.50 (CH_2), 28.11 (3 × CH_3), 11.73 (CH_3), 8.56 (CH_3). HRMS (ESI) for $C_{23}H_{25}NO_6$ calcd 434.1580 $[M + Na]^+$; found 434.1726 $[M + Na]^+$.

General procedure for the synthesis of 5c/5c′ and 5d/5d′.

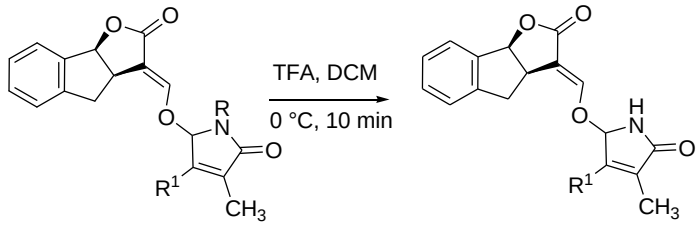

(±) **5a/a'**: R = Boc; R^1 = H
(±) **5b/b'**: R = Boc; R^1 = CH_3
(±) **5c/c'**: R^1 = H
(±) **5d/d'**: R^1 = CH_3

In a round bottom flask an anhydrous solution of the corresponding GR24-N-Boc-lactam D1 (**5a**, **5b**) or D2 (**5a′**, **5b′**) (1.00 eq.) in 2.00 ml of CH_2Cl_2 was prepared. The solution was then cooled to 0 °C and TFA (19.00 eq.) was added. The mixture was stirred at 0 °C with monitoring by TLC (PE/EtOAc 1:1). After 15 min, TFA and CH_2Cl_2 were immediately removed under reduced pressure. The crude product was purified by column chromatography on silica gel.

3-Methyl-5- ((*E*) - (2-oxo-4,8b-dihydro-2*H*-indeno [1,2-*b*] furan-3 (3a*H*)-ylidene)methoxy)-1,5-dihydro-2*H*-pyrrol-2-one (±5c).

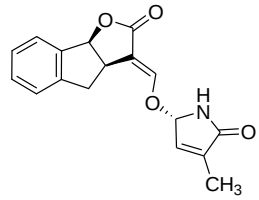

The crude was purified by column chromatography (PE/EtOAc 1:1, Rf = 0.30) to give the final product as a white solid in 24% yield. ^{1}H-NMR (600 MHz, $CDCl_3$): δ 7.50 – 7.49 (m, 1H, Ar*H*), 7.41 (br s, 1H, $H_{6'}$), 7.33 – 7.32 (m, 1H, Ar*H*), 7.28 – 7.27 (m, 1H, Ar*H*), 7.24 – 7.23 (m, 1H, Ar*H*), 6.62 (br s, 1H, $H_{3'}$), 5.94 (d, *J* = 7.9 Hz, 1H, H_{8b}), 5.86 (br s, 1H, $H_{2'}$), 3.94 – 3.90 (m, 1H, H_{3a}), 3.43 (dd, *J* = 16.8 Hz, *J* = 9.2 Hz, 1H, H_4), 3.10 (dd, *J* = 16.8 Hz, *J* = 2.9 Hz, 1H, H_4), 1.96 (s, 3H, CH_3); ^{13}C-NMR (150 MHz, $CDCl_3$): δ 172.87 (CON), 172.14 (COO), 150.79 (6′CH),

142.81 (ArC), 140.00 (ArC), 139.11 (4′Cq), 136.90 (3′CH), 130.09 (ArCH), 127.58 (ArCH), 126.56 (ArCH), 125.32 (ArCH), 111.60 (3Cq), 85.99 (2′CH), 85.67 (8bCH), 39.04 (3aCH), 37.59 ($4CH_2$), 10.81 (CH_3). HRMS (ESI) for $C_{17}H_{15}NO_4$ calcd 336.0633 $[M + K]^+$; found 336.0642 $[M + K]^+$.

3-Methyl-5- ((*E*) - (2-oxo-4,8b-dihydro-2*H*-indeno [1,2-*b*] furan-3 (3a*H*)-ylidene)methoxy)-1,5-dihydro-2*H*-pyrrol-2-one (±5c′).

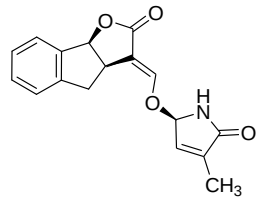

The crude was purified by column chromatography (PE/EtOAc 1:1, Rf = 0.26) to give the final product as a white solid in 22% yield. ^{1}H-NMR (600 MHz, $CDCl_3$): δ 7.49 – 7.47 (m, 1H, Ar*H*), 7.39 (br s, 1H, $H_{6'}$), 7.32 – 7.31 (m, 1H, Ar*H*), 7.27 – 7.26 (m, 1H, Ar*H*), 7.23 – 7.22 (m, 1H, Ar*H*), 6.60 (br s, 1H, $H_{3'}$), 5.93 (d, *J* = 8.0 Hz, 1H, H_{8b}), 5.84 (br s, 1H, $H_{2'}$), 3.93 – 3.90 (m, 1H, H_{3a}), 3.41 (dd, *J* = 16.6 Hz, J = 9.0 Hz, 1H, H_4), 3.10 (dd, *J* = 16.8 Hz, *J* = 3.0 Hz, 1H, H_4), 1.95 (s, 3H, CH_3); ^{13}C-NMR (150 MHz, $CDCl_3$): δ 172.89 (CON), 172.16 (COO), 150.78 (6′CH), 142.83 (ArC), 139.99 (ArC), 139.13 (4′Cq), 136.92 (3′CH), 130.11 (ArCH), 127.60 (ArCH), 126.57 (ArCH), 125.34 (ArCH), 111.61 (3Cq), 86.00 (2′CH), 85.69 (8bCH), 39.05 (3aCH), 37.61 ($4CH_2$), 10.83 (CH_3). HRMS (ESI) for $C_{17}H_{15}NO_4$ calcd 336.0633 $[M + K]^+$; found 336.0649 $[M + K]^+$.

(3,4-Dimethyl-5- ((*E*) -2-oxo- 4,8b-dihydro-2*H*-indeno [1,2-*b*] furan-3 (3a*H*)-ylidene)methoxy)-1,5-dihydro-2*H*-pyrrol-2-one (±5d).

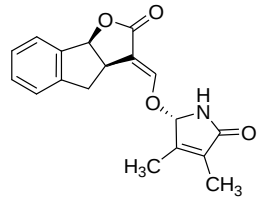

The crude was purified by column chromatography (DCM/EtOAc 4 : 1, Rf = 0.21) to give the final product as a white solid in 21% yield. ^{1}H-NMR (600 MHz, $CDCl_3$): δ 7.50 (d, *J* = 7.5 Hz, 1H, Ar*H*), 7.35 (d, *J* = 2.4 Hz, 1H, $H_{6'}$), 7.33 (d, *J* = 6.6 Hz, 1H, Ar*H*), 7.28 (d, *J* = 7.5 Hz, 1H, Ar*H*), 7.24 (d, *J* = 7.5 Hz, 1H, Ar*H*), 6.70 (s, 1H, NH), 5.95 (d, *J* = 7.9 Hz, 1H, H_{8b}), 5.65 (s, 1H, $H_{2'}$), 3.96 – 3.93 (m, 1H, H_{3a}), 3.45 (dd, *J* = 16.8 Hz, *J* = 9.2 Hz, 1H, H_4), 3.12 (dd, *J* = 16.8 Hz, *J* = 3.0 Hz, 1H, H_4), 1.95 (s, 3H, CH_3), 1.86 (s, 3H, CH_3); ^{13}C-NMR (150 MHz, $CDCl_3$): δ 173.42 (CON), 172.01 (COO), 150.47 (6′CH), 147.23 (ArC), 142.71 (ArC), 139.08 (3′Cq), 132.62 (4′Cq), 130.04 (ArCH), 127.55 (ArCH), 126.53 (ArCH), 125.24 (ArCH), 110.60 (3Cq), 87.89 (2′CH), 85.88 (8bCH), 38.98 (3aCH), 37.51 (CH_2), 11.64 (CH_3), 8.44 (CH_3). HRMS (ESI) for $C_{18}H_{17}NO_4$ calcd 334.1055 [M + Na]$^+$; found 334.1132 [M + Na]$^+$.

(3,4-Dimethyl-5- ((*E*)-2-oxo-4,8b-dihydro-2*H*-indeno [1,2-*b*] furan-3 (3a*H*)-ylidene)methoxy)-1,5-dihydro-2*H*-pyrrol-2-one (±5d′).

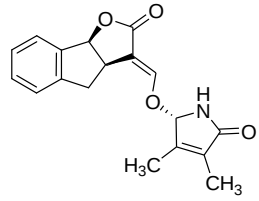

The crude was purified by column chromatography (DCM/ EtOAc 4 : 1, Rf = 0.17) to give the final product as a white solid in 25% yield. ^{1}H-NMR (600 MHz,

$CDCl_3$): δ 7.48 (d, *J* = 7.4 Hz, 1H, Ar*H*), 7.34 (d, *J* = 2.5 Hz, 1H, $H_{6'}$), 7.31 (d, *J* = 6.4 Hz, 1H, Ar*H*), 7.27 (d, *J* = 7.5 Hz, 1H, Ar*H*), 7.22 (d, *J* = 7.5 Hz, 1H, Ar*H*), 6.69 (s, 1H, NH), 5.93 (d, *J* = 8.0 Hz, 1H, H_{8b}), 5.64 (s, 1H, $H_{2'}$), 3.95–3.91 (m, 1H, H_{3a}), 3.43 (dd, *J* = 16.9 Hz, *J* = 9.2 Hz, 1H, H_4), 3.11 (dd, *J* = 17.0 Hz, *J* = 3.0 Hz, 1H, H_4), 1.95 (s, 3H, CH_3), 1.84 (s, 3H, CH_3); ^{13}C-NMR (150 MHz, $CDCl_3$): δ 173.48 (CON), 172.06 (COO), 150.52 (6′CH), 147.29 (ArC), 142.77 (ArC), 139.09 (3′Cq), 132.68 (4′Cq), 130.09 (ArCH), 127.60 (ArCH), 126.58 (ArCH), 125.30 (ArCH), 111.65 (3Cq), 87.94 (2′CH), 85.93 (8bCH), 39.04 (3aCH), 37.56 (CH_2), 11.70 (CH_3), 8.49 (CH_3). HRMS (ESI) for $C_{18}H_{17}NO_4$ calcd 334.1055 [M + Na]$^+$; found 334.1148 [M + Na]$^+$.

***tert*-Butyl (*E*) -3-methyl-5-((4-methyl-3-oxo-3,4-dihydrocyclopenta [*b*] indol-2(1*H*)-ylidene)methoxy)-2-oxo-2,5-dihydro-1*H*-pyrrole-1-carboxylate (±5e).**

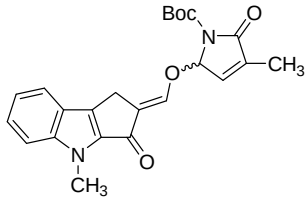

To a solution of the ABC-framework **6**[46] (1.00 eq, 0.498 mmol, 92.0 mg) in anhydrous ethyl formate (10.0 mL), cooled to 0 °C and under a nitrogen atmosphere, were added sublimated *t*-BuOK (3.00 eq, 1.49 mmol, 167 mg). The pink reaction mixture was stirred at room temperature with monitoring using TLC (PE/EtOAc, 3:2). After complete consumption of the substrate (1 h), the solvent was removed under nitrogen stream leaving a solid residue to which, after cooling to 0 °C, a solution of the suitable brominated lactam **3a** (1.70 eq, 0.847 mmol, 234 mg) in anhydrous DME (10.0 mL) was added. The resulting pale brown mixture was stirred at room temperature overnight. Then it was quenched by the addition of water (10.0 mL) and extracted with CH_2Cl_2 (3 × 10 mL). The combined organic

layers were dried over Na_2SO_4, filtered and concentrated under vacuum. The crude product was purified by column chromatography on silica gel with PE/EtOAc 1:1 to give **5e** as a pale yellow solid in 44% yield (89 mg). TLC Rf = 0.40 (PE/EtOAc 1:1); ^{1}H-NMR (200 MHz, $CDCl_3$): δ 7.68 (dt, *J* = 8.11 Hz, 1H, Ar*H*), 7.51 – 7.50 (m, 1H, Ar*H*), 7.41 – 7.38 (m, 2H, Ar*H* + $H_{6'}$), 7.22 – 7.14 (m, 1H, Ar*H*), 6.70 – 6.66 (m, 1H, $H_{3'}$), 6.11 – 6.10 (m, 1H, $H_{2'}$), 3.97 (s, 3H, NCH_3), 3.57 (s, 2H, CH_2), 1.99 – 1.97 (m, 3H, vCCH_3), 1.54 (s, 9H, Boc); ^{13}C-NMR (50.2 MHz, $CDCl_3$): δ 183.64 (CO), 167.93 (CON), 148.66 (6′CH), 148.27 (CO Boc), 144.53 (ArC), 141.03 (ArC), 138.25 (4′Cq), 136.77 (Cq), 136.42 (3′CH), 126.56 (ArCH), 122.96 (Cq), 121.75 (ArCH), 121.69 (Cq), 120.51 (ArCH), 111.00 (ArCH), 88.76 (2′CH), 84.46 (CqBoc), 30.40 (NCH_3), 28.22 (3 × CH_3), 22.57 (CH_2), 10.96 (CH_3). HRMS (ESI) for $C_{23}H_{24}N_2O_5$ calcd 431.1583 $[M + Na]^+$; found 431.1570 $[M + Na]^+$.

General procedure for the synthesis of ±5f and ±5g.

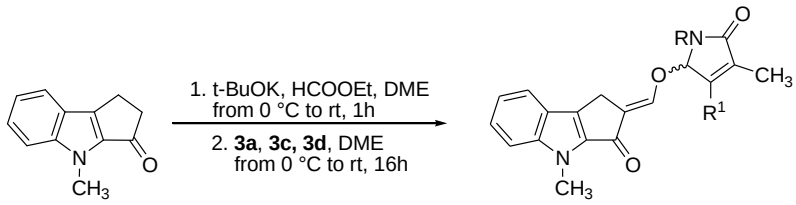

6

(±) **5e**: R = Boc; R^1 = H, 44%
(±) **5f**: R = Cbz; R^1 = H, 55%
(±) **5g**: R = Cbz; R^1 = CH_3, 55%

To a solution of ±**6**[46] (1.00 eq., 0.470 mmol, 82 mg) in anhydrous DME (10 mL), cooled to 0 °C and under a nitrogen atmosphere anhydrous ethyl formate (10.0 eq, 4.70 mmol, 0.40 mL) and sublimated *t*-BuOK (2.00 eq, 0.94 mmol, 105.3 mg) were added. The pink reaction mixture was stirred at room temperature until a TLC control (PE/EtOAc 6:4) showed the disappearance of the starting material. After complete consumption of the substrate (2 h), the reaction mixture was cooled to 0 °C and a solution of the suitable brominated lactam **3c**/**3d** (1.70 eq) in

anhydrous DME (5 mL) was added dropwise. The reaction mixture turned pale orange and it was stirred at room temperature under a N_2 atmosphere overnight. The reaction was quenched by the addition of water and the aqueous layer was extracted with CH_2Cl_2 (3 × 20 mL). The combined organic layers were dried over Na_2SO_4, filtered and concentrated under vacuum. The crude product was purified by flash chromatography.

Benzyl (*E*)-3-methyl-5- ((4-methyl-3-oxo-3,4-dihydrocyclopenta [*b*] indol-2(1*H*)-ylidene)methoxy)-2-oxo-2,5-dihydro-1*H*-pyrrole- 1-carboxylate (±5f).

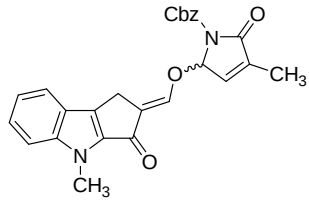

The crude was purified by column chromatography (PE/EtOAc 1:1, Rf = 0.23) to give the final product as a pale yellow solid in 55% yield. ^{1}H-NMR (600 MHz, $CDCl_3$): δ 7.67 (d, *J* = 8.0 Hz, 1H, Ar*H*), 7.46 (s, 1H, $H_{6'}$), 7.42 – 7.37 (m, 5H, Ar*H*), 7.27 – 7.25 (m, 2H, Ar*H*), 7.21 – 7.17 (m, 2H, Ar*H*), 6.72 (s, 1H, $H_{3'}$), 6.17 (s, 1H, $H_{2'}$), 5.39 (d, *J* = 12.2 Hz, 1H, CH_2 Cbz), 5.24 (d, *J* = 12.2 Hz, 1H, CH_2 Cbz), 3.97 (s, 3H, NCH_3), 3.50 – 3.42 (m, 2H, CH_2), 1.99 (s, 3H, CH_3); ^{13}C-NMR (150 MHz, $CDCl_3$): δ 183.60 (CO), 167.38 (CON), 149.99 (CO Cbz), 147.63 (6′CH), 144.51 (Cq), 138.23 (ArC), 137.04 (3′CH), 136.81 (Cq), 134.92 (Cq), 128.68 (4′Cq), 128.63 (2 × ArCH), 128.61 (ArCH), 126.52 (2 × ArCH), 122.95 (ArC), 122.34 (Cq), 121.74 (ArCH), 120.47 (ArCH), 110.98 (ArCH), 88.19 (2′CH), 68.58 (CH_2 Cbz), 30.37 (NCH_3), 22.53 (CH_2), 10.98 (CH_3). HRMS (ESI) for $C_{26}H_{22}N_2O_5$ calcd 465.1426 $[M + Na]^+$; found 465.1396 $[M + Na]^+$.

Benzyl (*E*)-3,4-dimethyl-2- ((4-methyl-3-oxo-3,4-dihydrocyclopenta[*b*]indol-2(1*H*)-ylidene) methoxy)-5-oxo-2,5-dihydro-1*H*pyrrole- 1-carboxylate (±5g).

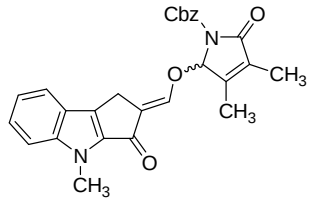

The crude was purified by column chromatography (PE/EtOAc 1:1, Rf = 0.55) to give the final product as a pale yellow solid in 55% yield. Mp 84.3 °C–85.1 °C. ^{1}H-NMR (600 MHz, $CDCl_3$): δ 7.67 (d, *J* = 8.9 Hz, 1H, Ar*H*), 7.45 – 7.37 (m, 5H, Ar*H* + $H_{6'}$), 7.27 – 7.25 (m, 2H, Ar*H*), 7.21 – 7.17 (m, 2H, Ar*H*), 5.95 (s, 1H, $H_{2'}$), 5.38 (d, *J* = 12.2 Hz, 1H, CH_2 Cbz), 5.24 (d, *J* = 12.2 Hz, 1H, CH_2 Cbz), 3.97 (d, *J* = 3.4 Hz, 3H, NCH_3), 3.52 – 3.44 (m, 2H, CH_2), 1.98 (s, 3H, CH_3), 1.88 (s, 3H, CH_3); ^{13}C-NMR (150 MHz, $CDCl_3$): δ 183.57 (CO), 167.72 (CON), 150.06 (CO Cbz), 148.00 (ArC), 147.84 (6′CH), 144.52 (3′Cq), 141.05 (ArC), 136.75 (Cq), 135.03 (Cq), 131.33 (4′Cq), 128.68 (3 × ArCH), 128.58 (2 × ArCH), 126.47 (ArCH), 122.96 (ArC), 122.40 (Cq), 121.73 (ArCH), 120.48 (ArCH), 111.00 (ArCH), 90.51 (2′CH), 68.45 (CH_2 Cbz), 30.37 (NCH_3), 22.58 (CH_2), 11.84 (CH_3), 8.61 (CH_3). HRMS (ESI) for $C_{27}H_{24}N_2O_5$ calcd 479.1583 $[M + Na]^+$; found 479.1594 $[M + Na]^+$.

General procedure for the synthesis of (±5h) and (±5i).

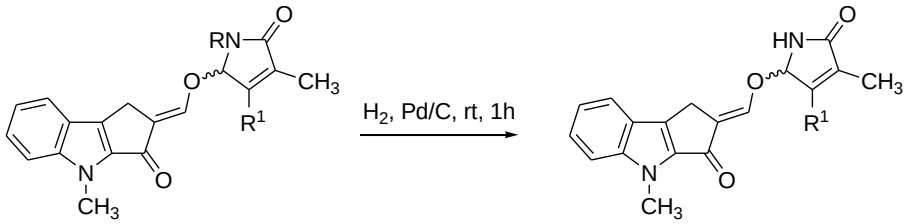

(±) **5e**: R = Boc; R^1 = H, 44%
(±) **5f**: R = Cbz; R^1 = H, 55%
(±) **5g**: R = Cbz; R^1 = CH_3, 55%

(±) **5h**: R^1 = H, 100%
(±) **5i**: R^1 = CH_3,100%

To a solution of compound **±5f** or **±5g** (0.100 mmol) in anhydrous THF (10.0 mL) was added Pd/C 10% (13.0 mg) under a nitrogen atmosphere. The reaction mixture was stirred under a saturated hydrogen atmosphere for 10 min. The mixture was filtered through Celite and the filter was washed with CH_2Cl_2. After evaporation of the solvent the crude product did not require any further purification.

(*E*) -4- Methyl -2- (((4-methyl -5- oxo- 2,5 –dihydro -1*H*- pyrrol-2-yl) oxy) methylene)-1,4-dihydrocyclopenta[*b*]indol-3(2*H*)-one (±5h).

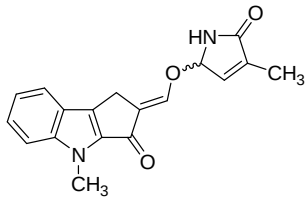

The product was obtained as a pale yellow solid in 100% yield. TLC PE/EtOAc 3:7, Rf = 0.25. ^{1}H-NMR (600 MHz, $CDCl_3$): δ 7.67 (d, *J* = 8.0 Hz, 1H, Ar*H*), 7.41 – 7.35 (m, 2H, Ar*H* + $H_{6'}$), 7.30 (t, *J* = 1.3 Hz, 1H, Ar*H*), 7.17 (ddd, *J* = 8.0 Hz, *J* = 6.8 Hz, *J* = 1.1 Hz, 1H, Ar*H*), 6.50 (s, 1H, NH), 6.42 (s, 1H, $H_{2'}$), 5.86 (s, 1H, $H_{3'}$), 3.95 (s, 3H, NCH_3), 3.60 (s, 2H, CH_2), 1.98 (s, 3H, CH_3); ^{13}C-NMR (150 MHz, $CDCl_3$): δ 183.74 (CO), 173.51 (CON), 147.84 (ArC), 145.30 (6′CH), 137.15 (3′CH), 136.79 (ArC + Cq), 132.27 (4′Cq), 126.55 (ArCH), 123.09 (Cq), 122.93 (Cq), 121.72 (ArCH), 120.48 (ArCH), 110.99 (ArCH), 87.01 (2′CH), 30.35 (NCH_3), 22.60 (CH_2), 10.81 (CH_3). HRMS (ESI) for $C_{18}H_{16}N_2O_3$ calcd 331.1059 $[M + Na]^+$; found 331.1127 $[M + Na]^+$.

(*E*)-2- (((3,4-Dimethyl-5-oxo-2,5-dihydro-1*H*-pyrrol-2-yl) oxy) methylene)-4-methyl-1,4-dihydrocyclopenta[*b*]indol-3(2*H*)-one (±5i).

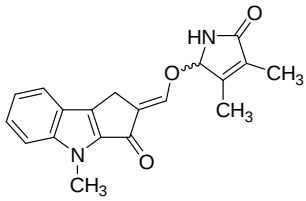

The product was obtained as a pale yellow solid in 100% yield. TLC PE/EtOAc 1:1, Rf = 0.20. ^{1}H-NMR (600 MHz, $CDCl_3$): δ 7.68 (d, *J* = 8.1 Hz, 1H, Ar*H*), 7.42 – 7.37 (m, 2H, ArH + $H_{6'}$), 7.31 (t, *J* = 1.2 Hz, 1H, ArH), 7.18 (ddd, *J* = 8.1 Hz, *J* = 6.7 Hz, *J* = 1.1 Hz, 1H, Ar*H*), 6.53 (s, 1H, NH), 5.66 (s, 1H, $H_{2'}$), 3.96 (s, 3H, NCH_3), 3.60 (s, 2H, CH_2), 1.96 (s, 3H, CH_3), 1.88 (s, 3H, CH_3); ^{13}C-NMR (150 MHz, $CDCl_3$): δ 183.72 (CO), 173.48 (CON), 147.82 (ArC), 145.27 (6′CH), 144.53 (3′Cq), 141.06 (ArC), 136.75 (Cq), 132.28 (4′Cq), 126.54 (ArCH), 123.10 (Cq), 122.94 (Cq), 121.72 (ArCH), 120.47 (ArCH), 111.01 (ArCH), 87.59 (2′CH), 30.38 (NCH_3), 22.69 (CH_2), 11.71 (CH_3), 8.49 (CH_3). HRMS (ESI) for $C_{19}H_{18}N_2O_3$ calcd 361.0954 $[M + K]^+$; found 361.0998 $[M + K]^+$.

Synthesis of 5j and 5k.

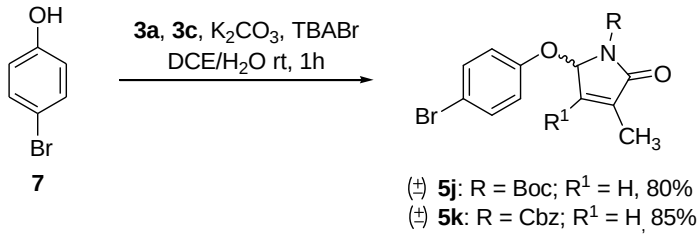

To a solution of a brominated lactam **3a** or **3c** (1.00 eq) in CH_2Cl_2 (1.50 mL) TBABr (1.00 eq), K_2CO_3 (1.20 eq), p-bromophenol (1.00 eq) and water (1.00 mL) were added. The reaction mixture was stirred at room temperature overnight. Then it was quenched with a saturated solution of Na_2CO_3 and the aqueous phase was

extracted with CH_2Cl_2 (3 × 5 mL). The collected organic layers were dried (Na_2SO_4), filtered and evaporated. The crude product was purified by chromatography on silica gel.

***tert*-Butyl 5-(4-bromophenoxy)-3-methyl-2-oxo-2,5-dihydro- 1*H*-pyrrole-1-carboxylate (±5j).**

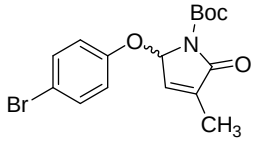

The crude product was purified by column chromatography (PE/EtOAc 4:1, Rf = 0.57) to give **5j** as a white solid in 80% yield. Mp 105.3 – 106.3 °C. ^{1}H-NMR (200 MHz, $CDCl_3$): δ 7.42 (dd, *J* = 2.22 Hz, *J* = 9.05 Hz, 2H, Ar*H*), 6.88 (dd, *J* = 2.22 Hz, *J* = 8.96 Hz, 2H, Ar*H*), 6.74 – 6.71 (m, 1H, $H_{3'}$), 6.27 – 6.26 (m, 1H, $H_{2'}$), 1.93 – 1.91 (m, 3H, CH_3), 1.44 (s, 9H, Boc); ^{13}C-NMR (50.2 MHz, $CDCl_3$): δ 167.91 (CON), 155.62 (CO Boc), 148.28 (ArCO), 137.75 (3′CH), 136.80 (4′Cq), 132.62 (2ArCH), 119.55 (2ArCH), 115.53 (ArCBr), 85.73 (2′ CH), 83.53 (CqBoc), 27.93 (3 × CH_3), 10.79 (CH_3). HRMS (ESI) for $C_{16}H_{18}BrNO_4$ calcd 406.0056 $[M + K]^+$; found 406.0082 $[M + K]^+$.

Benzyl 5-(4-bromophenoxy)-3-methyl-2-oxo-2,5-dihydro-1*H*pyrrole- 1-carboxylate (±5k).

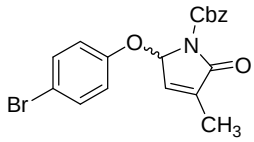

The crude product was purified by column chromatography (PE/EtOAc 4:1, Rf = 0.42) to give **5j** as a white solid in 85% yield. Mp 143.5 – 145.0 °C. ^{1}H-NMR (600 MHz, $CDCl_3$): δ 7.34 (dd, *J* = 2.40 Hz, *J* = 9.00 Hz, 2Ar*H*), 7.32 (s, 5H, Ar*H* Cbz),

6.81 (dd, *J* = 2.40 Hz, *J* = 9.00 Hz, 2Ar*H*), 6.77 – 6.76 (m, 1H, $H_{3'}$), 6.31 – 6.30 (m, 1H, $H_{2'}$), 5.26 (s, 2H, CH_2Cbz), 1.94 – 1.93 (m, 3H, CH_3); ^{13}C-NMR (150 MHz, $CDCl_3$): δ 167.65 (CON), 155.27 (CO Cbz), 150.05 (ArCO), 137.56 (3′CH), 137.42 (4′Cq), 135.00 (ArC), 132.71 (2ArCH), 128.72 (2ArCH), 128.62 (ArCH), 128.40 (2ArCH), 120.00 (2ArCH), 116.04 (ArCBr), 85.91 (2′CH), 68.44 (CH_2Cbz), 10.88 (CH_3). HRMS (ESI) for $C_{19}H_{16}BrNO_4$ calcd 424.0160 [M + Na]$^+$; found 424.0296 [M + Na]$^+$.

5-(4-Bromophenoxy)-3-methyl-1,5-dihydro-2*H*-pyrrol-2-one (±5l).

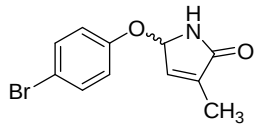

A solution of debranone **±5j** (1.00 eq, 0.375 mmol, 138 mg) in CH_2Cl_2 (2.00 mL) was cooled at 0 °C and after 2 min TFA (19.0 eq, 1.24 mmol, 0.10 mL) was added. The mixture was stirred at 0 °C with monitoring by TLC (PE/EtOAc 4 : 1). After complete consumption of **±5j** (25 min), TFA and CH_2Cl_2 were immediately evaporated under vacuum. The crude product was purified by column chromatography (PE/EtOAc 7:3, Rf = 0.82) to give **±5l** as a white solid (80 mg, 80%). Mp 156 – 157.5 °C. ^{1}H-NMR (600 MHz, $CDCl_3$): δ 7.42 (dd, *J* = 2.22 Hz, *J* = 9.05 Hz, 2Ar*H*), 6.84 (dd, *J* = 2.30 Hz, *J* = 9.05 Hz, 2Ar*H*), 6.72 – 6.70 (m, 1H, $H_{3'}$), 6.58 (br, 1H, NH), 5.92 – 5.91 (m, 1H, $H_{2'}$), 1.93 (s, 3H, CH_3); ^{13}C-NMR (150 MHz, $CDCl_3$): δ 173.02 (CvO), 155.43 (ArCO), 138.45 (3′CH), 137.38 (4′Cq), 132.93 (2ArCH), 118.96 (2ArCH), 115.53 (ArCBr), 82.97 (2′CH), 10.73 (CH_3). HRMS (ESI) for $C_{11}H_{11}BrNO_2$ calcd 267.9973 [M + H]$^+$; found 267.9960 [M + H]$^+$.

Benzyl 3-methyl-5-(4-methyl-3-oxo-1,2,3,4-tetrahydrocyclopenta[*b*]indol-2-yl)-2-oxo-2,5 dihydro-1*H*-pyrrole-1-carboxylate (5m).

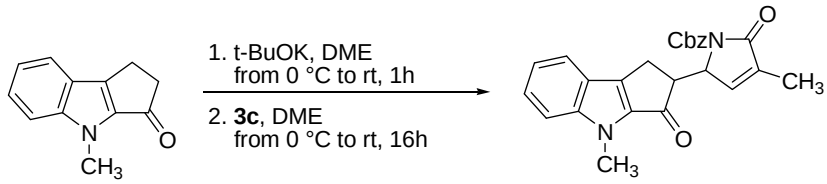

To a solution of **±6**[46] (1.00 eq, 0.60 mmol, 111 mg) in anhydrous DME (15 mL), cooled to 0 °C and under a nitrogen atmosphere sublimated *t*-BuOK (2.00 eq, 1.20 mmol, 134 mg) was added. The reaction mixture was stirred at room temperature until a TLC control (PE/EtOAc 6:4) showed the disappearance of the starting material. After complete consumption of the substrate (1.5 h), the reaction mixture was cooled to 0 °C and a solution of lactam **3c** (1.70 eq, 1.02 mmol, 316 mg) in anhydrous DME (5 mL) was added dropwise. The reaction mixture turned brown and was stirred at room temperature under a N_2 atmosphere overnight. Then the reaction was quenched by the addition of water and the aqueous layer was extracted with CH_2Cl_2 (3 × 20 mL). The combined organic layers were dried over Na_2SO_4, filtered and concentrated under vacuum. The crude product was purified by flash chromatography (PE/EtOAc 1:1, 0.1% Et_3N, Rf = 0.36) to give **5m** as a pale yellow solid (112 mg, 45%). ^{1}H-NMR (600 MHz, $CDCl_3$): δ 7.64 (dt, *J* = 8.1 Hz, *J* = 0.9 Hz, 1H. Ar*H*), 7.45 – 7.42 (m, 1H. Ar*H*), 7.36 – 7.33 (m, 1H, Ar*H*), 7.27 – 7.25 (m, 2H, Ar*H*), 7.20 – 7.14 (m, 4H, Ar*H*), 6.75 – 6.74 (m, 1H, $H_{3'}$), 5.22 – 5.14 (m, 3H, CH_2Cbz and $H_{2'}$), 3.64 – 3.62 (m, 1H, CH_2C*H*CvO), 3.14 (dd, *J* = 16.9 Hz, *J* = 6.9 Hz, 1H, CH_2CHCO), 2.73 (dd, *J* = 16.9 Hz, *J* = 2.6 Hz, 1H, CH_2CHCvO), 1.89 (t, *J* = 1.7 Hz, 3H, CH_3). ^{13}C-NMR (150 MHz, $CDCl_3$): δ 191.80 (CvO), 169.62 (CON), 151.48 (COO Cbz), 145.10 (Cq), 141.65 (3′CH), 138.25 (2 x ArC), 135.78 (ArC), 135.44 (4′Cq), 128.48 (2 x ArCH), 128.14 (ArCH), 127.75 (2 x ArCH), 127.15 (ArCH), 122.97 (Cq), 121.94 (ArCH), 120.59

(ArCH), 111.22 (ArCH), 67.93 (CH_2Cbz), 60.32 (2′CH), 52.44 (CH_2*C*HCO), 30.21 (NCH_3), 21.60 (CH_2), 11.13 (CH_3). HRMS (ESI) for $C_{25}H_{22}N_2O_4$ calcd 437.1477 $[M + Na]^+$; found 437.1594 $[M + Na]^+$.

4-Methyl-2- (4- methyl -5- oxo- 2,5- dihydro -1*H*- pyrrol-2-yl) -1,4-dihydrocyclopenta[*b*]indol-3(2*H*)-one (5n).

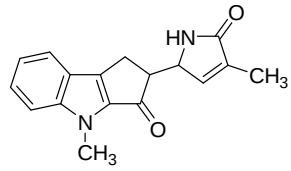

To a solution of the compound **5m** (0.050 mmol, 22.0 mg) in anhydrous THF (5.00 mL) was added Pd/C 10% (6.0 mg) under a nitrogen atmosphere. The reaction mixture was stirred under a saturated hydrogen atmosphere for 2 h. The mixture was filtered through Celite and the filtrate was evaporated to dryness to afford **5n** (32 mg, 100%) as a pale yellow solid. The product did not require any further purification. TLC Rf = 0.11 (PE/ EtOAc 1:1); ^{1}H-NMR (600 MHz, $CDCl_3$): δ 7.63 (d, *J* = 8.1 Hz, 1H, Ar*H*), 7.44 (ddd, *J* = 8.2 Hz, *J* = 7.0 Hz, *J* = 1.1 Hz, 1H, Ar*H*), 7.36 (d, *J* = 8.5 Hz, 1H, Ar*H*), 7.18 – 7.16 (m, 1H, Ar*H*), 6.82 – 6.81 (m, 1H, $H_{3'}$), 5.86 (br, 1H, NH), 4.81 (br, 1H, $H_{2'}$), 3.91 (s, 3H, NCH_3), 3.30 – 3.28 (m, 1H, CH_2C*H*CvO), 2.93 (dd, *J* = 16.8 Hz, *J* = 6.6 Hz, 1H, CH_2CHCO), 2.47 (dd, *J* = 16.8 Hz, *J* = 2.6 Hz, 1H, CH_2CHCO), 1.95 (t, *J* = 1.7 Hz, 3H, CH_3). ^{13}C-NMR (150 MHz, $CDCl_3$): δ 193.28 (CvO), 174.70 (CON), 145.61 (Cq), 144.98 (ArC), 141.79 (3′CH), 136.21 (ArC and 4′Cq), 127.77 (ArCH), 123.01 (Cq), 122.15 (ArCH), 120.73 (ArCH), 111.16 (ArCH), 56.87 (2′CH), 53.84 (CH_2*C*HCO), 30.36 (NCH_3), 20.29 (CH_2), 11.04 (CH_3). HRMS (ESI) for $C_{17}H_{16}N_2O_2$ calcd 303.1109 $[M + Na]^+$; found 303.1210 $[M + Na]^+$.

Modeling. All compounds were docked into the protein binding site with the docking software GOLD, version 5.5 (http://www.ccd.cam.ac.uk). For each compound, 25 diverse poses were generated and analysed. A radius of 10 Å was used to define the pocket extension. Automatic default parameters were set for the Genetic Algorithm. Shape constraints were imposed using as template the structure of GR24 as co-crystallized within the target. ChemScore was used as scoring function. All calculations were performed on a Dell Precision workstation, having two Intel Xeon processors, twelve core, 1 TB 7.2K 6GBPS SAS hard drive, NVidia GTX 980 graphic card, and a Linux operating system centos 7, kernel version 3.10.0- 514.10.2.el7.x86_64. Molecular interaction fields were calculated by FLAP[82] using the DRY probe to describe potential hydrophobic interactions, the sp^2 carbonyl oxygen O and the amide N1 probes for hydrogen-bond donor and acceptor regions, respectively.

X-ray analysis. Colourless crystalline platelets suitable for the analysis of compound **(+)-5a** have been obtained by the slow evaporation of a methanol solution. X-ray diffraction analysis of compound **(+)-5a** was performed at room temperature using an Oxford Diffraction Gemini R-Ultra diffractometer equipped with an Enhanced Ultra Cu X-ray Source (λ = 1.54184 Å). Copper radiation has been chosen to enhance the anomalous scattering of light atoms for a more significant Bijvoet intensity difference and more reliable statistic of the absolute configuration determination.[83] The intensities were corrected for absorption with the numerical correction based on Gaussian integration over a multifaceted crystal model. Software used: CrysAlisPro (Agilent Technologies, Version 1.171.38.43) for data collection, data reduction and absorption correction; SHELXT[84] for structure solution using Direct Methods and ShelXL[84] for refinement through least squares minimization; Mercury[85] for graphics. All non-hydrogen atoms were

anisotropically refined. All the hydrogens have been calculated with a riding atom model. The Flack parameter(x) has been calculated using the SHELX "hole-in-one" post-refinement method[86] and the value of 0.01(8) confirms the absolute configuration reported.[87]

Stability. Compounds were dissolved in methanol to give 1 g/L stock solutions, which were added to buffer solution (10 μL in 1 mL) at 40 °C in HPLC vials for direct measurement of compound loss *versus* time. A Waters HPLC 2695 Alliance system with a Waters 2996 photodiode array were used with a Hichrom reverse-phase column (ACE3 C18, 4.6×100–250 mm) (Hichrom, Reading, UK) and acetonitrile acidified water (0.2% formic acid) mobile phase at a flow rate of 1 mL/min. Peak detection was at the optimum wavelength (230 – 250 nm), and peak areas were used for quantification. Initial and subsequent measurements of peak area attributable to the test compound were used to fit exponential half-lives and calculate first-order rate constants. Stability data ($t_{1/2}$) indicated the time in hours for half of the test compound to be hydrolysed.

Germination activity. Seeds of *Phelipanche aegyptiaca* were collected from field-grown tomato in the West Galilee of Israel. The seeds were stored in glass vials in the dark at room temperature until use in germination tests. Preparation of test solutions: the compound to be tested was weighed out very accurately, dissolved in 1 mL of acetone and then diluted with sterile distilled water to reach the desired concentrations. All solutions were prepared just before use. Seeds were surface-sterilized and preconditioned as published.[45] Briefly, seeds were exposed for 5 min to 50% (v/v) aqueous solutions of commercial bleach (2% hypochlorite) and rinsed with sterile distilled water. For preconditioning, seeds were placed on a glass fibre filter paper disc using a sterile toothpick (approximately 20 seeds per disc); the glass fibre discs were placed on two filter paper discs, wetted with sterile

distilled water, and incubated at 25°C in the dark for 6 d. The preconditioned seeds were then allowed to dry completely in the laminar flow, treated with all the compounds at six different concentrations: 10^{-5} M, 10^{-6} M, 10^{-7} M, 10^{-8} M, 10^{-9} M and 10^{-10} M; their germination rate was evaluated under a stereomicroscope 7 d after the beginning of the treatment. For each concentration, at least 100 seeds were scored; synthetic strigolactone *rac*-GR24 was included as positive control, while a solution of 0.1% acetone in sterile distilled water was included as negative control. Seeds were considered to be germinated if the radicle protruded through the seed coat.

Luminometer assays. Seeds of transgenic Arabidopsis expressing luciferase as a translational fusion to the SL receptor protein D14 under the control of D14 native promoter (pD14::D14::LUC) were obtained. Seeds were surface-sterilized with 8 % commercial bleach (sodium hypochlorite) in distilled water for 5 minutes and rinsed 5 times with sterile distilled water. Sterile seeds were plated on MS medium (Murashige & Skoog 1962) solidified with 4 % Phytagel and kept at 4°C for 3 d (stratification). Seeds were then transferred to a growth chamber at 25°C 16 h light/8 h dark photoperiod for 7 d. SL mimic and derivative compounds were accurately weighed and dissolved in acetone at 10^{-2} M. Five different concentrations (10^{-4}M, 10^{-5}M, 10^{-6}M, 10^{-7} M, 10^{-8} M) were prepared by 1:10 serial dilutions in liquid MS, along with blank controls containing corresponding water and acetone volumes in MS. D-Luciferin (potassium salt) stock was prepared at 25mg/mL M in DMSO, aliquoted and stored at -80°C until use; all other solutions were prepared just before the assay. With the help of tweezers, 7-day-old Arabidopsis seedlings were placed in a 96-well microtiter plate with their cotyledons facing up (one seedling per well, in 170 µL of liquid MS). Fifteen µL of luciferin (0.125 mg/mL, diluted 1:200 in MS from stock) was added to each

well, corresponding to 1.875 µg. Plate was covered with a transparent film poked in correspondence of each well to allow for gas exchanges. Measurements were taken every 15 minutes in a multimode reader (LB942 Tristar2 S, Berthold Technologies) and the signal was allowed to stabilize for 2-3 h in the light before treatments were started by adding 15 µL per well of different SLs in MS, thus reaching a final volume of 200 µL and 9.4 µg/mL of luciferin; luminescence was measured every 15 minutes for the following 24 hours. Appropriate blank controls were included; each treatment was imposed on a minimum of 16 wells and seedlings, measured individually over time. The percent efficacy of each molecule was calculated 6 h after treatment as a function of decrease in D14::LUC-emitted luminescence with respect to (+)-GR24 1 µM, assuming that the latter, minus the drift of the corresponding blank control, has 100% efficacy.

Author contribution:

X-ray were recorded by the PhD Emanuele Priola (Department of Chemistry, Turin); Modelling has been performed by the PhD student Piermichele Kobauri, (Department of Drug Science and Technology, Turin); Stability tests have been made by the PhD Emma Artuso (Department of Chemistry, Turin); Germination activity has been evaluated by the PhD Beatrice Lace and PhD Wajeeha Saeed (Department of Chemistry, Turin; Department of Agricultural, Forestry and Food Science, Turin); Luminometer assays were performed by the PhD student Helena Sanchez (Centro Nacional de Biotecnología-CSIC, Plant Molecular Genetics Department, Madrid, Spain).

Scientific group supervisors: Dr. Marco Lolli, Professor Francesca Spirakys, PhD Zahid Ali, Professor Cristina Prandi, Professor Francesca Cardinale, Dr. Ivan Visentin, PhD Pilar Cubas.

CHAPTER 4

- SYNTHESIS OF FLUORESCENT DERIVATIVES -

4.1 – Results and discussion

4.1.1. – Fluorescent SL analogues[88]

In strigolactone field, the convergence between chemistry and biology derives from the need to elucidate, at molecular level, the cellular processes involved in AM fungi, host and parasitic plants.

Since Strigolactone are produced in tiny amounts by hosts, there is a need for chemical supply of these plant hormones in view of applications in various fields as agriculture and medicine. To this purpose, the aim is to device simpler structural analogues retaining the bioactivity. In this sense, in recent years the library of SL is constantly growing. As described in detail in Chapter 1, the stereochemistry of natural strigolactones plays a central role in affecting not only the activity, but also the selectivity of target effects. As a consequence, enantioselective synthesis and elucidation of absolute configuration become crucial.

An unambiguous assignment of the configuration would allow to correlate the stereochemistry with the high specificity of the response. As a matter of fact, in *Arabidopsis thaliana* system two different α,β-hydrolases have been identified: KAI2 and AtD14, respectively responsible for the perception of karrikins and strigolactones.[89,29] AtD14 selectively responds to SLs showing R configuration at the C-2', whilst KAI2 is able to mediate the response to KARs but also to some SLs analogues, whose configuration at C-2' is S.[90]

The consequences of a missing configuration assignment could lead to the activation of responses that are completely unrelated to strigolactones and then to misinterpretated results.

We decided to focus our study on the indolyl-derived family of SLs analogues, known also as the “EGO family”. This class of compounds presents some interesting features which persuaded us to chose them as lead candidates: starting from cheap regents, few synthetic steps are required for a multigram preparation.[46] In addition, these class of compounds is characterized by a simplified stereochemistry, as only the stereocenter C-2’ is retained.

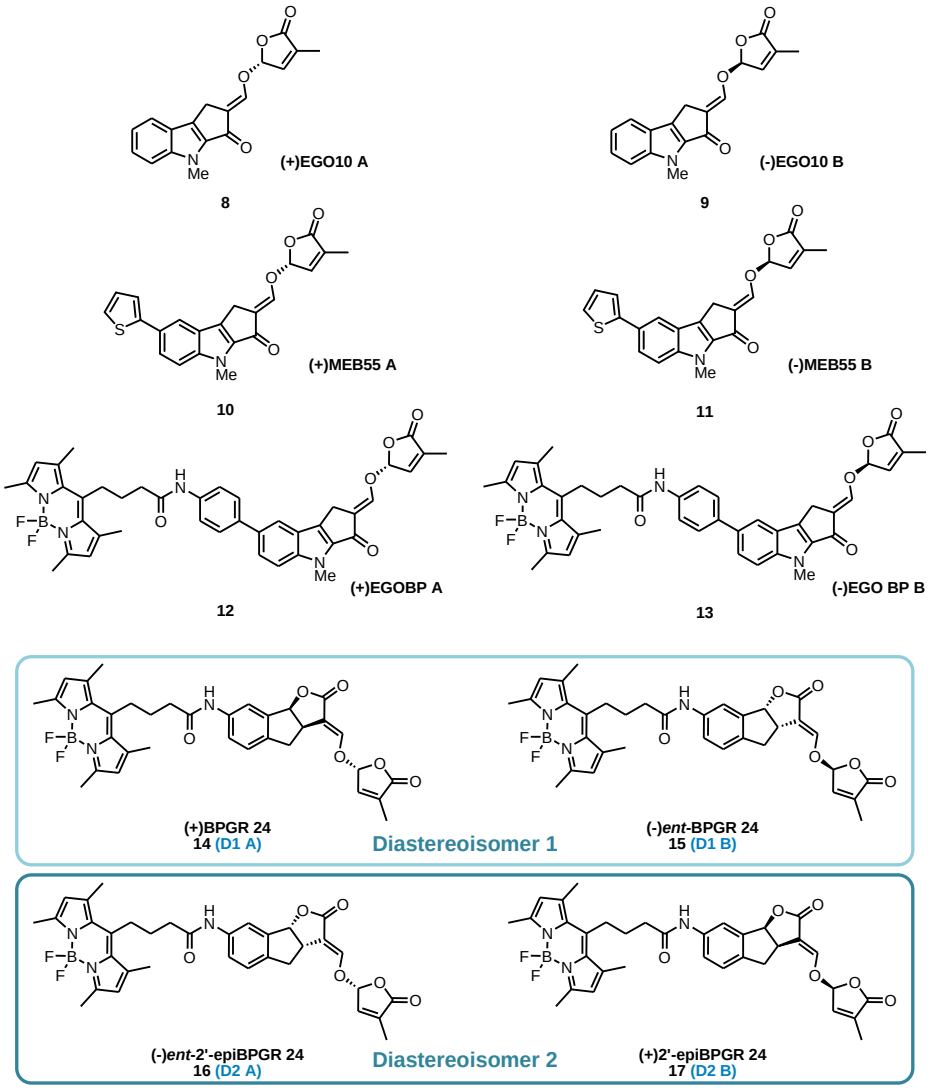

Figure 47. SL analogues as pure enantiomers.

Furthermore, these molecules possess interesting luminescent properties which can be strengthened through easy functionalization and introduction of substituents on the A ring, with the resulting opportunity to use them as probes for *in vivo* mapping by means of confocal microscopy studies.

Keeping in mind 405 nm as the minimum excitation wavelength required for confocal investigations, the BODIPY family of fluorophores was considered suitable as possible *in vivo* tracer.[52]

The stereochemical study was then targeted at EGO10 (**8**, **9**) and MEB55 (**10**, **11**), at the EGO10 fluorescent version, called EGOBP A (**12**) and EGOBP B (**13**), and, due to the GR24 widespread use as standard in biological assays, at the GR24 fluorescent version BPGR24.

EGO10, MEB55, EGOBP A and B were synthesized as previously reported,[46] apart for amino-GR24 which was obtained through a slight modification of the already published procedure (Figure 48).[91]

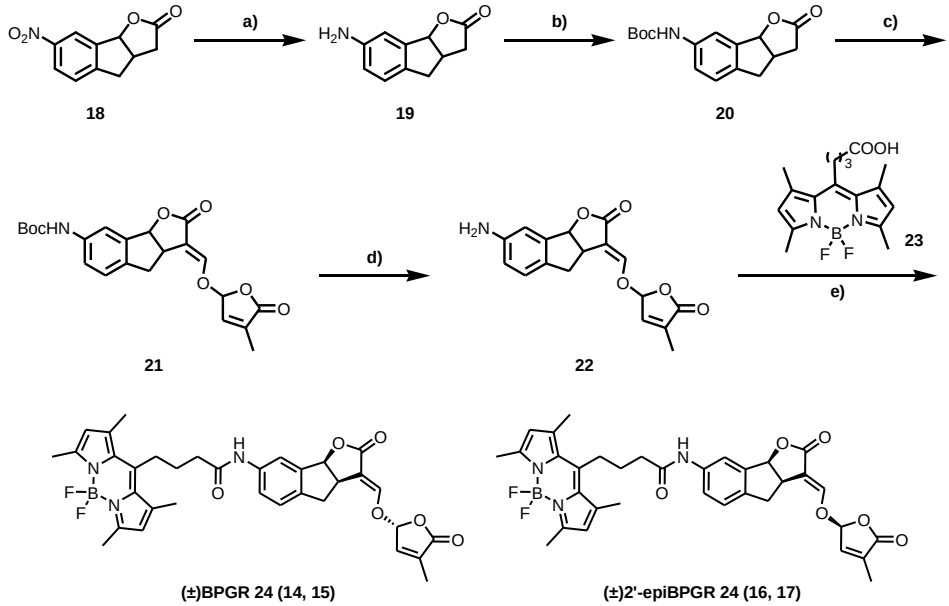

Figure 48. Synthetic procedure of BPGR24. Reagents and conditions: a) Zn/$CaCl_2$, EtOH-H_2O, reflux, 2h (80%); b) t-Boc_2O, DMAP, THF, reflux, 18h (80%); c) HCOOEt, t-BuOK, DME, rt, 2h, then 5-bromo-3-methyfuran-2-(5H)-one, rt, 18h (62%); d) TFA, DCM, rt, 2h (93%); e) CDMT, NMM, DCM, rt, 18h (78%).

Once realized the D-ring attack to the ABC system, **21** was obtained as a couple of diastereoisomers. These were separated by column chromatography, and the following reactions were carried out separately on the two diastereoisomers. After Boc deprotection of the amino group, the NH_2-GR24 (**22**) was then labelled with the previously mentioned BODIPY (**23**) according to the Kaminski procedure.[92] Each fluorescent diastereoisomer was obtained as racemic mixture of two enantiomers and separated through chiral HPLC[88] to obtain (+)-BPGR24 (**14**), (-)-*ent*-BRGR24 (**15**), (+)-2'-*epi*-BPGR24 (**17**) and (-)-*ent*-2'-*epi*-BPGR24 (**16**) (Figure 47).

ECD measurements.

For the assessment of the absolute configuration of the aforementioned analogues, ECD spectra were recorded and compared with those of all the stereoisomers of GR24. At the beginning, the labels "A" and "B" of EGO10, EGOBP, MEB55 and BPGR24 stereoisomers were assigned on the basis of the HPLC behaviour: "A" for the first eluted, and "B" for the second, as reported in Table 6.

SL analogue	Retention times (min)	
	A	B
EGO10[a]	12.25	30.24
EGOBP[b]	4.88	12.37
MEB55[a]	6.32	16.09
BPGR24[c]	6.18	9.56
***Epi*-BPGR24**[d]	11.79	13.62

Table 6. Retention times of SL analogues in HPLC. *a*: isocratic, DCM/EtOH 99/1, flow: 1mL/min; *b*: isocratic, DCM/EtOH 95/5, flow: 1mL/min; *c*: isocratic, DCM/EtOH 97/3, flow: 1mL/min; *d*: isocratic, DCM/EtOH 97/3, flow: 0.5 mL/min.

In ECD spectra the stereochemical assignment of the SLs C2' stereocenter is usually based on the Frischmuth's rule.[93] The key concept of this rule is that a 2'R configuration corresponds to compounds showing a negative Cotton effect at 270 nm, while 2'S corresponds to a positive Cotton effect in the same spectral region. This principle has been successfully applied for the stereochemical assignment of various SL stereoisomers.[94] Also in this case, with our SLs analogues, the rule is applicable and leads to unequivocal configuration assignment (Figure 49).

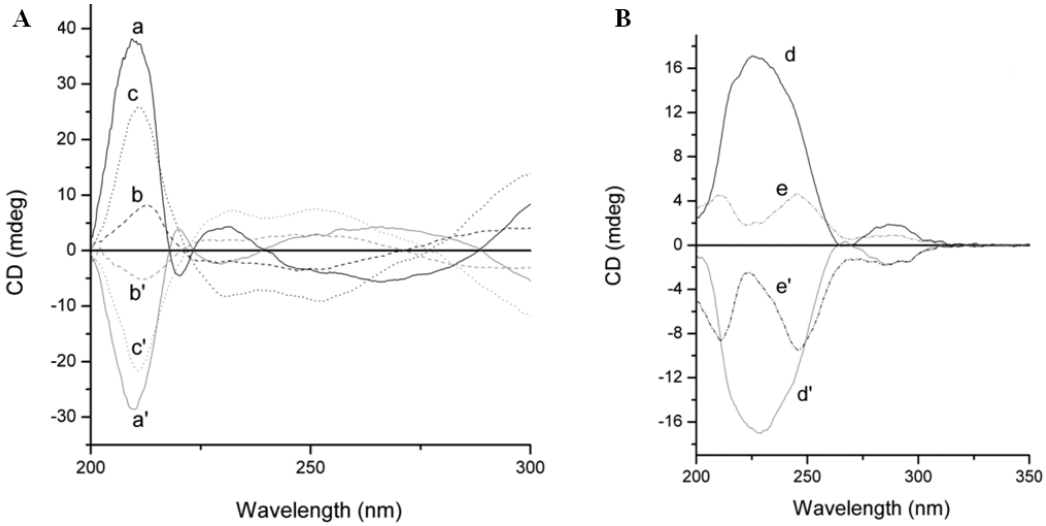

Figure 49. ECD spectra of A. EGO10 A (**8**, a) and B (**9**, a'), EGOBP A (**12**, b), and B (**13**, b'), and MEB55 A (**10**, c) and B (**11**, c'); B. BPGR24 (**14**, d), *ent*-BPGR24 (**15**, d'), *ent*-2'-*epi*-BPGR24 (**16**, e), and 2'-*epi*-BPGR24 (**17**, e'). All stereoisomers were dissolved in MeCN.

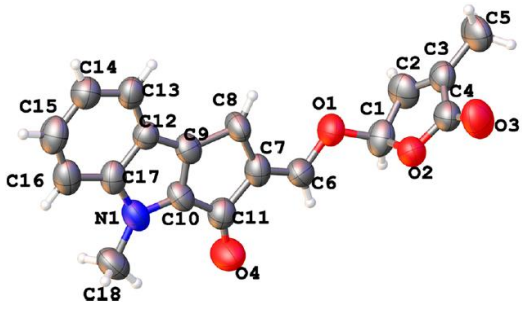

To support the assigned configurations we performed a X-ray analysis of EGO10 A crystals. As shown in Figure 50, EGO10 A clearly shows a R configuration at C-2'.

Figure 50. X-ray of EGO10 A compound.

Furthermore, considering the similarities in CD patterns between the molecules belonging to set A, EGOBP A and MEB55 A should retain the same spatial arrangement of EGO10A, and equally should happen for set B.

By contrast the tagged stereoisomers of GR24 (i.e. BPGR24, *ent*-BPGR24, 2'-*epi*-BPGR24, *ent*-2'-*epi*-BPGR24) display a different ECD profile, with no sign inversion in the 250-300 nm range (Figure 49B). Hence, in this case the Frischmuth's rule is not applicable.

However, it is possible to determine the stereochemistry of these fluorescent compounds combining different experimental evidences. The most appropriate approach is consider as a reference the CD spectra of all stereoisomers of GR24. As can be observed in Figure 51, the similarity with its BP-labelled version (Figure 49B)is clearly detectable.

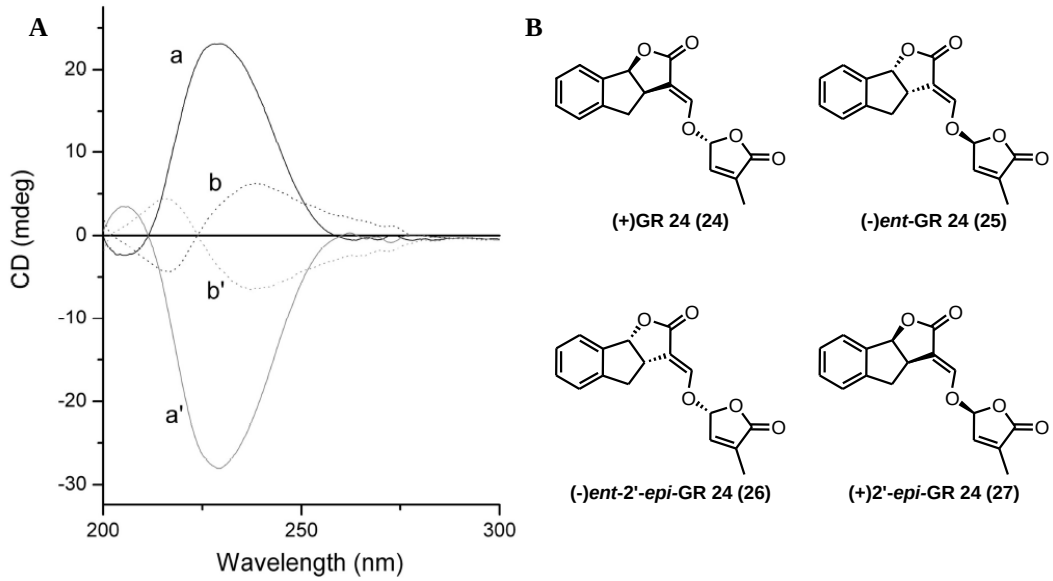

Figure 51. A. CD spectra of GR24 (a), *ent*-GR24 (a'), 2'-*epi*-GR24 (b), and *ent*-2'-*epi*-GR24 (b'). All stereoisomers were dissolved in acetonitrile at submillimolar concentration; B. GR24 stereoisomers.

(+)-GR24, whose configuration was established to be R at C-2' by Scaffidi and co-workers,[90] exhibits a positive Cotton effect in the 210-260 range, and the same

effect is evident both in BPGR24 (**14**) and *ent*-2'-*epi*-BPGR24 (**16**). This evidence suggests a similar spatial arrangement for both **14** and **16** compounds. Furthermore, their chemical correlation and correspondence in the chromatographic behaviour respect to GR24 provide additional evidences in support of the stereochemical assignment.

To sum up, in the synthesized molecules the C2' stereocenter presents an R configuration for EGO10 A (**8**), EGOBP A (**12**), MEB55 A (**10**), BPGR24 (**14**), and *ent*-2'-*epi*-BPGR24 (**16**).

Biological activity.

Once elucidated the configuration of our compounds we were interested in investigating the different biological response ascribable to each of the stereoisomers. *Pelipanche aegyptiaca* was used as a model for the parasitic seed germination, *Gigaspora margarita* for hyphal branching, and *Arabidopsis thaliana* for root-hair elongation bioactivity tests.

EGO10 – As we can observe in bar graph reported in Figure 52 EGO10 A (**8**), which now has been confirmed as showing a R configuration, does not show any statistical difference in activity with respect to EGO10 B (**9**) when tested as seed germination inducer. By contrast, it was found to be the most active stereoisomer for hyphal branching test in *Gigaspora margarita* and for root elongation in *Arabidopsis thaliana*. We also wanted to gain evidence that the bioactiphore of the compounds was the enol ether function linking the C and D ring. To this purpose, we synthesized a compound related to EGO10 but lacking the D-ring (EGO10-mD), and proved unable to trigger the biological response (Figure 52 C).

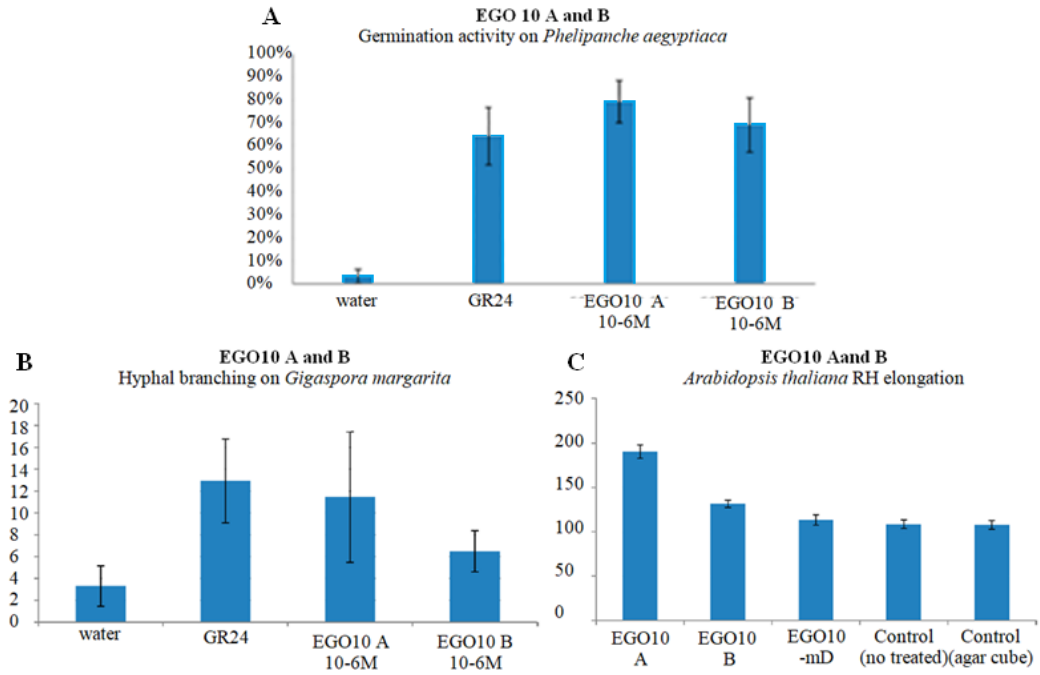

Figure 52. Activity of pure enantiomers of EGO10 A (R) and B (S). A. Germination percentages (y axis) of *Phelipanche aegyptiaca;* B. Branching number per hyphal apex of *Gigaspora margarita*; C. Root hair length (μm) in root segments of *Arabidopsis thaliana*. EGO10-mD at 0.1M concentration.

MEB55 – The activity of this racemic thiophene-indolyl-derived analogue was already reported.[46] This preliminary study gave us the possibility to directly test the two enantiomers A and B at the concentration which led to the highest activity (i.e. 10^{-6} M). As can be observed in Figure 53 MEB55 A with C-2' R proved to be more effective than both MEB55 B (C-2' S), and even racemic GR24.

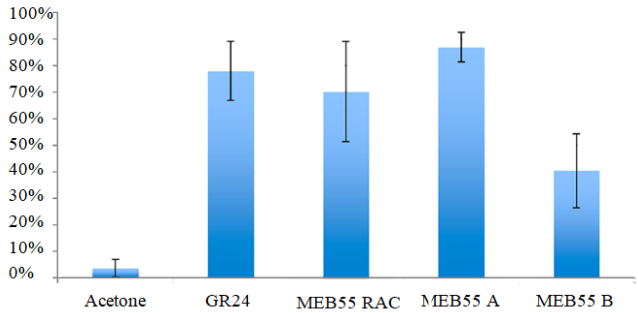

Figure 53. Percentages of germinated (y axis) *Peliphanche aegyptiaca* seeds after exposure to MEB55 as recemic mixture or pure enantiomer (**10**, **11**) at 0.1 μM concentration.

EGOBP – The racemic fluorescent BP-labelled EGO10 was tested towards *Phelipanche aegyptiaca* seeds disclosing a remarkable bioactivity, even if not high as racemic GR24.[53] Since little is known about the dynamic transport of SLs within the plant, our interest was focused on the evaluation of the molecule distribution. Enantiomers A (2'R) and B (2'S) were separated by chiral HPLC chromatography, and their effect was evaluated on root hair elongation in *Arabidopsis* (Figure 54). The results revealed the 2'R as the most active, while naked-BP and EGO10BP without the D-ring (EGO10-mD-BP) were found to be inactive and aspecific in the distribution.[95]

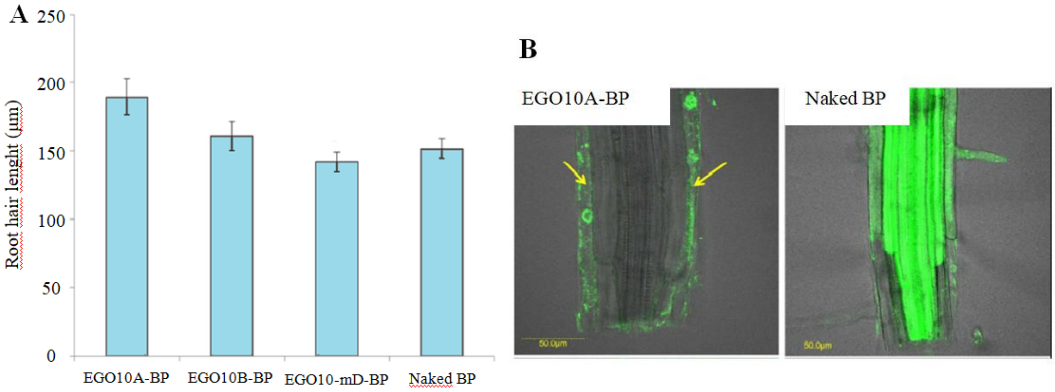

Figure 54. A) Root-hair length (µm) in root segments of *Arabidopsis* system containing EGO10A-BP, EGO10B-BP, EGO10-mD-BP or naked-BP; B) Images of roots treated with EGO10A-BP or naked-BP. Green: EGO10A-BP or Naked-BP signals. Yellow arrows denote the epidermis cell layer.[96]

BPGR24 – Since GR24 remains the reference point in the trade, we decided to label it with the BODIPY fluorophore by means of a three carbon linker hooked to NH_2-GR24. HPLC provided a successful separation into the four stereoisomers, whose germination activity was measured towards *Phelipanche aegyptiaca* seeds.

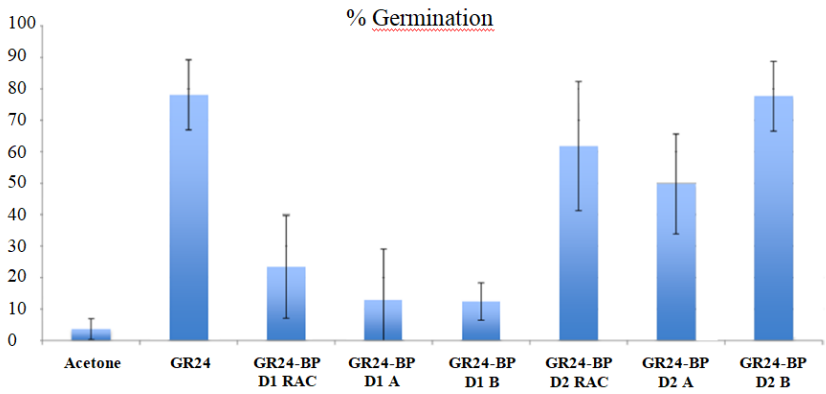

Figure 55. Percentages of germinated seeds (y axis) of *Peliphanche aegyptiaca* after exposure to pure enantiomers of the GR24 BP series at 0.1 μM concentration.

As reported in Figure 55 the results surprisingly revealed the D2 diastereoisomer (*ent*-2'-*epi*-BPGR24 **16** and 2'-*epi*-BPGR24 **17**) as the most active. The D1 (BPGR24 **14** and *ent*-BRGR24 **15**), on the contrary, was disclosed as inactive and statistically comparable with the negative control, even though the germination activity of GR24 D1, not bearing the fluorophore (Figure 56), confirmed the expected activity results when measured both as racemate and as pure enantiomer. Therefore the fluorescent GR24 epimers, 2'-*epi*-GR24BP (**17**) and *ent*-2'-*epi*-GR24BP (**16**), seem to be the more promising for further bioimaging studies.

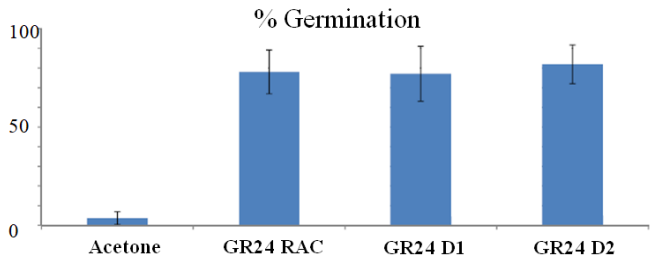

Figure 56. Germination activity on *Peliphanche aegyptiaca* seeds at 10^{-7} M of racemic GR24, GR24 D1 (**24**, **25**) and 2'-*epi* GR24 D2 (**26**, **27**) respectively.

4.1.2 – The CL-BP compound

The BP-labelled analogues constitute a suitable tool to *in vivo* monitor SLs distribution and transport in both plants and AM fungi. However what has to be considered is that, following perception of these fluorescent analogs by D14-type receptors, the ABC part bearing the fluorophore could be cleaved at the ether bond as a consequence of the enzyme hydrolytic activity, possibly leaving the unlabeled D-ring inside the binding pocket and releasing the ABC part. Being the hydrolysis a rapid event, it would be therefore difficult to use these compounds as markers to label the receptor site.

Bearing in mind the model proposed by Nakamura and coworkers in 2013,[32] according to which the SL recognition and regulation by D14 provide the transition from an open binding cavity to a capped structure, our aim was to devise an active SL agonist, whose corresponding fluorescent version should be non-hydrolysable.

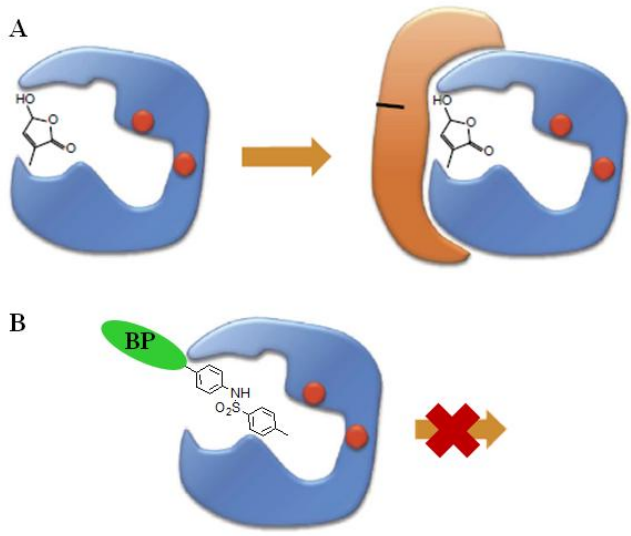

Figure 57. A. Model proposed by Nakamura for the SL recognition and hydrolyzation;[33] B. Principle of the non hydrolysable agonist applied to the CL-BP compound.

Preventing the removal of the linkage between the active molecule and the fluorophore, the compound would be too hindered for the transition to the receptor capped structure (Figure 57 B). As a consequence the fluorescent non-hydrolysable agonist would be able to enter in the receptor site and get trapped inside of it retaining the fluorescent probe.

In 2010 Tsuchiya and co-workers[96] identified some sulphonamide-related compounds as capable to perturb the strigolactone biology. These were collectively named cotylimides.

On this basis we devised a sulphonamide *core* for the design of fluorescent non hydrolysable SLs agonist. A p-Iodo phenyl sulphonamide (**28**), also called CL compound, was synthesized and coupled to the fluorescent BODIPY (**29**) according to a Sonogashira procedure to obtain the CL-BP molecule with 51% yield (**30**).

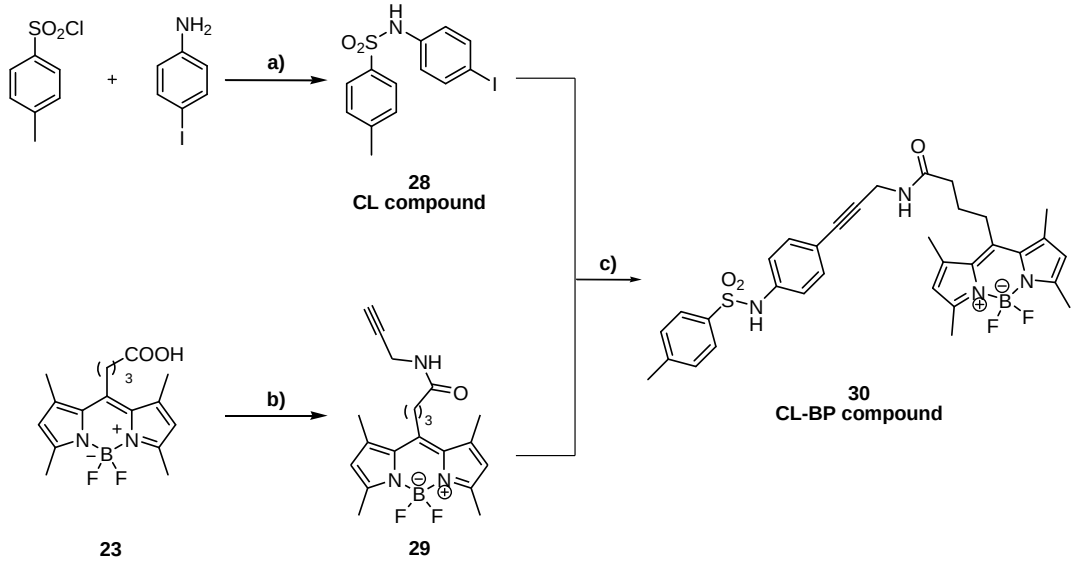

Figure 58. Synthetic pathway of CL-BP: a) H_2O, 25', r.t. (76%); b) propargylamine, ClCOOEt, 4-MMP, THF, 1h, r.t. (99%); c) CuI, $(PPh_3)_2PdCl_2$ 5%, Et_3N, THF, o.n., r.t. (51%).

CL **28** and CL-BP **30** have been evaluated by means of D14:Luciferase bioactivity tests thanks to the collaboration with Dr. Pilar Cubas and PhD student Elena Sanchez (National Center for Biotechnology, Madrid).

In its essence the luciferase test is an *in vivo* enzymatic assay where the D14 receptor is labelled to a fluorescent protein called luciferin. This can be defined as

an "imaging reporter": given the so far accounted mechanism of perception of SLs, when the active molecule interacts with the D14, the final degradation of the receptor itself is detected as a decrease of fluorescence, measured by luminometer.

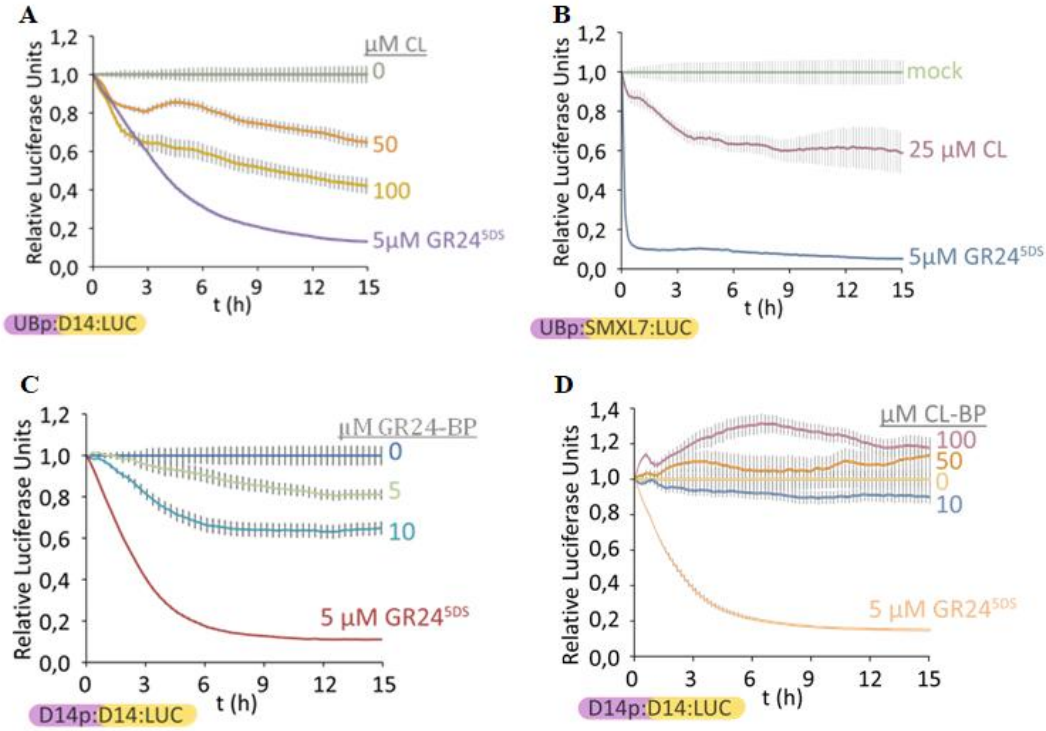

Figure 59. A. **B**. **C**. **D**. Analysis of D14:Luciferase Arabidopsis transgenic lines in combination with hydrolysable and non-hydrolysable SL derivatives. Monitoring of D14:LUC degradation *vs* time (h).

As reported in Figure 59A the detected loss of fluorescence reveals that CL compound (**28**) is able to trigger the D14 degradation. Even though the hormone concentration required for the activity is higher compared to GR24 and not feasible with physiological conditions, these evidence suggest that the hydrolytic mechanism is not required to promote the receptor disruption.

To confirm the occurred interaction it was performed a second assay in which the luciferin protein was tagged to SMXL7 (SUPPRESSOR OF MAX2 7), a MAX2

interacting protein required for SL signaling and D14 dependent. When tested the CL activity the detected loss of fluorescence recorded for SMXL7 (Figure 59B), being AtD14 dependent, supported the hypothesis of an interaction with the SL receptor.

Concerning the fluorescent versions of the tested molecules, from the luciferase assays we can see that GR24-BP is able to trigger certain level of D14 degradation, but not as much as GR24 (Figure 59C). On the other hand, as expected CL-BP is not able to activate the D14 degradation even at high concentrations (Figure 59D). Indeed the fluorophore hindrance and the lacking of the hydrolytic mechanism wouldn't allow to have the transition from the open binding cavity of D14 to the capped structure hypothesized by Nakamura in 2013.[32]

4.1.3 – Profluorescent probes

During the second year of my PhD I had the opportunity to gain a working and learning experience abroad at the Institute de Chimie des Substances Naturelles (ICSN), in Gif sur Yvette (France). Under the supervision of the Dr. François-Didier Boyer I was introduced to an innovative project regarding the synthesis of profluorescent probes. The aim of the work was related to the main topic of my PhD project, i.e. to shed some light on the mechanism of action of the strigolactone receptor.[36]

Pisum sativum, whose RMS3 (RAMOSUS3) receptor was demonstrated as the pea ortholog of D14, was selected as biological system for the study.

The tool conceived for the investigation on the receptor bioactivity is essentially a "switch on/off" system based on fluorescence. More in detail, the designed probes were composed by two different parts: a cumarine (DiFMU), and a butenolide ring mimicking the D ring present in SLs, with one methyl group in 4' position or two methyl groups respectively in 3' and 4'. The DiFMU scaffold is basically a phenol fluorophore whose luminescence is quenched when engaged in a covalent bond. This means that, when bound to the D ring fragment, the molecule is non fluorescent.

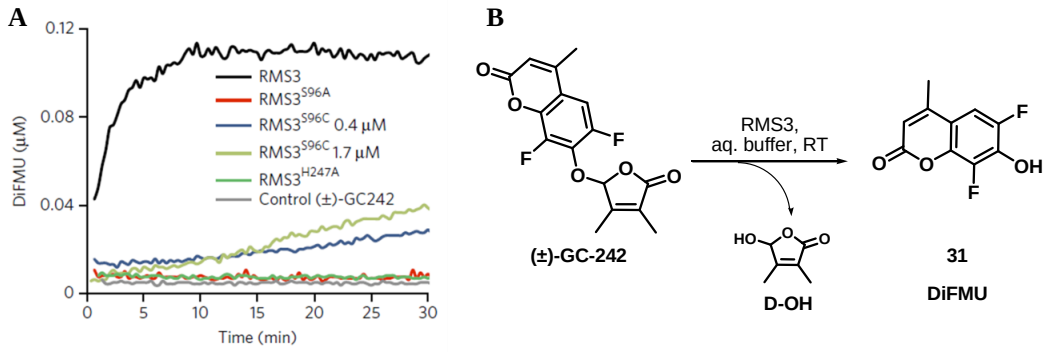

Figure 60. A. Progress curves deriving from the interaction of (±)-GC242 profluorescent probe with RMS3 or RMS3 mutants; B. Hydrolytic mechanism of the profluorescent probe.[37]

When the molecule undergoes an hydrolysis reaction, the phenol group became unmasked and an increase in fluorescence is observed, thus allowing to obtain a readout of the receptor activity.

Monitoring the fluorescence level obtained from the DiFMU fragment release, the group in ICSN discovered that the pea receptor acts as a single-turnover enzyme. Furthermore RMS3 mutants were tested, demonstrating the importance of the catalytic triad to retain the bioactivity.

Intrigued by the strigolactone-like bioactivity of the (±)-GC242 compound and considered its complete different structure respect to the ABC SL tricycle, our target has been to investigate how the SL reception would be influenced using profluorescent probes presenting different cumarine scaffolds.

Thinking about the type of scaffolds which could be synthesized our attention was drawn towards a possible implementation of the project.

Previous studies had successfully reported the possibility to obtain controlled protein functions by a photoactivable approach. In this strategy, to obtain a temporally inactive protein poised for activation by light, the side-chain carboxyl group was caged as a 2-nitrobenzyl ester, in which the ester function and 2-NO_2 substituent were essential for light removal.[97]

Along this line our aim has been the synthesis of caged and inactive probes, whose lack of action was due to a photo-removable moiety linked to the *core* framework.

In this case, the light will trigger the removal of the NO_2 phenyl fragment and the in situ release of the less-hindered, profluorescent and active molecule.

To maintain the chemical requirements for photoactivation, the first step was the synthesis of several cumarine derivatives (Figure 61) showing the same framework but presenting substituents which could be bound to a NO_2-benzyl or NO_2-benzoate moiety. Afterwards each *core* was labelled to D-rings possessing one or

two methyl groups respectively. In case of compound **33** the D-ring attack brought to two different products, one with the free carboxylic acid group, and the other bound to two butenolide rings.

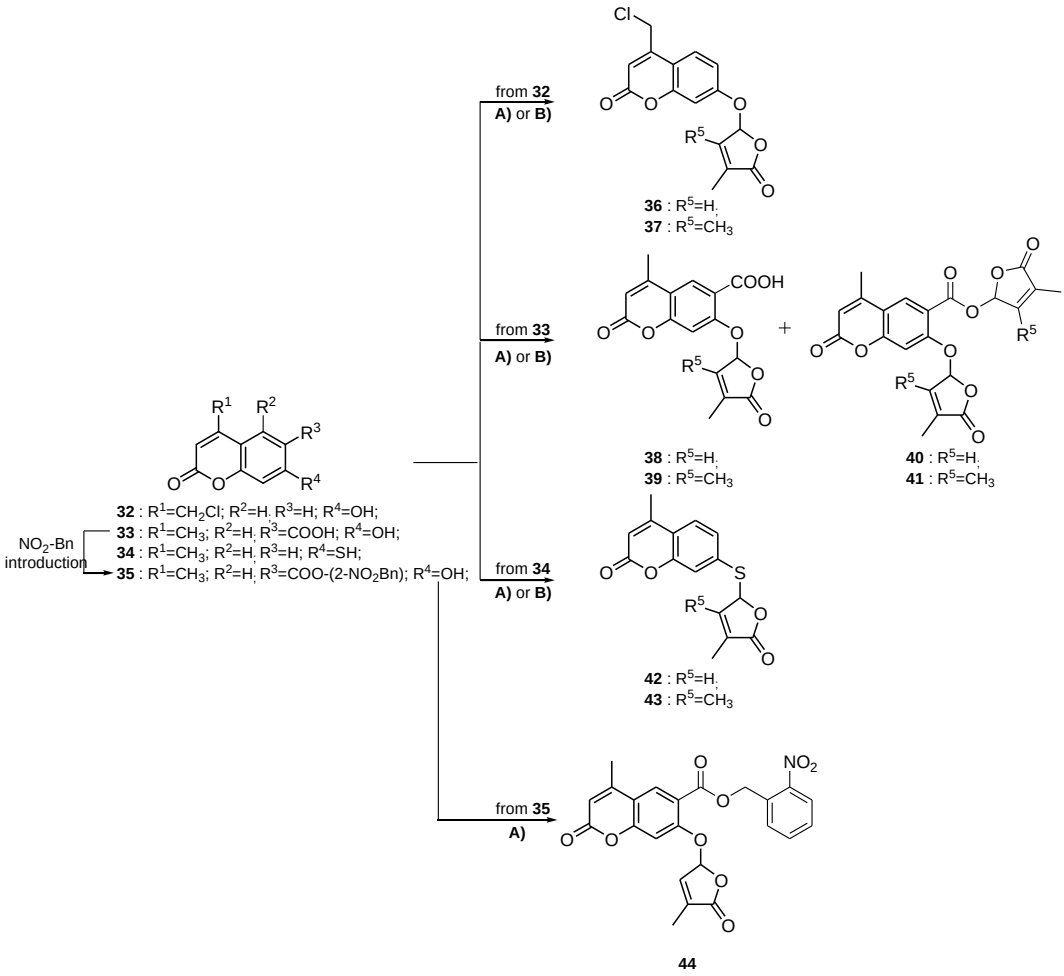

Figure 61. Synthetic procedure for the synthesis of several profluorescent probes presenting different cumarine scaffolds. Procedure A) for R^5 = H: 5-bromo-3-methylfuran-2(5H)-one, DIEA, ACN, o.n., r.t.; Procedure B) for R^5 = CH_3: 5-chloro-3,4-dimethylfuran-2(5H)-one, DIEA, ACN, o.n., r.t.

Furthermore, aside from this strategy, a commercially available cumarine having a thiol functional group instead of a phenol group was labelled to a 4'-methyl (**42**) or 3',4'-dimethyl (**43**) D-ring.

Finally, in the light-activable version of the designed derivatives the NO_2-phenyl fragment was introduced before (compound **35**) or after (compound **45**) the D ring attack respectively.

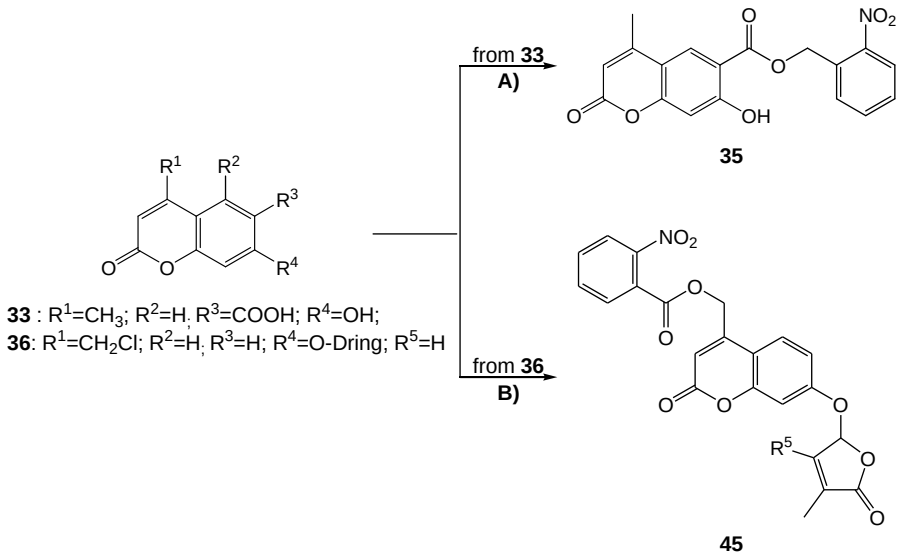

Figure 62. Synthetic pathway of cumarine derivatives having a light-removable fragment. Procedure A): 1-(bromomethyl)-2-nitrobenzene, K_2CO_3, DMF, 30', r.t.; Procedure B): 2-nitrobenzoic acid, K_2CO_3, DMF, 30', r.t.

At the time this PhD thesis is being written the purified molecules are being tested on the *Pisum sativum* system, looking forward to see the effects on bioactivity derived from the cumarine scaffold modifications.

4.2 – Experimental

4.2.1. – Fluorescent SL analogues

All the chemicals and solvents were purchased from Sigma-Aldrich and were used as received unless specified. Reactions involving air-sensitive reagents were performed under a dry nitrogen atmosphere with purified solvents. Glassware for sensitive reactions were oven-dried at 150 °C and assembled under nitrogen. Reactions were monitored by TLC carried out on 0.25 mm silica gel plates (Merck F254). Chromatographic purifications were carried out on silica gel (Merck grade 7734, pore size 60 Å, 70–230 mesh) using flash-column or classical techniques; Rf values refer to TLC carried out on 0.25 mm silica gel plates (Merck F254), with the same eluent indicated for column chromatography. ^{1}H-NMR, ^{13}C-NMR and COSY spectra were recorded on a Bruker Avance-200 spectrometer or on a Jeol JNM-ECZR600 in $CDCl_3$. ^{1}H NMR spectra were recorded at 200 MHz or 600 MHz; ^{13}C NMR spectra were recorded at 50.2 MHz or 150 MHz with complete proton decoupling. Multiplicity is indicated as the following: s (singlet), br (broad signal), d (doublet), t (triplet), dd (doublet doublet), td (triplet–doublet), m (multiplet). Chemical shifts were reported in ppm from the peak residual solvent as an internal standard. The coupling constants *J* are expressed in Hz. HRMS data were recorded on an LTQ Orbitrap Hybrid mass spectrometer. MS data were recorded at an ionizing voltage of 70 eV. The abbreviation 'M' indicates molecular ion. Enantiomers were separated on either a semipreparative or an analytical Chiralpak IC column (particle size 5 μm, Daicel, Osaka, Japan). Dimensions: analytical column 4.6Ø × 250 mmL; semipreparative column 10Ø × 250 mL. A Jasco P-2000 polarimeter was used for the determination of optical rotations. ECD measurements were performed on a JASCO J-815 instrument at

RT, in quartz cells with a 1 mm optical path, scanning speed 100 nm/min, bandwidth 1 nm.

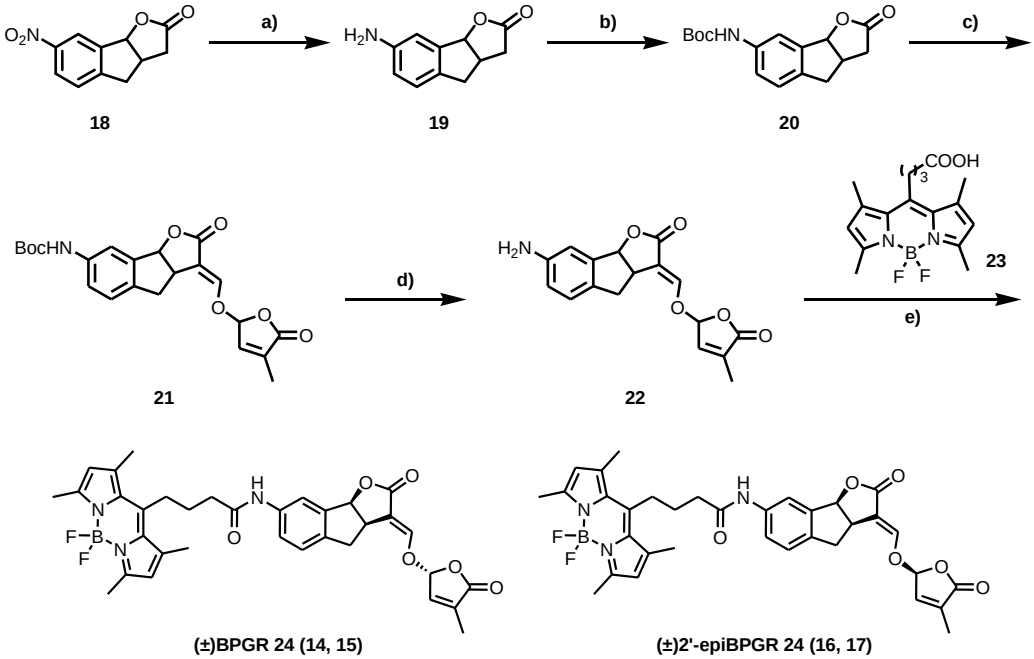

Figure 63. Synthetic pathway for the synthesis of BP-GR24 and 2'-*epi*-BP-GR24. Reagents and conditions: a) Zn/$CaCl_2$, EtOH-H_2O, reflux, 2h (80%); b) *t*-Boc_2O, DMAP, THF, reflux, 18h (80%); c) HCOOEt, *t*-BuOK, DME, rt, 2h, then 5-bromo-3-methyfuran-2-(5*H*)-one, rt, 18h (62%); d) TFA, DCM, rt, 2h (93%); e) CDMT, NMM, DCM, rt, 18h (78%).

7-Amino-3,3*a*,4,8*b*-tetrahydro-2*H*-indeno[1,2-b]furan-2-one (19).

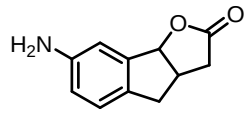

A solution of **18**[91] (3.12 mmol, 0.684 g) in 4.8 mL of EtOH was added to an aqueous solution of $CaCl_2$ (2.18 mmol, 0.684 g in 3.6 mL of water) in a three-necked round-bottom flask. Zn powder was then added (27.52 mmol, 1.80 g), and the resulting suspension was heated to reflux temperature (80 °C) and reacted for 2

h. Upon TLC control (PE/EtOAc, 1:1, Rf = 0.21) the reaction mixture was filtered on a Büchner funnel and washed with CH_2Cl_2. The organic phases were washed with brine (1 × 25 mL) and H_2O (2 × 25 mL), dried over K_2CO_3, and filtered, and the solvent was evaporated. Compound **19** (0.420 g, 80%yield) was obtained as a white solid and did not require further purification: ^{1}H-NMR ($CDCl_3$, 200 MHz) δ 2.30 (1H, dd, *J* = 18 Hz, *J* = 5.8 Hz, H_{3a}), 2.63−2.86 (2H, m, H_3), 3.05−3−51 (2H, m, H_4), 3.57 (2H, br, NH_2), 5.73 (1H, d, *J* = 7.0 Hz, H_{8b}), 6.61 (1H, dd, *J* = 2.0 Hz, *J* = 8.0 Hz, H_6), 6.71 (1H, d, *J* = 2.0 Hz, H_8), 6.98 (1H, d, *J* = 8.4 Hz, H_5). Spectroscopic data correspond to those reported in literature.[51]

***rac*-BPGR24 (and *rac*-2′-*epi*-BPGR24).** (**14** - **17**)

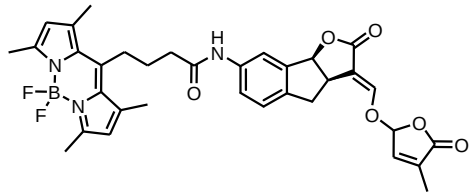

A solution of **23**[46] (0.15 mmol, 50 mg) was prepared in 3 mL of DCM in a three-neck round bottom flask, 2-chloro-4,6-dimethoxy-1,3,5-triazine (CDMT, 0.18 mmol, 32 mg) was then added, and the solution was cooled to −5 °C. N-Methylmorpholine (NMM) was added, and the mixture reacted for 2 h. When the TLC control (PE/EtOAc, 2:3) confirmed the formation of the activated BODIPY complex after 2 h), *rac*-amino-GR24 (**22**) (or *rac*-2′-*epi*-GR24, 0.150 mmol, 47 mg) was added via cannula. The mixture was reacted at room temperature overnight. A 10% solution of citric acid was added, and the aqueous phases were extracted with DCM (10 mL × 3). The organic phases were then dried over Na_2SO_4, and the solvent was evaporated under reduced pressure. The crude was purified by flash chromatography with hexanes/EtOAc, 2:3 (Rf 0.20 green

fluorescence), to give 74 mg (78% yield) of an orange solid of BPGR24/*ent*-BPGR24. Separation on chiral HPLC gives pure enantiomers.

BPGR24 (14): $[\alpha]^{25}_{D}$ +86 (*c* 0.2, CH_2Cl_2); ^{1}H-NMR ($CDCl_3$, 200 MHz) δ 2.04 (5H, s, CH_3 D ring and CH_2), 2.39−2.49 (14H, m, CH_3 BODIPY and CH_2), 2.98−3.06 (3H, m, H_4 and CH_2), 3.29−3.42 (1H, m, H_4), 3.88−3.97 (1H, m, H_{3a}), 5.88 (1H, d, *J* = 7.8 Hz, H_{8b}), 6.03 (2H, s, BODIPY), 6.17 (1H, br, $H_{3'}$), 6.96 (1H, br, $H_{2'}$), 7.13 (1H, d, *J* = 8.0 Hz, H_5), 7.47−7.56 (3H, m, H_6, $H_{6'}$, and H_8); ^{13}C-NMR ($CDCl_3$, 50 MHz) δ 10.7 (2 CH_3 BODIPY), 14.4 (2 CH_3 BODIPY), 16.4 (CH_3 D ring), 27.2 ($CH_2CH_2CH_2CONH$), 27.4 (CH_2CH_2CONH), 36.9 ($CH_2CH_2CH_2CONH$), 37.0 (CH_2 C-4a), 39.2 (C-3a), 85.9 (C-8b), 100.7 (C-2′), 113.2 (C-4), 117.5 (C-3′), 121.8 (CH-BODIPY), 122.3 (phenyl C-5), 125.6 (C-6′), 131.5 (phenyl, C-3), 135.9 (2C, BODIPY), 137.5 (2C, BODIPY), 138.2 (C, BODIPY), 139.3 (2C, BODIPY), 140.7 (C-4a), 141.0 (phenyl, C-6), 145.3 (C-8a), 151.3 (phenyl, C-8), 154.0 (C-7), 170.2, 171.5 (CONH); ESIMS *m/z* 652,3 $[M + Na]^+$; HRESIMS *m/z* 629.2339 (calcd for $C_{34}H_{34}BF_2N_3O_6$ 629.2509).

***ent*-BPGR24 (15)**: $[\alpha]^{25}_{D}$ −82 (*c* 0.2, CH_2Cl_2); ^{1}H-NMR ($CDCl_3$, 200 MHz) δ 2.05 (5H, s, CH_3 D ring and CH_2), 2.39−2.51 (14H, m, CH_3 BODIPY and CH_2), 2.98−3.06 (3H, m, H_4 and CH_2), 3.30−3.43 (1H, m, H_4), 3.90−3.98 (1H, m, H_{3a}), 5.90 (1H, d, *J* = 7.8 Hz, H_{8b}), 6.04 (2H, s, BODIPY), 6.19 (1H, br, $H_{3'}$), 6.99 (1H, br, $H_{2'}$), 7.14 (1H, d, *J* = 8.0 Hz, H_5), 7.50−7.57 (3H, m, H_6, $H_{6'}$, and H_8); ^{13}C-NMR ($CDCl_3$, 50 MHz) δ 10.9 (2 CH_3 BODIPY), 14.6 (2 CH_3 BODIPY), 16.5 (CH_3 D ring), 27.5 ($CH_2CH_2CH_2CONH$), 27.6 (CH_2CH_2CONH), 37.1 ($CH_2CH_2CH_2CONH$), 37.2 (CH_2 C-4a), 39.3 (C-3a), 86.2 (C-8b), 100.9 (C-2′), 113.4 (C-4), 117.7 (C-3′), 121.9 (CH-BODIPY), 122.5 (phenyl C-5), 125.7 (C-6′),

131.7 (phenyl, C-3), 136.0 (2C, BODIPY), 137.7 (2C, BODIPY), 138.3 (C, BODIPY), 139.4 (2C, BODIPY), 140.9 (C-4a), 141.2 (phenyl, C-6), 145.6 (C-8a), 151.6 (phenyl, C-8), 154.1 (C-7), 170.4, 171.8 (CONH); ESIMS *m/z* 652,3 $[M + Na]^+$; HRESIMS *m/z* 629.1416 (calcd for $C_{34}H_{34}BF_2N_3O_6$ 629.2509).

2′-*epi*-BPGR24 (17): $[\alpha]^{25}_D$ +148 (*c* 0.2, CH_2Cl_2); ^{1}H-NMR ($CDCl_3$, 200 MHz) δ 2.05 (3H, s, CH_3 D ring), 2.42−2.51 (16H, m, CH_3 BODIPY and 2 × CH_2), 3.02−3.10 (3H, m, H_4 and CH_2), 3.32−3.45 (1H, m, H_4), 3.90−4.01 (1H, m, H_{3a}), 5.91 (1H, d, *J* = 7.8 Hz, H_{8b}), 6.04 (2H, s, BODIPY), 6.18 (1H, br, $H_{3'}$), 6.97 (1H, br, $H_{2'}$), 7.16 (1H, d, *J* = 8.0 Hz, H_5), 7.46−7.61 (3H, m, H_6, $H_{6'}$; and H_8); ^{13}C-NMR ($CDCl_3$, 50 MHz) δ 10.9 (2 CH_3 BODIPY), 14.6 (2 CH_3 BODIPY), 16.5 (CH_3 D ring), 27.4 ($CH_2CH_2CH_2CONH$), 27.6 (CH_2CH_2CONH), 37.1 ($CH_2CH_2CH_2CONH$), 37.2 (CH_2 C-4a), 39.3 (C-3a), 86.1 (C-8b), 100.9 (C-2′), 113.4 (C-4), 117.7 (C-3′), 121.9 (CH-BODIPY), 122.5 (phenyl C-5), 125.8 (C-6′), 131.7 (phenyl, C-3), 136.1 (2C, BODIPY), 137.6 (2C, BODIPY), 138.4 (C, BODIPY), 139.5 (2C, BODIPY), 140.8 (C-4a), 141.2 (phenyl, C-6), 145.5 (C-8a), 151.5 (phenyl, C-8), 154.2 (C-7), 170.4, 171.7 (CONH); ESIMS *m/z* 652,2 $[M + Na]^+$; HRESIMS *m/z* 629.3516 (calcd for $C_{34}H_{34}BF_2N_3O_6$ 629.2509).

***ent*-2′-*epi*-BPGR24 (16):** $[\alpha]^{25}_D$ −175 (*c* 0.1, CH_2Cl_2); ^{1}H-NMR ($CDCl_3$, 200 MHz) δ 2.01 (3H, s, CH_3 D ring), 2.38−2.48 (16H, m, CH_3 BODIPY and 2 × CH_2), 2.98−3.04 (3H, m, H_4 and CH_2), 3.29− 3.40 (1H, m, H_4), 3.87−3.98 (1H, m, H_{3a}), 5.88 (1H, d, *J* = 7.8 Hz, H_{8b}), 6.01 (2H, s, BODIPY), 6.15 (1H, br, $H_{3'}$), 6.94 (1H, br, $H_{2'}$), 7.13 (1H, d, *J* = 8.0 Hz, H_5), 7.43−7.58 (3H, m, H_6, $H_{6'}$, and H_8); ^{13}C-NMR ($CDCl_3$, 50 MHz) δ 10.9 (2 CH_3 BODIPY), 14.6 (2 CH_3 BODIPY), 16.6 (CH_3 D ring), 27.5 ($CH_2CH_2CH_2CONH$), 27.6 (CH_2CH_2CONH), 37.0 ($CH_2CH_2CH_2CONH$), 37.2 (CH_2 C-4a), 39.5 (C-3a), 86.0 (C-8b), 100.8 (C-2′),

113.2 (C-4), 117.7 (C-3′), 121.9 (CH-BODIPY), 122.4 (phenyl C-5), 125.7 (C-6′), 131.7 (phenyl, C-3), 136.2 (2C, BODIPY), 137.8 (2C, BODIPY), 138.4 (C, BODIPY), 139.6 (2C, BODIPY), 140.8 (C-4a), 141.1 (phenyl, C-6), 145.5 (C-8a), 151.4 (phenyl, C-8), 154.2 (C-7), 170.4, 171.6 (CONH); ESIMS *m/z* 652.2 $[M + Na]^+$; HRESIMS *m/z* 629.2211 (calcd for $C_{34}H_{34}BF_2N_3O_6$ 629.2509).

X-ray Analysis. Crystals that were suitable for X-ray diffraction analyses were obtained via slow evaporation of a methanol solution. X-ray data were collected on an Oxford Diffraction Gemini R-Ultra diffractometer equipped with an Enhanced Ultra (Cu) X-ray source (mirror monochromatized Cu Kα radiation, λ = 1.5418 Å). The ω scan was performed with a frame width of 1.0°. The intensities were corrected for absorption with the numerical correction based on a Gaussian integration over a multifaceted crystal model. Software used: CrysAlisPro (Agilent Technologies, version 1.171.37.31) for data collection, data reduction, and absorption correction; SHELXT[98] for data solution; SHELXL-2014/7[98] for refinement; OLEX2 (version 1.2.5)[99] for structure analysis and drawing preparation. All non-hydrogen atoms were anisotropically refined. Hydrogen atoms were calculated and refined riding with $U_{iso} = 1.2U_{eq}$ or $1.5U_{eq}$ of the atom connected. The absolute configuration was determined using Parson's method.[100]

Plant Material. Seeds of Peliphanche aegyptiaca were collected from field-grown tomato in the West Galilee in Israel. The seeds were stored in glass vials in the dark at room temperature until used in germination tests. For the preparation of test solutions, the compounds to be tested were weighed out accurately, dissolved in 1 mL of acetone, and then diluted with sterile distilled H_2O to reach the appropriate concentrations. All solutions were prepared just before use. Seeds

were surface sterilized and preconditioned.[101] Briefly, seeds were exposed to 50% (v/v) aqueous solutions of commercial bleach for 5 min (2% hypochlorite) and rinsed with sterile distilled H_2O. For preconditioning, seeds were sown on a glass fiber filter paper disc using a sterile toothpick (approximately 20 seeds per disc), and the glass fiber discs were placed on two filter paper discs, dampened with sterile distilled H_2O, and incubated at 25 °C in the dark for 6 days. The preconditioned seeds were then allowed to dry completely in the laminar flow and treated with the strigolactone analogue solutions, and germination rate was evaluated under a stereomicroscope 7 days after treatment. At least 100 seeds were analyzed at each concentration. Synthetic strigolactone GR24 (10^{-7} M) was included as the positive control, while an aqueous solution of 0.1% acetone and sterile distilled H_2O was included as the negative control. Seeds were considered to be germinated if the radicle protruded through the seed coat.

Fungal Material. Spores of Gigaspora margarita Becker and Hall were collected from a previously established trap culture of clover, sterilized with a solution of chloramine T (3% P/V) and streptomycine sulfate (0.03% P/V), rinsed with distilled H_2O, and placed in a Petri plate filled with 0.2% Phytagel gel (Sigma-Aldrich) containing 3 mM $MgSO_4$. The plates were incubated vertically for 5 days at 30 °C in the dark. Paper discs (6 mm diameter), loaded with the appropriate strigolactone analogue solution, were positioned on either side of the germinating hyphae tips. The number of newly formed hyphal apexes was recorded 24 h after treatment. GR24 (10^{-7} M) was included as a positive control, while an aqueous solution of 0.1% acetone and sterile distilled H_2O was included as negative control.

XTT Cell Proliferation Assay. Cells were seeded into 96-well plates at 2500 cells per well in triplicates in normal growing media. The following day, the media was replaced with phenol red-free DMEM supplemented with 10% FBS (fetal bovine serum) and 5% penicillin-streptomycin solution. Cells were incubated overnight at 37 °C in a humidified 5% CO_2/95% air atmosphere and then were treated as indicated below for 48 h. An XTT (2,3-bis(2-methoxy-4-nitro-5-sulfophenyl)-5-[(phenylamino)carbonyl]-2H-tetrazolium inner salt) was used to quantify viability according to the manufacturer's instruction (Biological Industries, IL, USA). Cells were incubated with XTT reagent for 2 h at 37 °C in a humidified 5% CO_2/95% air atmosphere. Absorbance was recorded on a VersaMax ELISA microplate reader (Molecular Devices, USA) at 450 nm with 650 nm being the reference wavelength. Cell survival was estimated from the following equation: % cell survival of control = $100 \times (A_t - A_c)$(treatment)/$(A_t - A_c)$(control), where A_t and A_c are the absorbencies (450 nm) of the XTT colorimetric reaction in treated and control cultures, respectively, minus nonspecific absorption measured at 650 nm. Absorbance of the medium alone was also deduced from specific readings. Data points were connected by nonlinear regression lines of the sigmoidal dose−response relation in dose−response assays.

4.2.2 - The CL-BP compound

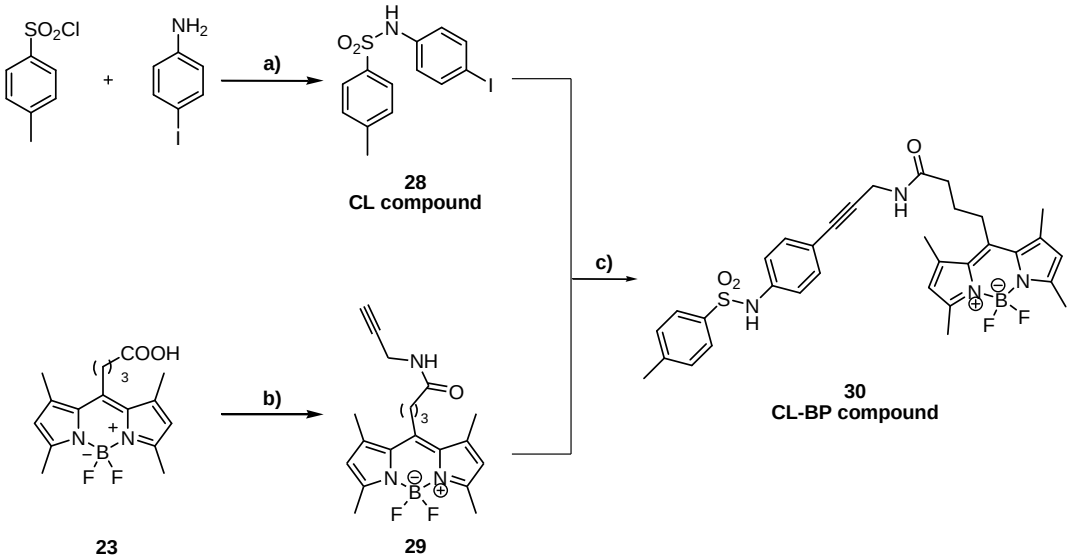

Figure 64. Synthetic pathway for the synthesis of the CL-BP compound. a) H_2O, 25', r.t. (76%); b) propargylamine, ClCOOEt, 4-MMP, THF, 1h, r.t. (99%); c) CuI, $(PPh_3)_2PdCl_2$ 5%, Et_3N, THF, o.n., r.t. (51%).

Synthesis of *N*-(4-iodophenyl)-4-methylbenzenesulfonamide (28)

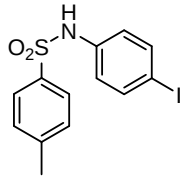

In a round bottom flask a suspension of 4-iodobenzenamine (4.6 mmol, 1g) in water (15 mL) was treated with *p*-toluensulfonyl chloride (5.45 mmol, 1.04 g) at room temperature for 30 minutes. The product was extracted with EtOAc (20 mL x 3), the organic phases were then dried over Na_2SO_4, and the solvent was evaporated under reduced pressure. The crude was purified by chromatography with PE/EtOAc, 8:2 (Rf 0,48) to give the final product (1,29 g, 76%) as a pale yellow solid. ^{1}H-NMR ($CDCl_3$, 200 MHz) δ 7.68 (2H, d, J = 8.4 Hz), 7.52 (2H, d,

J = 8.7 Hz), 7.25 (2H, d, *J* = 8.0 Hz), 6.86 (2H, d, *J* = 8.8 Hz), 2.38 (3H, s). Spectral data correspond to those previously reported in literature.[102]

Synthesis of *N*-(prop-2-ynyl)-4-(4,4-difluoro-1,3,5,7-tetramethyl-4-bora-3a,4a-diaza-s-indacene-8-yl)butyramide (29)

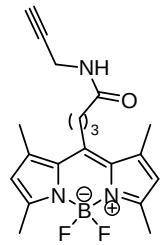

In a three necks round bottom flask under anhydrous conditions, BODIPY (**23**, 0.3 mmol, 100 mg), ethyl chloroformate (0.3 mmol, 29 μL), and 4-methylmorpholine (0.3 mmol, 33 μL) were subsequentially added in THF (20 mL). The solution was stirred at ambient temperature for 10 min, then propargylamine (0.3 mmol, 19 μL) was added to the solution and stirred for 1 h. The product was extracted with EtOAc and 2 M HCl aqueous solution (10 mL x 3), and then with saturated $NaHCO_3$ aqueous solution for neutralization. Afterward, the solution was dried, filtered, and the solvent was evaporated under reduced pressure. The crude was purified by column chromatography on silica gel (EtOAc/PE 7:3 + 0.1 % Et_3N) to give 110 mg of the final product (Rf = 0.46, 99 % yield). ^{1}H-NMR ($CDCl_3$, 200 MHz) δ 6.05 (s, 2H, 2 x CH), 5.66 (br s, 1H, NH), 4.04 – 4.03 (dd, 2H, *J* = 5.2, 2.5 Hz, NHCH_2), 3.06 – 2.97 (m, 2H, CH_2), 2.51 (s, 6H, 2 x CH_3), 2.42 (s, 6H, 2 x CH_3), 2.36 (t, 2H, *J* = 7.1 Hz, CH_2), 2.24 (t, 1H, J = 2.5 Hz, ≡C*H*), 2.05 – 1.90 (m, 2H, CH_2); ^{13}C-NMR ($CDCl_3$, 50 MHz) δ 171.07 (CO), 154.10 (Cq), 145.04 (Cq), 140.44 (Cq), 131.43 (Cq), 121.77 (CH), 79.26 (NHCH$_2$*C*≡), 71.78 (≡CH), 35.91 (CH_2), 29.21 (CH_2), 27.39 (CH_2), 27.15 (CH_2), 16.41 (CH_3), 14.43 (CH_3). HRESIMS *m/z* 343.1761 (calcd for $C_{18}H_{20}BF_2N_3O$ 343.1667).

Synthesis of the CL-BP compound (30)

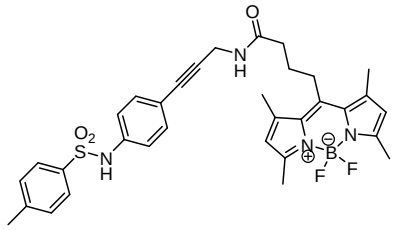

In a glass vial under N_2, *N*-(4-iodophenyl)-4-methylbenzenesulfonamide (**28**, 0.07 mmol, 25 mg) was introduced and, after few minutes anhydrous THF (4 mL) was added and properly degassed by bubbling N_2. Then Et_3N (0.3 mmol, 40 μL), CuI (10%, 1 mg) and $(PPh_3)_2PdCl_2$ (5%, 2 mg) were sequentially added and degassed again. Lastly the alkyne (**29**, 0.08 mmol, 30 mg) was introduced and the system was degassed one more time. The reaction was stirred at room temperature overnight. After TLC analyses, the mixture was quenched with saturated solution of NH_4Cl and stirred for 20 minutes and then extracted with CH_2Cl_2 (15 mL x 3). The combined organic phases were washed brine, dried over Na_2SO_4 and the solvent was removed *in vacuo*. The crude product was purified by column chromatography on silica gel with EtOAc/PE 7 : 3 (Rf = 0.43) to give CL-BP (21 mg, 51%) as a pale yellow solid. ^{1}H-NMR ($CDCl_3$, 200 MHz): δ 7.66 – 7.62 (d, 2H, *J* = 8.3 Hz, 2 x CH), 7.23 – 7.19 (m, 4H, 4 x CH), 7.02 – 6.97 (d, *J* = 8.6 Hz, 2 x CH), 6.89 (s, 1H, NH), 6.03 (s, 2H, 2 x CH), 5.85 – 5.80 (br t, 1H, NH), 4.25 – 4.22 (d, 2H, *J* = 5.1 Hz, NHC*H*$_2$), 3.05 – 2.97 (m, 2H, CH_2), 2.51 (s, 6H, 2 x CH_3), 2.41 (s, 6H, 2 x CH_3), 2.37 – 2.33 (m, 5H, CH_3 + CH_2), 2.01 – 1.91 (m, 2H, CH_2); ^{13}C-NMR ($CDCl_3$, 50 MHz): δ 171.39 (CO), 154.28 (Cq), 145.26 (Cq), 144.33 (Cq), 140.63 (Cq), 136.99 (Cq), 136.02 (Cq), 132.95 (2 x CH), 131.66 (Cq), 131.62 (Cq), 129.89 (2 x CH), 127.34 (2 x CH), 121.96 (CH), 121.92 (CH), 120.79 (2 x CH), 119.14 (Cq), 84.99 (Cq), 82.88 (Cq), 36.12 (CH_2), 30.21 (CH_2),

27.58 (CH_2), 27.40 (CH_2), 21.69 (CH_3), 16.58 (2 x CH_3), 14.64 (CH_3), 14.61 (CH_3); HRESIMS *m/z* 616.2496 (calcd for $C_{33}H_{35}BF_2N_4O_3S$ 616.2491).

Luminometer assays. Luciferase activity was monitored using the LB942 Tristar2 S luminometer reader (Berthold Technologies). Seven-days-old *Ub:D14:LUC* (Col-0), *Ub:SMXL7:LUC* (Col-0) or *D14p:D14:LUC* Arabidopsis transgenic plants grown in Murashige and Skoog (MS) medium, 1.2 % agar and 1% sucrose were transferred to 96-well microtiter plates containing 170µl of MS 1% Sucrose medium. D-luciferin substrate (Molecular Probes) was added to a final concentration of 9.4 µg/mL per well. Plates were incubated 2-3 h in the light, 15µl of each treatment was added per well and measures were taken every 15 min. Luciferase activity is represented relative to the activity of the mock (solvent) treated plants. For each treatment, at least 16 plants were analyzed.

4.2.3 – Profluorescent probes

Unless otherwise specified, all the reactions were run under an inert atmosphere (argon), following standard procedures for manipulating air-sensitive compounds. All glassware was stored in the oven and/or was flame-dried prior to use. Anhydrous solvents were obtained by filtration through drying columns. Analytical thin-layer chromatography (TLC) were performed on plates pre-coated with silica gel layers. Compounds were visualized by illumination with a short wavelength UV lamp (i.e. = 254 nm). Flash column chromatography was performed using 40-63 mesh silica. Nuclear magnetic resonance spectra (^{1}H; ^{13}C NMR) were recorded respectively at 300 and 75 MHz on a Bruker DPX 300 spectrometer. IR spectra are reported in reciprocal centimeters (cm^{-1}). High-resolution mass spectra (HRMS) were determined by electrospray ionization (ESI) coupled to a time-of-flight analyzer (Waters LCT Premier XE).

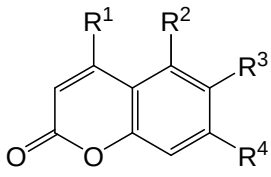

Cumarine derivative

Entry

32 : R^1=CH_2Cl; R^2=H; R^3=H; R^4=OH;
33 : R^1=CH_3; R^2=H; R^3=COOH; R^4=OH;
34 : R^1=CH_3; R^2=H; R^3=H; R^4=SH;
35 : R^1=CH_3; R^2=H; R^3=COO-(2-NO_2Bn); R^4=OH.

General synthetic procedures:

- D-ring attack -

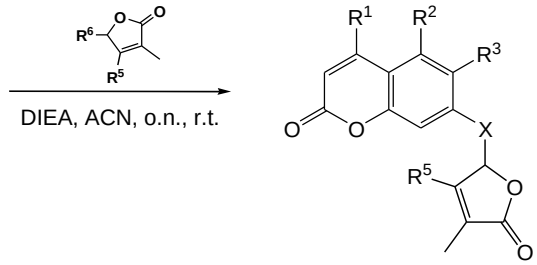

Entry	R^1	R^2	R^3	R^4	R^5	R^6	X	Product	Yield (%)
32	CH_2Cl	H	H	OH	H	Br	O	**36**	43.8
32	CH_2Cl	H	H	OH	CH_3	Cl	O	**37**	26
33	CH_3	H	COOH	OH	H	Br	O	**38 + 40**	12.8 + 1.4
33	CH_3	H	COOH	OH	CH_3	Cl	O	**39 + 41**	19 + 2.6
34	CH_3	H	H	SH	H	Br	S	**42**	53.7
34	CH_3	H	H	SH	CH_3	Cl	S	**43**	59.2
35	CH_3	H	COO-(2-NO_2Bn)	OH	H	Br	O	**44**	33

- Nitrobenzyl introduction -

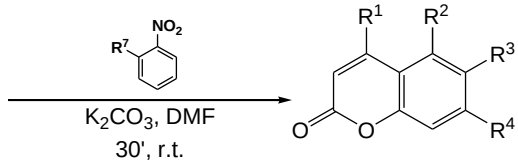

Entry	R^1	R^2	R^3	R^4	R^7	Prod	Yield (%)
33	CH_3	H	-COO-(2-NO_2Bn)	OH	-CH_2Br	**35**	2.5
36	(2-NO_2Ph)$COOCH_2$-	H	H	-O-Dring	COOH	**45**	29

Figure 65. Synthetic pathway for the synthesis of profluorescent probes having cumarine scaffolds.

Synthesis of 4-(chloromethyl)-7-hydroxy-2H-chromen-2-one (32).

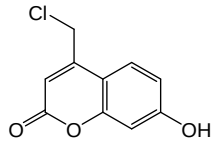

In a round bottom flask resorcinol (20 mmol, 2.20 g) and ethyl 4-chloroacetoacetate (20 mmol, 2.72 mL) were introduced and stirred. The solution was brought to 0 °C, and then H_2SO_4 60% (50 mL) was added dropwise. The reaction was stirred at room temperature over night. After complete conversion, ice cold water was slowly added some ice cold water and stirred for 1 h. The resulting precipitate was collected by filtration, washed with iced water and dried giving the desired product as a white solid (yield: 2.10 g, 50.2 %). ^{1}H-NMR (300 MHz, DMSO): δ 10.66 (s, 1H), 7.67 (d, 1H), 6.84 (dd, 1H), 6.75 (d, 1H), 6.42 (s, 1H), 4.96 (s, 2H) ppm. Spectral data correspond to those previously reported in literature.[103]

Synthesis of 7-hydroxy-4-methyl-2-oxo-2H-chromene-6-carboxylic acid (33).

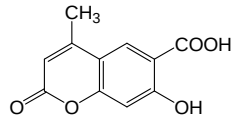

A solution of 2,4-dihydroxy benzoic acid (6.49 mmol, 1.0 g) in ethyl acetoacetate (19.5 mmol, 2.46 mL) was slowly added under constant stirring to ice cold H_2SO_4 (5.0 ml). Once the addition was completed, the reaction mixture was stirred for 6 h at room temperature and the progress of the reaction was monitored by TLC. Upon complete conversion, some ice cold water was slowly added and stirring continued. The resulting precipitate was collected by filtration, washed with ice water and dried giving the desired product as a pale yellow solid (yield: 0.8 g,

56%). ^{1}H-NMR (300 MHz, DMSO): δ 8.12 (s, 1H), 6.91 (s, 1H), 6.27 (s, 1H), 2.41 (s, 3H) ppm. Spectral data correspond to those previously reported in literature.[104]

General procedure for the introduction of the D-ring.

To a solution of 5-bromo-3-methylfuran-2(5*H*)-one or 5-chloro-3,4-dimethylfuran-2(5*H*)-one (1.2 eq) in anhydrous CH_3CN (4 mL for 100 mg of cumarine), the cumarine derivative (1 eq) and *N*,*N*-Diisopropylethylamine (DIEA, 4.7 eq) were sequentially added under argon atmosphere. The resulting mixture was stirred at room temperature for 2 h and checked for completion by TLC. The solvent was removed under vacuum and the resulting residue filtrated and purified on a silica gel column.

4-(chloromethyl)-7- (4-methyl-5-oxo-2,5-dihydrofuran-2-yloxy) -2H-chromen-2-one (36)

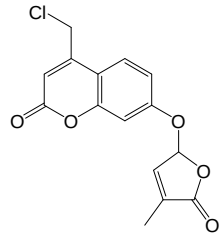

The product was purified by a silica gel column (CH_2Cl_2/MeOH 95:5) and obtained as a white solid (32 mg, 43.8%). ^{1}H-NMR (300 MHz, $CDCl_3$): δ 7.64 (d, 1H, *J* = 8.9 Hz, CH), 7.12 – 7.09 (m, 2H, 2 x CH), 7.03 (br s, 1H, CH), 6.48 (s, 1H, CH), 6.37 (s, 1H, CH), 4.64 (s, 2H, CH_2), 2.04 (s, 3H, CH_3); ^{13}C-NMR (75 MHz, $CDCl_3$): δ 170.86 (Cq), 160.30 (Cq), 159.35 (Cq), 155.40 (Cq), 149.34 (Cq), 141.71 (CH), 135.18 (Cq), 125.78 (CH), 114.36 (CH), 113.62 (CH), 113.20 (Cq), 105.27 (CH), 98.13 (CH), 41.37 (CH_2), 10.83 (CH_3); IR ν_{max} (film, cm^{-1}): 1615, 1730, 1778, 2972; HRMS (ESI): *m/z* calc. for $C_{15}H_{12}ClO_5$ $[M + H]^+$: 307.0373, found: 307.0369.

4- (chloromethyl) -7- (3,4- dimethyl -5- oxo -2,5- dihydrofuran -2- yloxy) -2H-chromen-2-one (37)

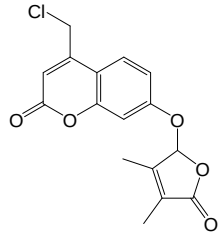

The product was purified by a silica gel column (CH_2Cl_2/MeOH 95:5) and obtained as a white solid (20 mg, 26 %). ^{1}H-NMR (300 MHz, $CDCl_3$): δ 7.64 (d, 1H, *J* = 9.6 Hz, CH), 7.13 – 7.10 (m, 2H, 2 x CH), 6.47 (s, 1H, CH), 6.16 (s, 1H, CH), 4.64 (s, 2H, CH_2), 2.11 (s, 3H, CH_3), 1.92 (s, 3H, CH_3); ^{13}C-NMR (75 MHz, $CDCl_3$): δ 171.38 (Cq), 160.32 (Cq), 159.64 (Cq), 155.40 (Cq), 153.21 (Cq), 149.36 (Cq), 127.61 (Cq), 125.77 (CH), 114.26 (CH), 113.56 (CH), 113.11 (Cq), 105.17 (CH), 99.77 (CH), 41.37 (CH_2), 11.73 (CH_3), 8.72 (CH_3); IR ν_{max} (film, cm^{-1}) : 1614, 1726, 1771, 2059, 2334, 2854, 2925, 3087, 3535; HRMS (ESI): *m/z* calc. for $C_{16}H_{14}ClO_5$ $[M + H]^+$: 321.0522, found: 321.0530.

4-methyl-7- (4-methyl-5-oxo-2,5-dihydrofuran-2-yloxy) -2-oxo -2H-chromene-6-carboxylic acid (38)

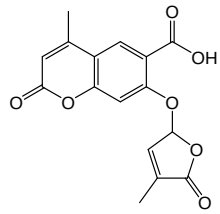

The product was purified by a silica gel column (CH_2Cl_2/EtOAc 8:2) giving **31** as a pale yellow solid (92 mg, 12.8 %). ^{1}H-NMR (300 MHz, $CDCl_3$): δ 10.66 (s, 1H, OH), 8.03 (s, 1H, CH), 7.14 – 7.08 (m, 2H, 2 x CH), 6.89 (s, 1H, CH), 6.18 (s, 1H, CH), 2.41 (s, 3H, CH_3), 2.07 (s, 3H, CH_3); ^{13}C-NMR (75 MHz, $CDCl_3$): δ 170.78 (Cq), 167.84 (Cq), 164.70 (Cq), 159.90 (Cq), 159.39 (Cq), 151.97 (Cq), 141.54

(CH), 135.58 (Cq), 127.99 (CH), 113.78 (Cq), 113.47 (CH), 108.42 (Cq), 105.41 (CH), 93.45 (CH), 18.93 (CH_3), 11.01 (CH_3); IR ν_{max} (film, cm^{-1}) : 1578, 1630, 1685, 1733, 1780, 2927, 2987, 3093, 3193; HRMS (ESI): *m/z* calc. for $C_{16}H_{13}O_7$ $[M + H]^+$: 317.0661, found: 317.0648.

4-methy l-5- oxo -2,5- dihydrofuran-2-yl 4-methyl-7- (4-methyl -5 –oxo -2,5-dihydrofuran-2-yloxy)-2-oxo-2H-chromene-6-carboxylate (40)

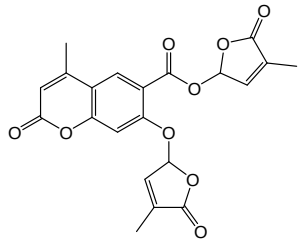

The product was purified by preparative TLC (CH_2Cl_2/EtOAc 8:2) and obtained as a pale yellow solid (13 mg, 1.4 %) and as a mixture of two diastereoisomers 1:1. ^{1}H-NMR (300 MHz, $CDCl_3$): δ 8.06 (s, 1H, CH), 8.02 (s, 1H, CH), 7.24 – 7.20 (m, 1H, CH), 7.05 – 6.97 (m, 3H, 3 x CH), 6.27 (s, 1H, CH), 6.20 (s, 1H, CH), 2.38 (s, 3H, CH_3), 1.97 (s, 6H, 2 x CH_3); ^{13}C-NMR (75 MHz, $CDCl_3$): δ 170.75 (Cq), 159.51 (Cq), 158.95 (Cq), 158.71 (Cq), 157.76 (Cq), 151.63(Cq), 142.08 (CH), 141.74 (CH), 135.24 (Cq), 134.94 (Cq), 134.88 (Cq), 129.19 (CH), 116.29 (Cq), 115.91 (Cq), 114.74 (CH), 106.66 (CH), 99.30 (CH), 93.23 (CH), 18.85 (CH_3), 10.85 (2 x CH_3); IR ν_{max} (film, cm^{-1}) : 1567, 1612, 1625, 1725, 1775, 2926, 3093; HRMS (ESI): *m/z* calc. for $C_{21}H_{17}O_9$ $[M + Na]^+$: 413.0873, found: 413.0871.

7- (3,4- dimethyl -5- oxo -2,5- dihydrofuran -2- yloxy) -4- methyl -2- oxo -2H- chromene-6-carboxylic acid (39)

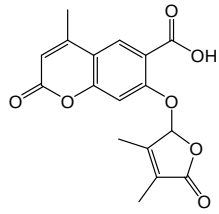

The product was purified by silica gel column (CH_2Cl_2/EtOAc 9:1) and obtained as a white solid (164 mg, 19 %). ^{1}H-NMR (300 MHz, $CDCl_3$): δ 10.69 (s, 1H, OH), 8.02 (s, 1H, CH), 7.04 (s, 1H, CH), 6.90 (s, 1H, CH), 6.18 (s, 1H, CH), 2.41 (s, 3H, CH_3), 2.07 (s, 3H, CH_3), 1.95 (s, 3H, CH_3); ^{13}C-NMR (75 MHz, $CDCl_3$): δ 171.24 (Cq), 168.09 (Cq), 164.68 (Cq), 159.83 (Cq), 159.36 (Cq), 152.84 (Cq), 151.86 (Cq), 128.72 (Cq), 127.80 (CH), 113.71 (Cq), 113.41 (CH), 108.41 (Cq), 105.38 (CH), 94.52 (CH), 18.84 (CH_3), 11.68 (CH_3), 8.85 (CH_3); IR ν_{max} (film cm^{-1}) : 1573, 1631, 1686, 1732, 1781, 2262, 2973, 3096, 3197; HRMS (ESI): *m/z* calc. for $C_{17}H_{15}O_7$ $[M + H]^+$: 331.0818, found: 331.0829.

3,4- dimethyl -5- oxo -2,5- dihydrofuran -2- yl 7-(3,4-dimethyl -5- oxo -2,5-dihydrofuran -2-yloxy) -4- methyl -2- oxo -2H- chromene -6- carboxylate (41)

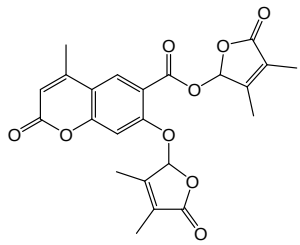

The product was purified through preparative TLC (CH_2Cl_2/EtOAc 9:1) and obtained as a white solid (27 mg, 2.6 %) and as mixture of two diastereoisomers 1:1. ^{1}H-NMR (300 MHz, $CDCl_3$): δ 8.18 (s, 1H, CH), 8.07 (s, 1H, CH), 7.34 (s, 1H, CH), 7.31 (s, 1H, CH), 6.99 – 6.98 (2 x s, 2H, 2 x CH), 6.26 (s, 2H, 2 x CH),

6.18 (br s, 2H, 2 x CH), 2.45 – 2.44 (2 x s, 6H, 2 x CH_3), 2.17 (s, 3H, CH_3), 2.09 (s, 3H, CH_3), 2.04 – 2.01 (2 x s, 6H, 2 x CH_3), 1.92 – 1.90 (2 x s, 12H, 4 x CH_3); ^{13}C-NMR (75 MHz, $CDCl_3$): δ 171.66 (Cq), 171.52 (Cq), 171.19 (Cq), 163.26 (Cq), 162.20 (Cq), 159.59 (Cq), 159.19 (Cq), 159.98 (Cq), 157.96 (Cq), 157.86 (Cq), 153.59 (Cq), 153.52 (Cq), 151.65 (Cq), 129.97 (CH), 129.20 (CH), 127.68 (Cq), 127.55 (Cq), 127.50 (Cq), 127.44 (Cq), 115.85 (Cq), 115.69 (Cq), 115.52 (Cq), 115.46 (Cq), 114.56 (CH), 105.44 (CH), 105.06 (CH), 100.59 (CH), 100.29 (CH), 94.49 (CH), 94.30 (CH), 18.87 (CH_3), 18.80 (CH_3), 11.76 (2 x CH_3), 11.62 (2 x CH_3), 8.75 (2 x CH_3), 8.66 (2 x CH_3); IR ν_{max} (film, cm^{-1}): 1567, 1613, 1625, 1697, 1730, 1773, 2255, 2856, 2925, 3537; HRMS (ESI): *m/z* calc. for $C_{23}H_{21}O_9$ $[M + H]^+$: 441.1186, found: 441.1188.

4-methyl-7- (4-methyl-5-oxo-2,5-dihydrofuran-2-ylthio) -2H- chromen -2- one (42)

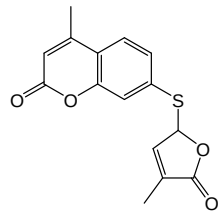

The product was purified on a silica gel column (CH_2Cl_2 100%) and obtained as a white solid (80 mg, 53.7 %). ^{1}H-NMR (300 MHz, $CDCl_3$): δ 7.57 – 7.43 (m, 3H, 3xCH), 7.04 (s, 1H, CH), 6.30 (s, 1H, CH), 6.22 – 6.21 (m, 1H, CH), 2.43 (s, 3H, CH_3), 1.92 (s, 3H, CH_3); ^{13}C-NMR (75 MHz, $CDCl_3$): δ 172.34 (CO), 160.22 (CO), 153.54 (Cq), 151.84 (Cq), 144.07 (CH), 136.27 (Cq), 133.19 (Cq), 127.75 (CH), 125.24 (CH), 120.10 (CH), 120.0 (Cq), 115.79 (CH), 85.16 (CH), 18.75 (CH_3), 10.80 (CH_3); IR ν_{max} (film, cm^{-1}) : 1602, 1653, 1688, 1717, 1765, 2033, 2333, 2924, 2946, 3068, 3515; HRMS (ESI): *m/z* calc. for $C_{15}H_{13}O_4S$ $[M + H]^+$: 289.0530, found: 289.0535.

7- (3,4-dimethyl-5-oxo-2,5-dihydrofuran-2-ylthio) -4- methyl -2H- chromen -2-one (43)

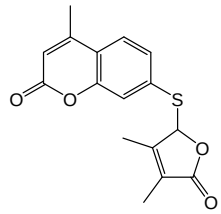

The product was purified on a silica gel column (CH_2Cl_2 100%) and obtained as a white solid (93 mg, 59.2 %). ^{1}H-NMR (300 MHz, $CDCl_3$): δ 7.56 – 7.53 (m, 1H, CH), 7.45 – 7.43 (m, 2H, 2 x CH), 6.30 (s, 1H, CH), 6.03 (s, 1H, CH), 2.43 (s, 3H, CH_3), 2.09 (s, 3H, CH_3), 1.78 (s, 3H, CH_3); ^{13}C-NMR (75 MHz, $CDCl_3$): δ 172.51 (CO), 160.24 (CO), 154.85 (Cq), 153.47 (Cq), 151.87 (Cq), 135.79 (Cq), 128.16 (CH), 126.93 (Cq), 125.19 (CH), 120.29 (CH), 120.06 (Cq), 115.81 (CH), 87.83 (CH), 18.75 (CH_3), 12.84 (CH_3), 8.86 (CH_3); IR ν_{max} (film, cm^{-1}) : 1602, 1621, 1686, 1719, 1735, 1761, 2342, 2924, 3065, 3519; HRMS (ESI): *m/z* calc. for $C_{16}H_{15}O_4S$ $[M + H]^+$: 303.0696, found: 303.0691.

2-nitrobenzyl 4-methyl-7- (4-methyl-5-oxo-2,5-dihydrofuran-2-yloxy) -2-oxo-2H-chromene-6-carboxylate (44)

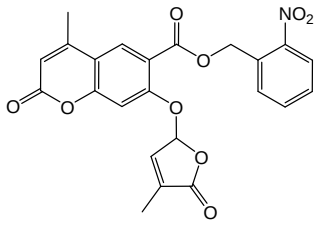

The product was purified on a silica gel column (heptane/EtOAc 6:4) and obtained as a light pink solid (9 mg, 33%). ^{1}H-NMR (300 MHz, $CDCl_3$): δ 8.17 (s, 1H, CH), 8.10 (d, 1H, *J* =, 7.9 Hz, CH), 7.66 – 7.64 (m, 2H, 2 x CH), 7.56 – 7.53 (m, 1H, CH), 7.30 (s, 1H, CH), 7.02 – 7.01 (m, 1H, CH), 6.35 – 6.34 (m, 1H, CH),

6.27 (d, 1H, *J* = 1.1 Hz, CH), 5.74 (s, 2H, CH_2), 2.46 (s, 3H, CH_3), 2.01 (s, 3H, CH_3); ^{13}C-NMR (75 MHz, $CDCl_3$): δ 170.74 (Cq), 163.98 (Cq), 159.79 (Cq), 158.51 (Cq), 157.43 (Cq), 151.88 (Cq), 141.80 (CH), 135.18 (Cq), 133.76 (CH), 131.42 (Cq), 130.19 (CH), 129.58 (CH), 129.48 (CH), 125.27 (CH), 117.39 (Cq), 115.90 (Cq), 114.58 (CH), 106.10 (CH), 99.52 (CH), 64.29 (CH_2), 18.77 (CH_3), 10.86 (CH_3); IR ν_{max} (film, cm^{-1}) : 1613, 1625, 1733, 1782, 2164, 2855, 2925, 2955; HRMS (ESI): *m/z* calc. for $C_{23}H_{18}NO_9$ $[M + H]^+$:452.1000, found: 452.0982.

General procedure for the introduction of the nitro-benzyl fragment.

In a round bottom flask, cumarine derivative **33** or **36** (1 eq) was dissolved in 2 mL of DMF. Then, K_2CO_3 was added (1.2 eq), followed by 1-(bromomethyl)-2-nitrobenzene (1eq) in case of **33**, or 2-nitrobenzoic acid in case of **36** precursor, and the reaction was stirred at room temperature for 30 minutes. The reaction mixture was then diluited with ethyl acetate and the organic phase washed with citric acid solution 10%, then with saturated $NaHCO_3$ aqueous solution, and finally with brine. The organic phase was dried (Na_2SO_4), and the solvents removed under vacuum. The product was then purified by column chromatography on silica gel.

2-nitrobenzyl 7-hydroxy-4-methyl-2-oxo-2H-chromene-6-carboxylate (35)

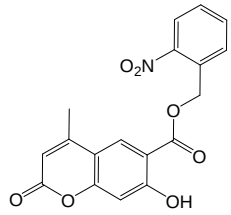

The product was purified by column chromatography (heptane/EtOAc from 95:5 to 9:1) and obtained as a white solid (80 mg, 2.5 %). ^{1}H-NMR (300 MHz,

$CDCl_3$): 10.91 (s, 1H, OH), 8.13 – 8.10 (m, 2H, 2 x CH), 7.72 – 7.76 (m, 1H, CH), 7.61 – 7.54 (m, 2H, 2 x CH), 6.89 (s, 1H, CH), 6.18 (s, 1H, CH), 5.82 (s, 2H, CH_2), 2.43 (s, 3H, CH_3); ^{13}C-NMR (75 MHz, $CDCl_3$): δ 168.28 (Cq), 164.03 (2 x Cq), 159.70 (Cq), 158.57 (Cq), 151.72 (Cq), 133.43 (CH), 130.30 (Cq), 129.35 (CH), 127.23 (CH), 124.95 (CH), 113.18 (CH), 112.78 (Cq), 108.92 (CH), 104.79 (Cq), 63.91 (CH), 29.42 (CH_2), 18.31 (CH_3); IR ν_{max} (film, cm^{-1}) : 1679, 1732, 2851, 2921; HRMS (ESI): *m/z* calc. for $C_{18}H_{14}NO_7$ $[M + H]^+$: 356.0757, found: 356.0770.

(7-(4-methyl-5-oxo-2,5-dihydrofuran-2-yloxy)-2-oxo-2H-chromen-4-yl)methyl 2-nitrobenzoate (45)

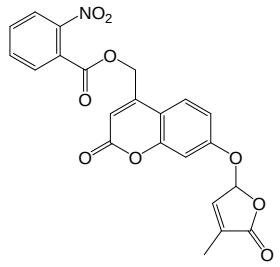

The product was purified through column chromatography (heptane/EtOAc 1:1) and obtained as a white solid. (26 mg, 29 %). ^{1}H-NMR (300 MHz, $CDCl_3$): 8.01 – 7.99 (d, 1H, *J* = 7.8 Hz, CH), 7.79 – 7.69 (m, 3H, 3 x CH), 7.55 – 7.53 (d, 1H, J = 8.6 Hz, CH), 7.12 – 7.02 (m, 3H, 3 x CH), 6.42 (s, 1H, CH), 6.37 (s, 1H, CH), 5.51 (s, 2H, CH_2), 2.04 (s, 3H, CH_3); ^{13}C-NMR (75 MHz, $CDCl_3$): δ 170.87 (Cq), 164.91 (Cq), 160.25 (Cq), 159.36 (Cq), 155.23 (Cq), 147.76 (Cq), 141.74 (CH), 135.15 (Cq), 133.47 (CH), 132.52 (CH), 129.97 (CH), 126.85 (Cq), 125.22 (CH), 124.40 (CH), 114.34 (Cq), 113.73 (CH), 112.97 (Cq), 112.61 (CH), 105.25 (CH), 98.14 (CH), 63.17 (CH_2), 10.81 (CH_3); IR ν_{max} (film, cm^{-1}): 1615, 1731, 1779, 2853, 2924, 3094; HRMS (ESI): *m/z* calc. for $C_{22}H_{16}NO_9$ $[M + H]^+$:438.0822, found: 438.0825.

Author contribution:

X-ray were recorded by the Dr. Domenica Marabello (Department of Chemistry, University of Turin); biological tests have been performed by the PhD Beatrice Lace (Department of Chemistry, University of Turin); CD spectra, presented in the "Results and discussion" section, have been recorded by the Dr. Elena Ghibaudi (Department of Chemistry, University of Turin); Luminometer assays were performed by the PhD student Elena Sanchez (Centro Nacional de Biotecnología-CSIC, Plant Molecular Genetics Department, Madrid, Spain).

Scientific group supervisors: Professor Hinanit Koltai and Professor Yoram Kalpunik (ARO Volcani Center, Israel), Dr. Mara Novero (DBIOS, University of Turin), Professor Ernesto Occhiato, Dr. Dina Scarpi (Department of Chemistry, University of Florence), Dr. Pilar Cubas (Centro Nacional de Biotecnología-CSIC, Plant Molecular Genetics Department, Madrid, Spain), Professor Cristina Prandi (Department of Chemistry, University of Turin).

CHAPTER 5

- SLs and DRUG DELIVERY SYSTEMS -

5.1 – Results and discussion

The last section of my PhD research project was focused on the delivery of SL derivatives, both for biomedical and biological/agriculture application.

In medicine, this study stemmed from the encouraging results published by the research group were I developed my PhD project, which had shown the activity of SLs analogues on different cancer cell lines (Section 2.1).[67,69] The high activity of the compounds is in some extends jeopardized by the the low stability of this class of molecules at pH higher than 7. Indeed, the high reactivity of the SL enol ether bridge would bring to hydrolysis in alkaline medium, with the consequent release of an ABC-formyl lactone and 5-hydroxybutenolide fragment. In addition, they suffer of a very poor aqueous solubility.

To overcome the aforementioned problems and to improve the SL therapeutic potential and possible applications in agriculture we undertook a study aimed at pinpointing efficient and biodegradable delivery systems. Our attention was drawn to β-cyclodextrin nanosponges, polymeric derivatives of natural cyclic oligosaccharides (i. e. cyclodextrins) cross-linked by means of carbonate or ester bonds.

The name comes from their ability of forming flexible structures similar to sponges, able to adapt and entrap small molecules in their matrix and to retain aqueous solutions up to 40 times their own weight. Contrary to the other polymers in the trade, they are totally biodegradable. In addition, they can be designed to perfectly adapt the occupant by the cross-linker connecting the cyclodextrins units. Consequence of the linker variation is the different swelling capability, key aspect to be considered. Indeed, changing the cross-linker and switching to a more flexible one might just enable to realize a delivery system which tend to give a better accommodation of the strigolactone molecule.

Furthermore, the dual nature of cyclodextrins is crucial: hydrophobic inside, perfect for a good interaction with the SL molecule, and hydrophilic outside, which would allow to solve the solubility problem.

We run preliminary studies on the possible use of cyclodextrin nanosponges as strigolactone analogs carriers.

We started our investigation with nanosponge βNS-CDI, obtained using 1,1'-carbonylimidazole as cross-linking agent between β-cyclodextrins monomers. We evaluated the characteristics of the nanosponge suspensions before and after compounds addition, and the amount of complexed drug (Table 7). Differential scanning calorimetry (DSC) analysis was used to investigate the complexation of SLs within the NS structure. Indeed, when an inclusion complex is formed the melting peak of guest compound is either shifted or decreased in intensity. In some cases it can even disappear.

Formulation	pH	Zeta potential ± SD (mV)	Title (% w/w)
βNS-CDI	7.40	- 31.2 ± 1.4	--
βNS-CDI + GR24	5.45	-28.5 ± 0.8	25.3
βNS-CDI + EGO10	6.70	- 23.6 ± 1.2	5.6
βNS-CDI + MEB55	6.33	- 29.2 ± 0.7	6.85
βNS-CDI + EDOT-EA	6.65	- 30.7 ± 1.5	24.5

Table 7. Chemico-physical characterization of nanosponges suspensions before and after the analogues addition.

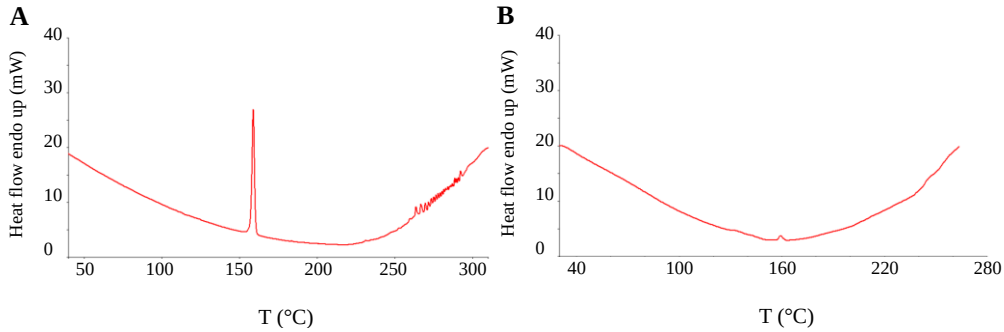

Figure 66. DSC thermograms of (±)-GR24 (A) before and (B) after the complexation inside β-CDI-NS.

Once confirmed the occurred complexation we thought about the different swelling capability of different nanosponges. As a matter of fact carbonate nanosponges are extremely compact.

MEB-55 was firstly selected as guest molecule because of the encouraging results obtained towards tumour cells. The incubation in pyromellitic nanosponges gave a title amount of 6.28 %, measured by HPLC analysis. The estimation of kinetic releases (Figure 67), performed using Franz cells and analyzed through HPLC, provided the evidence on how much the cross-linker difference can influence bioactivity.

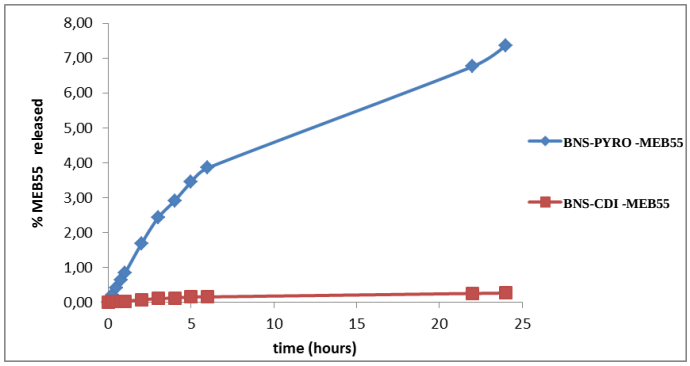

Figure 67. *In vitro* release kinetics of MEB55 from βNS-CDI and βNS-PYRO nanosponges.

Indeed, even if the strigolactone molecule was well incubated in two different nanosponges, the carbonate and the pyromellitic ones, only in this second case the percentage of analogue released was consistent, making them more suitable for practical applications.

The drug was then tested on living cells of the MDA-MB-231 breast cancer cell line. Figure 68 reports the percentage of tumor cells inhibited. The activity of free guest MEB55 molecule was evaluated at different concentrations and compared to its corresponding complexed versions in carbonate- or pyro-NS.

The results obtained suggest a MEB55 activity enhanced when loaded in pyro-NS formulations. By contrast the inclusion in βNS-CDI was revealed as not feasible, probably due to its compact structure which prevent the guest to go outside the delivery system, with a consequent no effect on cancer cells.

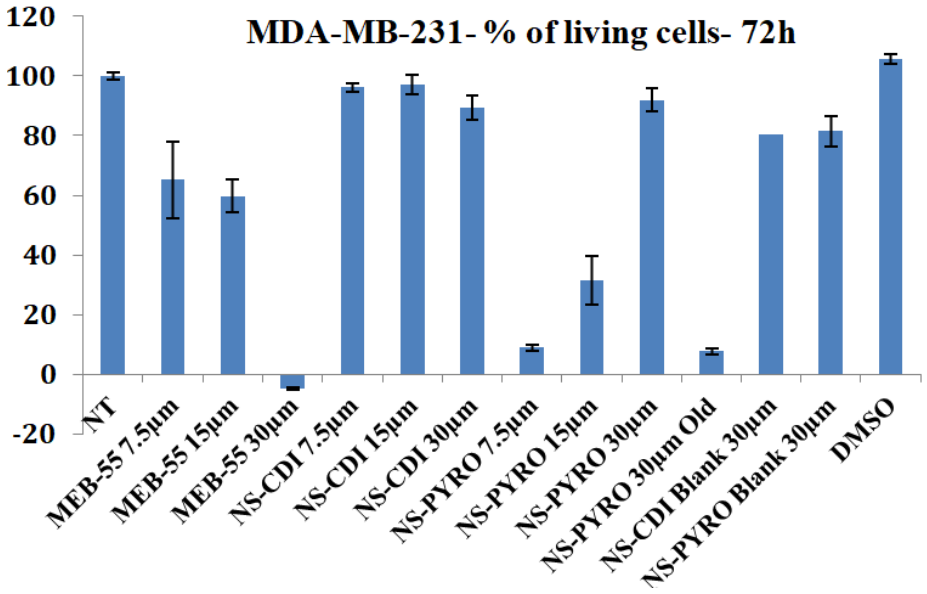

Figure 68. Percentages of living cells after the SLs treatment over 72 hours. Cancer cell line: MDA-MB-231 (breast cancer cells).

Intrigued by the noteworthy discrepancy in terms of bioactivity, we put forward an additional consideration: could be possible to have a selective release of the active compound towards cancer cells exclusively?

Therefore new cyclodextrin-based nanosponges responsive to intracellular stimuli have been evaluated as SL analogues carriers.[77]

Since the intracellular concentration of GSH (2–10 mM) was found to be greater than that of plasma (2-20 μM), and even higher in tumor cells, glutathione has been recognized as an internal stimulus for the selective release of active compounds towards tumor cells.[75,76]

Glutathione-responsive nanosponges (GSH-NS) have been recently developed as smart nanocarriers.[77] Essentially, for these systems the glutathione presence triggers a nanocarrier destabilization based on a redox reaction between the NS disulfide bridges and GSH thiol groups, which brings to the consequent guest

outflow. Along this line the MEB55 molecule was encapsulated inside GSH-nanosponge. The formulation was chemico-physically characterized to prove the stability of the system (Table 8). HPLC analysis demonstrate that the strigolactone molecule was loaded with a 13.9 percentage and an encapsulation efficiency of 87%.

Formulation	Average diameter ± SD (nm)	Polidispersity index	Zeta potential ± SD (mV)
Blank GSH-NS	203.4 ± 12.3	0.20 ± 0.01	-31.5 ± 3.8
GSH-NS + MEB55	217.3 ± 23.2	0.21 ± 0.02	-27.6 ± 2.3

Table 8. Chemico-physical characterization of blank and SL loaded GSH-NS formulations.

The occurred complexation was confirmed through DSC analysis (not shown) and FTIR (Figure 69), where the disappearance and the shift of the MEB55 peak respectively suggest an interaction with the delivery system.

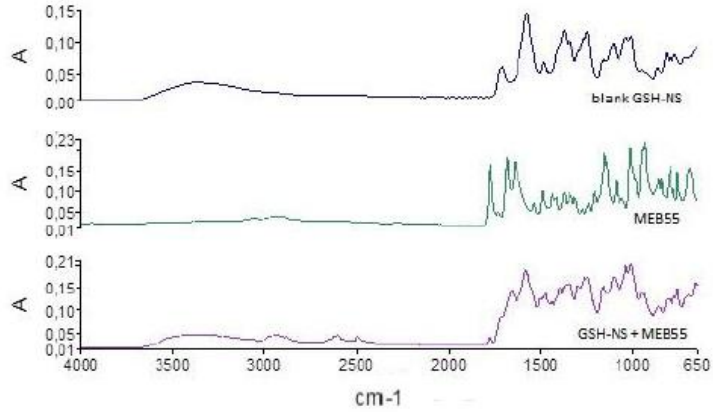

Figure 69. FTIR spectra of blank GSH-NS, MEB55 and MEB55 complexed in GSH-NS.

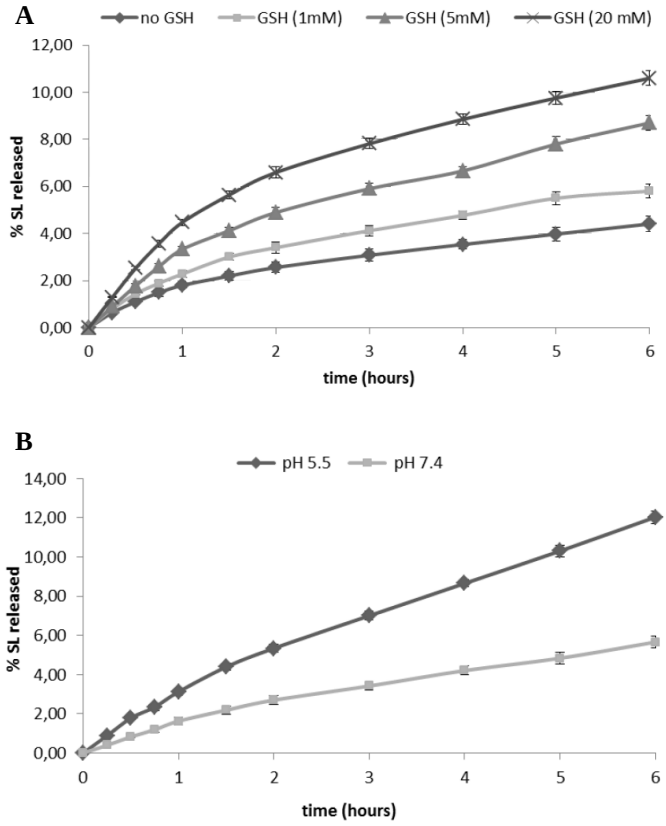

Figure 70. *In vitro* release kinetics of MEB55 from GSH-NS (A) at different glutathione concentrations (1, 5, 20 mM); (B) at different pH values (5.5, 7.4) in the presence of 1 mM of GSH.

Then, in order to prove the redox-sensitive release of the SL molecule from the GSH-NS, two different *in vitro* tests were carried out: one increasing the glutathione amount in the receiving phase, and the other varying the pH values. As shown in Figure 70 the percentage of strigolactone released was highly influenced by the GSH content, and more consistent at acidic pH values than at basic ones, perfectly in line with the polymeric structure of the nanosponge.

Since the strigolactone efficacy towards prostate cancer cells has already been proved,[105] two different cell lines belonging to this class were selected: DU145 and PC-3. These are characterized by an high (12 μM of GSH per mg of protein) and low (7 μM of GSH per mg of protein) GSH content respectively.[106]

MEB55 and the respective nanoformulations were tested in the 10-0.1 μM range (Figure 71). As expected, when the MEB55 was subministrated in the absence of the delivery system no difference was observed between the two cell lines. By

contrast, when incubated in the nanosponge structure, the cells disclosing a higher GSH content were more inhibited.

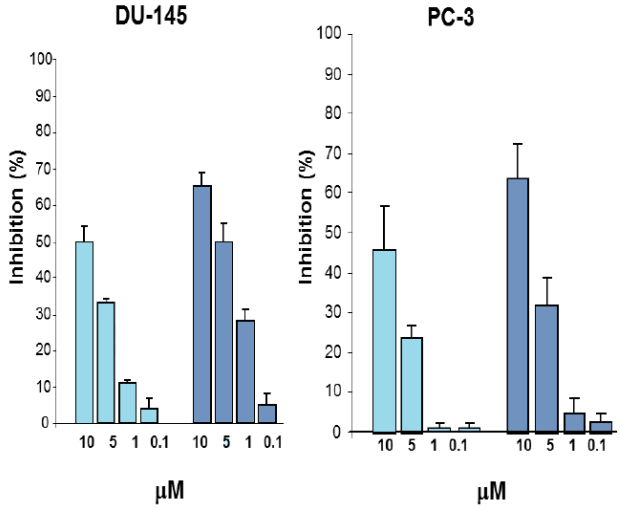

Figure 71. Cell viability after the SL and SL-loaded GSH-NS treatment. Results expressed as percentage of inhibition, obtained after 24h of treatment. MEB55; MEB55 GSH-NS.

Therefore, in accordance with the aforementioned results, MEB55 strigolactone analogue was successfully internalized in the GSH-NS carrier and released in significant extent at higher GSH concentrations and acidic pH. The selected delivery system thus seems to be a promising tool for the selective SL release in response to intracellular stimuli.

5.2 – Experimental

β-CDs were a gift from Roquette Italia (Cassano Spinola - Italy). All reagents were of analytical grade. Laboratory reagents were from Sigma-Adrich unless otherwise specified. Cell culture reagent were purchased from Gibco/Invitrogen (Life Technologies, Paisley, UK) except where otherwise indicated.

Cells. For strigolactone-loaded CDI-NS and PYRO-NS the study was performed on the MDA-MB-231 cell line. For strigolactone-loaded GSH-NS, the study was performed on two ATCC (Manassas) cell lines, PC-3 and DU145. Cells were grown in culture dishes as a monolayer in RPMI 1640 medium plus 10% FCS, 100 U·mL-1 penicillin, and 100 μg·mL-1 streptomycin at 37 °C in a 5% CO_2 humidified atmosphere.

Synthesis of CDI–NS. Briefly, 11.45 mmol of anhydrous β-CD (dehydrated in oven at 120° C for 12 h) was added to 78 mL anhydrous DMF in round bottom flask to achieve complete dissolution by observing transparent solution. Then a suitable amount of 1,1'-carbonyldiimidazole (CDI) was added as a cross-linker. This reaction mixture was heated up to 90° C in an oil bath. After approximately 20 min the gelation process occurred. Once the condensation reaction was completed, the transparent block of cross-linked CD was ground and filtered with excess of deionized water to remove excess of DMF. Lastly, residual by-products or unreacted reagents were completely removed by Soxhlet extraction with ethanol. After purification, CDI–NS were dried by exposure to air and then stored at ambient temperature until further use.

Synthesis of PYRO-NS. Briefly, 11.35 g of anhydrous β-CD (10.00 mmol) and a suitable amount of pyromellitic dianhydride were dissolved in 100 mL of DMSO containing 2.7 mL triethylamine (19.4 mmol), and were allowed to react at room temperature for 3 h. Once the reaction was over, the solid obtained was ground in a mortar, rinsed with an excess of deionized water, under vacuum filtration and Soxhlet extracted with acetone for 24 h. After purification, PYRO–NS was dried by exposure to air and then stored at ambient temperature until further use.

Synthesis of GSH-responsive nanosponge. GSH-responsive nanosponges (GSH-NS) were obtained in a one step synthetic route, by reacting β-cyclodextrin, pyromellitic dianhydride as cross-linking agent and 2-hydroxyethyl disulfide (DHES), in dimethylsulfoxide (DMSO) in order to insert disulfide bridges in the polymer matrix, following the procedure previously reported by Trotta et al.[77] Briefly, 4.00 g (3.52 mmol) of anhydrous β-CD (desiccated in oven at 100 °C, up to constant weight) were dissolved in 16 mL of DMSO in a 100 mL round bottom flask. Once a clear solution was obtained, 0.400 g (2.59 mmol) of DHES, 4.0 mL (28.70 mmol) of triethylamine were added and stirred for approximately 30 min. Finally, 11.01 g (48.96 mmol) of pyromellitic dianhydride were introduced. The gelation point was reached after a few minutes but the reaction was allowed to complete for 24 additional hours. Once the reaction was complete, the monolith block was crushed, rinsed with an excess of deionized water, filtered undervacuum and finally purified by means of Soxhlet extraction with acetone (for approximately 24 h). After drying in air, a white powder was collected and stored in a desiccator at room temperature.

Preparation of blank nanosponge nanoformulations. To obtain the nanoformulations from the coarse powder a top-down method was used. Firstly, a weighted amount of NS was suspended in saline solution (NaCl 0.9% w/v) at the concentration of 10 mg/mL under stirring at room temperature. The suspension was then dispersed using a high shear homogenizer (Ultraturrax®, IKA, Konigswinter, Germany) for 5 minutes at 24000 rpm. To further reduce the size of the nanosponges and obtain an almost homogenous nanoparticle distribution, the sample underwent to high pressure homogenization for 90 minutes at a back-pressure of 500 bar, using an EmulsiFlex C5 instrument (Avastin, USA). Then, the GSH-NS nanosuspension was purified by dialysis (Spectrapore, cellulose membrane, cutoff 12000 Da) to eliminate potential synthesis residues. The nanosuspensions were stored at 4 °C.

Preparation of nanosponge nanoformulations containing strigolactones. Strigolactone-loaded NSs were obtained by adding a weighted amount of strigolactone (1.5 mg/ml), solubilised in 100 μl of N-methylpyrrolidone, to the aqueous nanosuspension of NSs (10 mg/ml). The mixture was then stirred at room temperature in the dark for 48 h. Subsequently, a mild centrifugation step was performed to separate the unloaded SLs. The nanoformulations were stored at 4 °C. A volume was freeze-dried to obtain solid powders. Strigolactone solutions were prepared as control; firstly, a weighted amount of SLs was dissolved in N-methylpyrrolidone and then the organic solutions were diluted with saline solution (NaCl 0.9% w/v).

Characterization of nanosponge formulations. Blank and strigolactones-loaded NS formulations were *in vitro* characterized under the physico-chemical profile.

The average diameter and polydispersity index of NS nanoformulations were determined by photon correlation spectroscopy (PCS); the zeta potential was determined by electrophoretic mobility using a 90 Plus instrument (Brookhaven, NY, USA). The analyses were performed at a scattering angle of 90° at a temperature of 25° C, using NS suspension diluted with filtered distilled water. For zeta potential determination, samples of diluted NS formulations were placed in the electrophoretic cell, where an electric field of approximately 15 V/cm was applied. The morphology of NSs was evaluated by Transmission Electron Microscopy (TEM), using a Philips CM10 (Eindhoven, NL) instrument. NSs aqueous suspensions were sprayed on Formwar-coated copper grid and air-dried before observation.

Thermal analysis. Differential Scanning Calorimetry (DSC) was carried out by means of a Perkin Elmer DSC/7 differential scanning calorimeter (Perkin-Elmer, CT-USA) equipped with a TAC 7 /DX instrument controller. The instrument was calibrated with indium for melting point and heat of fusion. A heating rate of 10 °C/min was employed in the 25-250 °C temperature range. Standard aluminum sample pans (Perkin-Elmer) were used; an empty pan was used as reference standard. Analyses were performed in triplicate on 3 mg freeze-dried samples under nitrogen purge.

FTIR analysis. Fourier transformed infrared (FTIR) spectra of free SLs, blank GSH-NS and SL-loaded GSH-NS were obtained using a Perkin Elmer Spectrum 100 FT-IR in the region of 4000- 650 cm^{-1}. Data acquisition was done by spectrum software version 10.03.05 Perkin Elmer Corporation.

SL quantitative determination. The quantitative determination of SLs was carried out by High Performance Liquid Chromatography (HPLC) analysis, using an HPLC system consisting of a Perkin Elmer pump (Perkin Elmer PUMP 250B, Waltham, MA) equipped with a spectrophotometer detector (Flexar UV/Vis LC spectrophotometer detector, Perkin Elmer, Waltham, MA). A reversed phase Agilent TC C18 column (150 cm × 4.6 mm, pore size 5 μm; Agilent Technologies, Santa Clara, CA, USA) was used. The mobile phase was a mixture of acetonitrile and water (85:15 v/v), degassed and pumped through the column with a flow rate of 1 ml/min. Ultraviolet detection was set in the 200-450 nm range. The SL concentration was calculated using external standard method from standard calibration curves. For this purpose, 1 mg of each SL derivatives was weighted, placed in a volumetric flask, and dissolved in water:methanol solution (30:70 v/v) to obtain a stock standard solution. This solution was then diluted using the mobile phase, providing a series of standard solutions, subsequently injected into the HPLC system. Linear calibration curves were obtained over the concentration range of 0.5−25 μg/mL, with a regression coefficient of 0.999 for all the compounds.

Drug loading determination. The loading capacity was determined on freeze-dried SL-loaded NS samples. Briefly, a weighted amount of freeze-dried SL-loaded-NS was dissolved in 5 mL of water:methanol solution (30:70 v/v). After sonication and centrifugation, the supernatant was analyzed by HPLC for the SL quantitative determination. The loading capacity of the SL-loaded-NS formulations was calculated as [amount of SL/ weight of NS] X 100.

***In vitro* release kinetics of SL-loaded nanosponge formulations.** *In vitro* drug release experiments were conducted in a multi-compartment rotating cell,

comprising a donor chamber separated by a cellulose membrane (Spectrapore, cut-off = 12000 Da) from a receiving chamber. One mL of SL-loaded NS was placed in the donor chamber. The receiving compartment contained 1 mL of phosphate buffered saline (PBS) at pH 7.4 with 0.1% sodium dodecyl sulphate (SDS) to assure drug solubility. The receiving phase was withdrawn at regular intervals and completely replaced with the same amount of fresh solution, to maintain sink conditions. The concentration of SLs in the withdrawn samples was detected by HPLC. In the case of SL-loaded GSH-responsive nanosponge formulations, *in vitro* release studies were carried out in the presence of increasing amount of glutathione in the receiving compartment, ranging from 1 mM to 20 mM. Moreover, the influence of pH on the SL release profiles was investigated. At this purpose, *in vitro* drug release experiments were performed using as receiving phase phosphate buffer, containing 1 mM GSH, at two different pH values, i.e. 5.5 and 7.4.

Determination of SL intracellular content. The concentration of MEB55 in PC-3 and DU145 cells was investigated as a measure of the intracellular accumulation of the SL derivative. After incubation for 24 h with SL free or loaded in GSH-NS the cells were washed and lysed with a saturated solution of ammonium sulphate. 100 μL of a water:methanol mixture (30:70 v/v) were added to the samples and then centrifuged at 4°C for 10 minutes. The supernatants were withdrawn and diluted with the mobile phase, vortexed for 2 min and injected into the HPLC system, as described above, for the quantitative determination of SLs. The amount of compounds present inside the cells was calculated from the standard calibration curve. Cell uptake of MEB55 was expressed as a % of the total compound administered.

-Biological assays-

Cell viability assay. Cells (3x103/well) were seeded in 96-well plates and incubated at 37 °C, 5% CO_2, for 24 h. Then, cells were treated with different concentrations of the SLs or the SL-loaded-NSs (10-0.1 μM). After 24 h of incubation, viable cells were evaluated by 2,3-bis[2-methoxy-4-nitro-5sulphophenyl]-2H-tetrazolium-5carboxanilide (MTT) inner salt reagent at 570 nm, as described by the manufacturer's protocol. The controls (i.e. cells that had received no drug) were normalized to 100%, and the readings from treated cells were expressed as % of viability inhibition. Eight replicates were used to determine each data point and five different experiments were performed.

Author contribution:

The abovementioned section is the result of the cooperation between three research laboratories: for my own part I synthesized all the SL analogues as previously reported,[45,91,46,88] PhD Fabrizio Caldera (Department of Chemistry, University of Turin) synthesized the nanosponges, while the PhD Monica Argenziano (Department of Drug Science and Technology, University of Turin) formulated, *in vitro* characterized the nanoformulations, and performed cell culture experiments.

Scientific group supervisors: Professor Cristina Prandi (Department of Chemistry, University of Turin), Professor Francesco Trotta (Department of Chemistry, University of Turin) and Professor Roberta Cavalli (Department of Drug Science and Technology, University of Turin).

CHAPTER 6

- CONCLUSIONS -

In summary, during these three years of PhD I had the opportunity to deepen my knowledge on the chemistry and roles of strigolactones from different angles and using different type of approaches.

- A new generation of analogues was devised, the strigo D-lactams. Inspired by a isostheric approach and using a fine-tuned chemical design with a ring-closing metathesis as key step, the GR24, EGO10 and debranone mimic analogues as D-lactams were synthesized. The bioactivity of these molecules was evaluated by means of germination activity tests and by an innovative *in vivo* luminometer assay. All the compounds were disclosed as less active compared to SL-D-lactones. Furthermore, to support and rationalize the biological evidences, docking studies were performed to investigate the interactions occurring at receptor level and elucidate the reason of inactivity.

- To trace the strigolactone pathway in biological systems the natural luminescent properties of some bioactive analogues were implemented introducing an external fluorophore (BODIPY) having the appropriate features for bioimaging studies. X-ray analysis and ECD measurements were used to unequivocally assess the configuration of the synthesized molecules, while germination activity assays revealed the most promising candidates for bioimaging studies.

- Then, a fluorescent compound insensitive to the enzymatic activity of D14 was designed to track the destiny of the molecules *in vivo*, and called CL-BP. The unlabelled BP version of this molecule (CL, **28**) interestingly proved to promote the receptor degradation, whilst the tagged CL-BP compound was inactive. Speculations about the reasons behind this different behaviours have been proposed.

- To further explore the enzymatic receptor activity several profluorescent probes have been designed, some of them present an extended scaffold retaining a light-removable fragment. The aim was to achieve a photo-controlled interaction by means of a temporal and spatial controlled release of active probes. The evaluation of the activity is currently under study.

- Lastly, to improve the therapeutic and biological applications of strigolactones, several delivery systems were evaluated. Using a nanotechnological approach based on natural and totally biodegradable cyclic oligosaccharides cross-linked in a three-dimensional network, the SL scaffold was successfully incubated in carbonate and pyromellitic nanosponges respectively. A further improvement came through the use of glutathione-responsive nanosponges, drug carriers which have been revealed as capable to incorporate the strigolactone molecule and release it “on demand”. Therefore, the triggered SL outflow made GSH-NS specific nanocarriers for the controlled intracellular release of this phytohormone class.

Acknowledgements

At the end of these three years of my PhD I would like to conclude this thesis spending few words for all those who have been important and fundamental over this period.

First of all, I would like to express my deep gratitude to my supervisor, Professor Cristina Prandi, for all the things she has thought me, her motivation and support, for giving me the opportunity to dig deeply into this learning pathway and to have encouraged and supported such interesting experiences abroad.

A special thank also to Doctor Emma Artuso, who always represented a reference point during the lab life, for all the scientific discussions we had when “chemistry didn’t worked how we hoped”.

I would also like to show my gratitude to Dr. Francois-Didier Boyer and to Dr. Sandrinne Bonhomme for welcoming me in their team, and for being not only extraordinary scientists with always worthwhile advices for me, but also such amazing persons.

I would also like to thank the PhD commetee which will evaluate my work: Professor Antonio Evidente, Professor Francisco Macias and Professor Luisa Lanfranco.

Thanks to all my PhD companions Beatrice Lace, Elisa Acciardo, Stefano Nejrotti, Simone Ghinato and Chiara Bellomo. I could not hope to have better colleagues to share with funny moments, lunchtimes, and critical times overcome because of this cohesive team.

Thanks to all the people of the Organic Chemistry Department, especially to Dr. Silvano Cadamuro, Dr. Margherita Barbero, Dr. Stefano Dughera, Dr. Annamaria Deagostino and Dr. Marco Blangetti, and to all those I had the chance to meet in Gif sur Yvette, especially PhD Stéphanie Norsikian, PhD Lucy Buchardy, PhD Margaux Beretta and PhD Cedric Tresse.

Last but not the least, I would like to thank my family, especially my parents and grandparents, my friends Marco, Luca and Matteo, and Filippo, my best friend and fiance, which supported and helped me in every single moment…and who now also knows something about the Strigolactone chemistry.

Bibliography

1. Zwanenburg, B.; Pospisil, T.; Zeljkovic, S. C., Strigolactones: new plant hormones in action. *Planta* **2016,** *243* (6), 1311-1326.

2. Wigchert, S. C. M., *Chemical studies on germination stimulants for seeds of the parasitic weeds Striga and Orobanche*. [Sl: sn]: 1999.

3. (a) Parker, C.; Riches, C. R., *Parasitic weeds of the world: biology and control*. CAB international: 1993; (b) Parker, C., Observations on the current status of Orobanche and Striga problems worldwide. *Pest Manage. Sci.* **2009,** *65* (5), 453-459.

4. Butler, L. G., Chemical communication between the parasitic weed striga and its crop host - a new dimension in allelochemistry. In *Allelopathy: Organisms, Processes, and Applications*, Inderjit, A.; Dakshini, K. M. M.; Einhellig, F. A., Eds. 1995; Vol. 582, pp 158-168.

5. Akiyama, K.; Matsuzaki, K.; Hayashi, H., Plant sesquiterpenes induce hyphal branching in arbuscular mycorrhizal fungi. *Nature* **2005,** *435* (7043), 824-827.

6. Gomez-Roldan, V.; Fermas, S.; Brewer, P. B.; Puech-Pages, V.; Dun, E. A.; Pillot, J. P.; Letisse, F.; Matusova, R.; Danoun, S.; Portais, J. C.; Bouwmeester, H.; Becard, G.; Beveridge, C. A.; Rameau, C.; Rochange, S. F., Strigolactone inhibition of shoot branching. *Nature* **2008,** *455* (7210), 189-U22.

7. Cavar, S.; Zwanenburg, B.; Tarkowski, P., Strigolactones: occurrence, structure, and biological activity in the rhizosphere. *Phytochem. Rev.* **2015,** *14* (4), 691-711.

8. Cook, C.; Whichard, L. P.; Turner, B.; Wall, M. E.; Egley, G. H., Germination of witchweed (Striga lutea Lour.): isolation and properties of a potent stimulant. *Science* **1966,** *154* (3753), 1189-1190.

9. Cook, C.; Whichard, L. P.; Wall, M.; Egley, G. H.; Coggon, P.; Luhan, P. A.; McPhail, A., Germination stimulants. II. Structure of strigol, a potent seed germination stimulant for witchweed (Striga lutea). *J. Am. Chem. Soc.* **1972,** *94* (17), 6198-6199.

10. Brooks, D. W.; Bevinakatti, H. S.; Powell, D. R., The Absolute Structure of (+)-Strigol. *J. Org. Chem.* **1985,** *50* (20), 3779-3781.

11. Zwanenburg, B.; Pospisil, T., Structure and Activity of Strigolactones: New Plant Hormones with a Rich Future. *Molecular Plant* **2013,** *6* (1), 38-62.

12. Xie, X. N.; Yoneyama, K.; Kisugi, T.; Uchida, K.; Ito, S.; Akiyama, K.; Hayashi, H.; Yokota, T.; Nomura, T.; Yoneyama, K., Confirming Stereochemical Structures of Strigolactones Produced by Rice and Tobacco. *Molecular Plant* **2013,** *6* (1), 153-163.

13. Parker, C., Parasitic weeds: a world challenge. *Weed Sci.* **2012,** *60* (2), 269-276.

14. Xie, X. N.; Yoneyama, K.; Yoneyama, K., The Strigolactone Story. In *Annual Review of Phytopathology, Vol 48*, VanAlfen, N. K.; Bruening, G.; Leach, J. E., Eds. 2010; Vol. 48, pp 93-117.

15. Zwanenburg, B.; Mwakaboko, A. S.; Reizelman, A.; Anilkumar, G.; Sethumadhavan, D., Structure and function of natural and synthetic signalling molecules in parasitic weed germination. *Pest Manage. Sci.* **2009,** *65* (5), 478-491.

16. (a) Johnson, A. W.; Gowada, G.; Hassanali, A.; Knox, J.; Monaco, S.; Razavi, Z.; Rosebery, G., The preparation of synthetic analogues of strigol. *J. Chem. Soc., Perkin Trans. 1* **1981**, 1734-1743; (b) Kgosi, R. L.; Zwanenburg, B.; Mwakaboko, A. S.; Murdoch, A. J., Strigolactone analogues induce suicidal seed germination of Striga spp. in soil. *Weed Res.* **2012,** *52* (3), 197-203.

17. Schüßler, A.; Schwarzott, D.; Walker, C., A new fungal phylum, the Glomeromycota: phylogeny and evolution. *Mycol. Res.* **2001,** *105* (12), 1413-1421.

18. Harrison, M. J., Signaling in the arbuscular mycorrhizal symbiosis. *Annu. Rev. Microbiol.* **2005,** *59*, 19-42.

19. Bonfante, P.; Genre, A., Mechanisms underlying beneficial plant–fungus interactions in mycorrhizal symbiosis. *Nature communications* **2010,** *1*, 48.

20. Giovannetti, M.; Sbrana, C.; Citernesi, A. S.; Avio, L., Analysis of factors involved in fungal recognition responses to host-derived signals by arbuscular mycorrhizal fungi. *New Phytol.* **1996,** *133* (1), 65-71.

21. (a) Akiyama, K.; Hayashi, H., Strigolactones: chemical signals for fungal symbionts and parasitic weeds in plant roots. *Ann. Bot.* **2006,** *97* (6), 925-31; (b) Akiyama, K.; Ogasawara, S.; Ito, S.; Hayashi, H., Structural requirements of strigolactones for hyphal branching in AM fungi. *Plant Cell Physiol.* **2010,** *51* (7), 1104-17.

22. Lopez-Raez, J. A.; Kohlen, W.; Charnikhova, T.; Mulder, P.; Undas, A. K.; Sergeant, M. J.; Verstappen, F.; Bugg, T. D. H.; Thompson, A. J.; Ruyter-Spira, C.; Bouwmeester, H., Does abscisic acid affect strigolactone biosynthesis? *New Phytol.* **2010,** *187* (2), 343-354.

23. Domagalska, M. A.; Leyser, O., Signal integration in the control of shoot branching. *Nature Reviews Molecular Cell Biology* **2011,** *12* (4), 211-221.

24. Arite, T.; Kameoka, H.; Kyozuka, J., Strigolactone Positively Controls Crown Root Elongation in Rice. *J. Plant Growth Regul.* **2012,** *31* (2), 165-172.

25. Kapulnik, Y.; Delaux, P. M.; Resnick, N.; Mayzlish-Gati, E.; Wininger, S.; Bhattacharya, C.; Sejalon-Delmas, N.; Combier, J. P.; Becard, G.; Belausov, E.; Beeckman, T.; Dor, E.; Hershenhorn, J.; Koltai, H., Strigolactones affect lateral root formation and root-hair elongation in Arabidopsis. *Planta* **2011,** *233* (1), 209-216.

26. Smith, S. M.; Waters, M. T., Strigolactones: Destruction-Dependent Perception? *Curr. Biol.* **2012,** *22* (21), R924-R927.

27. Koltai, H., Implications of non-specific strigolactone signaling in the rhizosphere. *Plant Sci.* **2014,** *225*, 9-14.

28. Boyer, F. D.; de Saint Germain, A.; Pillot, J. P.; Pouvreau, J. B.; Chen, V. X.; Ramos, S.; Stevenin, A.; Simier, P.; Delavault, P.; Beau, J. M.; Rameau, C., Structure-activity relationship studies of strigolactone-related molecules for branching inhibition in garden pea: molecule design for shoot branching. *Plant Physiol.* **2012,** *159* (4), 1524-44.

29. (a) Zhou, F.; Lin, Q.; Zhu, L.; Ren, Y.; Zhou, K.; Shabek, N.; Wu, F.; Mao, H.; Dong, W.; Gan, L., D14–SCF D3-dependent degradation of D53 regulates strigolactone signalling. *Nature* **2013,** *504* (7480), 406; (b) Jiang, L.; Liu, X.; Xiong, G. S.; Liu, H. H.; Chen, F. L.; Wang, L.; Meng, X. B.; Liu, G. F.; Yu, H.; Yuan, Y. D.; Yi, W.; Zhao, L. H.; Ma, H. L.; He, Y. Z.; Wu, Z. S.; Melcher, K.; Qian, Q.; Xu, H. E.; Wang, Y. H.; Li, J. Y., DWARF 53 acts as a repressor of strigolactone signalling in rice. *Nature* **2013,** *504* (7480), 401-+.

30. Koltai, H., Receptors, repressors, PINs: a playground for strigolactone signaling. *Trends Plant Sci.* **2014,** *19* (11), 727-733.

31. Kagiyama, M.; Hirano, Y.; Mori, T.; Kim, S. Y.; Kyozuka, J.; Seto, Y.; Yamaguchi, S.; Hakoshima, T., Structures of D14 and D14L in the strigolactone and karrikin signaling pathways. *Genes Cells* **2013,** *18* (2), 147-160.

32. Nakamura, H.; Xue, Y. L.; Miyakawa, T.; Hou, F.; Qin, H. M.; Fukui, K.; Shi, X.; Ito, E.; Ito, S.; Park, S. H.; Miyauchi, Y.; Asano, A.; Totsuka, N.; Ueda, T.; Tanokura, M.; Asami, T., Molecular mechanism of strigolactone perception by DWARF14. *Nature Communications* **2013,** *4*.

33. Mangnus, E. M.; Zwanenburg, B., Tentative molecular mechanism for germination stimulation of Striga and Orobanche seeds by strigol and its synthetic analogs. *J. Agric. Food. Chem.* **1992,** *40* (6), 1066-1070.

34. Scaffidi, A.; Waters, M. T.; Bond, C. S.; Dixon, K. W.; Smith, S. M.; Ghisalberti, E. L.; Flematti, G. R., Exploring the molecular mechanism of karrikins and strigolactones. *Bioorg. Med. Chem. Lett.* **2012,** *22* (11), 3743-3746.

35. Zhao, L.-H.; Zhou, X. E.; Wu, Z.-S.; Yi, W.; Xu, Y.; Li, S.; Xu, T.-H.; Liu, Y.; Chen, R.-Z.; Kovach, A., Crystal structures of two phytohormone signal-transducing α/β hydrolases: karrikin-signaling KAI2 and strigolactone-signaling DWARF14. *Cell Res.* **2013,** *23* (3), 436-439.

36. de Saint Germain, A.; Clave, G.; Badet-Denisot, M. A.; Pillot, J. P.; Cornu, D.; Le Caer, J. P.; Burger, M.; Pelissier, F.; Retailleau, P.; Turnbull, C.; Bonhomme, S.; Chory, J.; Rameau, C.; Boyer, F. D., An histidine covalent receptor and butenolide complex mediates strigolactone perception. *Nat. Chem. Biol.* **2016,** *12* (10), 787-794.

37. Toh, S.; Holbrook-Smith, D.; Stogios, P. J.; Onopriyenko, O.; Lumba, S.; Tsuchiya, Y.; Savchenko, A.; McCourt, P., Structure-function analysis identifies highly sensitive strigolactone receptors in Striga. *Science* **2015,** *350* (6257), 203-7.

38. Lin, H.; Wang, R. X.; Qian, Q.; Yan, M. X.; Meng, X. B.; Fu, Z. M.; Yan, C. Y.; Jiang, B.; Su, Z.; Li, J. Y.; Wang, Y. H., DWARF27, an Iron-Containing Protein Required for the

Biosynthesis of Strigolactones, Regulates Rice Tiller Bud Outgrowth. *Plant Cell* **2009,** *21* (5), 1512-1525.

39. Crawford, S.; Shinohara, N.; Sieberer, T.; Williamson, L.; George, G.; Hepworth, J.; Muller, D.; Domagalska, M. A.; Leyser, O., Strigolactones enhance competition between shoot branches by dampening auxin transport. *Development* **2010,** *137* (17), 2905-2913.

40. (a) Walter, M. H.; Strack, D., Carotenoids and their cleavage products: biosynthesis and functions. *Nat. Prod. Rep.* **2011,** *28* (4), 663-692; (b) Waldie, T.; McCulloch, H.; Leyser, O., Strigolactones and the control of plant development: lessons from shoot branching. *Plant J.* **2014,** *79* (4), 607-622.

41. Alder, A.; Jamil, M.; Marzorati, M.; Bruno, M.; Vermathen, M.; Bigler, P.; Ghisla, S.; Bouwmeester, H.; Beyer, P.; Al-Babili, S., The Path from beta-Carotene to Carlactone, a Strigolactone-Like Plant Hormone. *Science* **2012,** *335* (6074), 1348-1351.

42. Seto, Y.; Sado, A.; Asami, K.; Hanada, A.; Umehara, M.; Akiyama, K.; Yamaguchi, S., Carlactone is an endogenous biosynthetic precursor for strigolactones. *Proc. Natl. Acad. Sci. U. S. A.* **2014,** *111* (4), 1640-1645.

43. Mangnus, E. M.; Dommerholt, F. J.; De Jong, R. L.; Zwanenburg, B., Improved synthesis of strigol analog GR24 and evaluation of the biological activity of its diastereomers. *J. Agric. Food. Chem.* **1992,** *40* (7), 1230-1235.

44. (a) Kondo, Y.; Tadokoro, E.; Matsuura, M.; Iwasaki, K.; Sugimoto, Y.; Miyake, H.; Takikawa, H.; Sasaki, M., Synthesis and seed germination stimulating activity of some imino analogs of strigolactones. *Biosci., Biotechnol., Biochem.* **2007,** *71* (11), 2781-2786; (b) Lachia, M.; Wolf, H. C.; Jung, P. J.; Screpanti, C.; De Mesmaeker, A., Strigolactam: new potent strigolactone analogues for the germination of Orobanche cumana. *Bioorg. Med. Chem. Lett.* **2015,** *25* (10), 2184-8.

45. Bhattacharya, C.; Bonfante, P.; Deagostino, A.; Kapulnik, Y.; Larini, P.; Occhiato, E. G.; Prandi, C.; Venturello, P., A new class of conjugated strigolactone analogues with fluorescent properties: synthesis and biological activity. *Org. Biomol. Chem.* **2009,** *7* (17), 3413-3420.

46. Prandi, C.; Occhiato, E. G.; Tabasso, S.; Bonfante, P.; Novero, M.; Scarpi, D.; Bova, M. E.; Miletto, I., New potent fluorescent analogues of strigolactones: synthesis and biological activity in parasitic weed germination and fungal branching. *Eur. J. Org. Chem.* **2011,** *2011* (20-21), 3781-3793.

47. Fukui, K.; Ito, S.; Asami, T., Selective Mimics of Strigolactone Actions and Their Potential Use for Controlling Damage Caused by Root Parasitic Weeds. *Molecular Plant* **2013,** *6* (1), 88-99.

48. Zwanenburg, B.; Nayak, S. K.; Charnikhova, T. V.; Bouwmeester, H. J., New strigolactone mimics: Structure-activity relationship and mode of action as germinating stimulants for parasitic weeds. *Bioorg. Med. Chem. Lett.* **2013,** *23* (18), 5182-5186.

49. Zwanenburg, B.; Mwakaboko, A. S., Strigolactone analogues and mimics derived from phthalimide, saccharine, p-tolylmalondialdehyde, benzoic and salicylic acid as scaffolds. *Biorg. Med. Chem.* **2011,** *19* (24), 7394-7400.

50. Tsuchiya, Y.; Yoshimura, M.; Sato, Y.; Kuwata, K.; Toh, S.; Holbrook-Smith, D.; Zhang, H.; McCourt, P.; Itami, K.; Kinoshita, T.; Hagihara, S., Probing strigolactone receptors in Striga hermonthica with fluorescence. *Science* **2015,** *349* (6250), 864-868.

51. Thuring, J. J.; Nefkens, G. L., Synthesis and biological evaluation of potential substrates for the isolation of the strigol receptor. *J. Chem. Soc., Perkin Trans. 1* **1997,** (5), 759-766.

52. Prandi, C.; Rosso, H.; Lace, B.; Occhiato, E. G.; Oppedisano, A.; Tabasso, S.; Alberto, G.; Blangetti, M., Strigolactone Analogs as Molecular Probes in Chasing the (SLs) Receptor/s: Design and Synthesis of Fluorescent Labeled Molecules. *Molecular Plant* **2013,** *6* (1), 113-127.

53. Prandi, C.; Ghigo, G.; Occhiato, E. G.; Scarpi, D.; Begliomini, S.; Lace, B.; Alberto, G.; Artuso, E.; Blangetti, M., Tailoring fluorescent strigolactones for in vivo investigations: a computational and experimental study. *Org. Biomol. Chem.* **2014,** *12* (18), 2960-2968.

54. Rasmussen, A.; Heugebaert, T.; Matthys, C.; Van Deun, R.; Boyer, F. D.; Goormachtig, S.; Stevens, C.; Geelen, D., A Fluorescent Alternative to the Synthetic Strigolactone GR24. *Molecular Plant* **2013,** *6* (1), 100-112.

55. Harrison, P. J.; Bugg, T. D., Enzymology of the carotenoid cleavage dioxygenases: reaction mechanisms, inhibition and biochemical roles. *Arch. Biochem. Biophys.* **2014,** *544*, 105-111.

56. Kitahata, N.; Ito, S.; Kato, A.; Ueno, K.; Nakano, T.; Yoneyama, K.; Yoneyama, K.; Asami, T., Abamine as a basis for new designs of regulators of strigolactone production. *J. Pestic. Sci.* **2011,** *36* (1), 53-57.

57. Kitahata, N.; Han, S.-Y.; Noji, N.; Saito, T.; Kobayashi, M.; Nakano, T.; Kuchitsu, K.; Shinozaki, K.; Yoshida, S.; Matsumoto, S., A 9-cis-epoxycarotenoid dioxygenase inhibitor for use in the elucidation of abscisic acid action mechanisms. *Biorg. Med. Chem.* **2006,** *14* (16), 5555-5561.

58. Nakamura, H.; Asami, T., Target sites for chemical regulation of strigolactone signaling. *Frontiers in Plant Science* **2014,** *5*.

59. Newman, D. J.; Cragg, G. M.; Snader, K. M., The influence of natural products upon drug discovery. *Nat. Prod. Rep.* **2000,** *17* (3), 215-234.

60. Cohen, S.; Flescher, E., Methyl jasmonate: a plant stress hormone as an anti-cancer drug. *Phytochemistry* **2009,** *70* (13-14), 1600-1609.

61. Clouse, S. D.; Sasse, J. M., Brassinosteroids: essential regulators of plant growth and development. *Annu. Rev. Plant Biol.* **1998,** *49* (1), 427-451.

62. Steigerová, J.; Oklešťková, J.; Levková, M.; Rárová, L.; Kolář, Z.; Strnad, M., Brassinosteroids cause cell cycle arrest and apoptosis of human breast cancer cells. *Chem. Biol. Interact.* **2010,** *188* (3), 487-496.

63. Umehara, M.; Hanada, A.; Yoshida, S.; Akiyama, K.; Arite, T.; Takeda-Kamiya, N.; Magome, H.; Kamiya, Y.; Shirasu, K.; Yoneyama, K.; Kyozuka, J.; Yamaguchi, S., Inhibition of shoot branching by new terpenoid plant hormones. *Nature* **2008,** *455* (7210), 195-U29.

64. Rameau, C., Strigolactones, a novel class of plant hormone controlling shoot branching. *C. R. Biol.* **2010,** *333* (4), 344-349.

65. Koltai, H.; Dor, E.; Hershenhorn, J.; Joel, D. M.; Weininger, S.; Lekalla, S.; Shealtiel, H.; Bhattacharya, C.; Eliahu, E.; Resnick, N.; Barg, R.; Kapulnik, Y., Strigolactones' Effect on Root Growth and Root-Hair Elongation May Be Mediated by Auxin-Efflux Carriers. *J. Plant Growth Regul.* **2010,** *29* (2), 129-136.

66. Hultzman, R. Plant Meristem: Definition & Function - Lesson Transcript
http://study.com/academy/lesson/plant-meristem-definition-function-quiz.html

67. Pollock, C. B.; Koltai, H.; Kapulnik, Y.; Prandi, C.; Yarden, R. I., Strigolactones: a novel class of phytohormones that inhibit the growth and survival of breast cancer cells and breast cancer stem-like enriched mammosphere cells. *Breast Cancer Res. Treat.* **2012,** *134* (3), 1041-1055.

68. Global Cancer Observatory. Data source: GLOBOCAN 2012 - International Agency for Research on Carcer 2017
http://gco.iarc.fr/.

69. Kapulnik, Y.; Koltai, H.; Yarden, R.; Prandi, C., Use of strigolactones and strigolactone analogs for treating proliferative conditions. Google Patents: 2014.

70. Hayeshi R., S. B., Kalombo L., Katata L., Lemmer Y., Melariri P., Nyamboli B., Swai H. , *Functional nanocarriers used in drug delivery, in Drug Discovery in Africa*. 2012.

71. Loftsson, T.; Duchêne, D., Cyclodextrins and their pharmaceutical applications. *Int. J. Pharm.* **2007,** *329* (1-2), 1-11.

72. Bender, M. L.; Komiyama, M., *Cyclodextrin chemistry*. Springer Science & Business Media: 1978; Vol. 6.

73. Duchêne, D., Cyclodextrins and their inclusion complexes. *Cyclodextrins in Pharmaceutics, Cosmetics, and Biomedicine: Current and Future Industrial Applications* **2011**, 1-18.

74. Trotta, F., Cyclodextrin nanosponges and their applications. *Cyclodextrins in pharmaceutics, cosmetics, and biomedicine: Current and future industrial applications* **2011**, 323-342.

75. Schafer, F. Q.; Buettner, G. R., Redox environment of the cell as viewed through the redox state of the glutathione disulfide/glutathione couple. *Free Radical Biol. Med.* **2001,** *30* (11), 1191-1212.

76. Traverso, N.; Ricciarelli, R.; Nitti, M.; Marengo, B.; Furfaro, A. L.; Pronzato, M. A.; Marinari, U. M.; Domenicotti, C., Role of glutathione in cancer progression and chemoresistance. *Oxid. Med. Cell. Longev.* **2013,** *2013*.

77. Trotta, F.; Caldera, F.; Dianzani, C.; Argenziano, M.; Barrera, G.; Cavalli, R., Glutathione bioresponsive cyclodextrin nanosponges. *ChemPlusChem* **2016,** *81* (5), 439-443.

78. Lombardi, C.; Artuso, E.; Grandi, E.; Lolli, M.; Spirakys, F.; Priola, E.; Prandi, C., Recent advances in the synthesis of analogues of phytohormones strigolactones with ring-closing metathesis as a key step. *Org. Biomol. Chem.* **2017,** *15* (38), 8218-8231.

79. Fürstner, A.; Thiel, O. R.; Ackermann, L.; Schanz, H.-J.; Nolan, S. P., Ruthenium carbene complexes with N, N '-bis (mesityl) imidazol-2-ylidene ligands: RCM catalysts of extended scope. *The Journal of organic chemistry* **2000,** *65* (7), 2204-2207.

80. Netz, N.; Opatz, T., A Modular Formal Total Synthesis of (±)-Cyclocla vine. *The Journal of organic chemistry* **2016,** *81* (4), 1723-1730.

81. Bermejo, F. A.; Rico-Ferreira, R.; Bamidele-Sanni, S.; García-Granda, S., Total synthesis of (+)-ampullicin and (+)-isoampullicin: Two fungal metabolites with growth regulatory activity isolated from Ampulliferina Sp. 27. *The Journal of organic chemistry* **2001,** *66* (25), 8287-8292.

82. (a) Baroni, M.; Cruciani, G.; Sciabola, S.; Perruccio, F.; Mason, J. S., A common reference framework for analyzing/comparing proteins and ligands. Fingerprints for ligands and proteins (FLAP): Theory and application. *J. Chem. Inf. Model.* **2007,** *47* (2), 279-294; (b) Spyrakis, F.; Benedetti, P.; Decherchi, S.; Rocchia, W.; Cavalli, A.; Alcaro, S.; Ortuso, F.; Baroni, M.; Cruciani, G., A Pipeline To Enhance Ligand Virtual Screening: Integrating Molecular Dynamics and Fingerprints for Ligand and Proteins. *J. Chem. Inf. Model.* **2015,** *55* (10), 2256-74.

83. Escudero-Adan, E. C.; Benet-Buchholz, J.; Ballester, P., The use of Mo K alpha radiation in the assignment of the absolute configuration of light-atom molecules; the importance of high-resolution data. *Acta Crystallographica Section B-Structural Science Crystal Engineering and Materials* **2014,** *70*, 660-668.

84. Sheldrick, G. M., Crystal structure refinement with SHELXL. *Acta Crystallographica Section C: Structural Chemistry* **2015,** *71* (1), 3-8.

85. Macrae, C. F.; Bruno, I. J.; Chisholm, J. A.; Edgington, P. R.; McCabe, P.; Pidcock, E.; Rodriguez-Monge, L.; Taylor, R.; Streek, J. v.; Wood, P. A., Mercury CSD 2.0–new features for the visualization and investigation of crystal structures. *J. Appl. Cryst.* **2008,** *41* (2), 466-470.

86. Flack, H.; Bernardinelli, G., Absolute structure and absolute configuration. *Acta Cryst.* **1999,** *55* (5), 908-915.

87. Flack, H.; Bernardinelli, G., Reporting and evaluating absolute-structure and absolute-configuration determinations. *J. Appl. Cryst.* **2000,** *33* (4), 1143-1148.

88. Artuso, E.; Ghibaudi, E.; Lace, B.; Marabello, D.; Vinciguerra, D.; Lombardi, C.; Koltai, H.; Kapulnik, Y.; Novero, M.; Occhiato, E. G.; Scarpi, D.; Parisotto, S.; Deagostino, A.;

Venturello, P.; Mayzlish-Gati, E.; Bier, A.; Prandi, C., Stereochemical Assignment of Strigolactone Analogues Confirms Their Selective Biological Activity. *J. Nat. Prod.* **2015,** *78* (11), 2624-2633.

89. Chiwocha, S. D. S.; Dixon, K. W.; Flematti, G. R.; Ghisalberti, E. L.; Merritt, D. J.; Nelson, D. C.; Riseborough, J.-A. M.; Smith, S. M.; Stevens, J. C., Karrikins: A new family of plant growth regulators in smoke. *Plant Sci.* **2009,** *177* (4), 252-256.

90. Scaffidi, A.; Waters, M. T.; Sun, Y. M. K.; Skelton, B. W.; Dixon, K. W.; Ghisalberti, E. L.; Flematti, G. R.; Smith, S. M., Strigolactone hormones and their stereoisomers signal through two related receptor proteins to Induce different physiological responses in arabidopsis. *Plant Physiol.* **2014,** *165* (3), 1221-1232.

91. Reizelman, A.; Wigchert, S. C. M.; del-Bianco, C.; Zwanenburg, B., Synthesis and bioactivity of labelled germination stimulants for the isolation and identification of the strigolactone receptor. *Org. Biomol. Chem.* **2003,** *1* (6), 950-959.

92. Kamiński, Z.; Paneth, P.; Rudziński, J., A study on the activation of carboxylic acids by means of 2-chloro-4, 6-dimethoxy-1, 3, 5-triazine and 2-chloro-4, 6-diphenoxy-1, 3, 5-triazine. *The Journal of Organic Chemistry* **1998,** *63* (13), 4248-4255.

93. Frischmuth K., W. U., Samson E., Weigelt D., Koll P., Meuer H., Sheldrick W. S., Welzel P. , Configurational assignment at C-2' of some strigol analogs. *Tetrahedron: Asymmetry* **1993,** *4*, 351−360.

94. Nomura, S.; Nakashima, H.; Mizutani, M.; Takikawa, H.; Sugimoto, Y., Structural requirements of strigolactones for germination induction and inhibition of Striga gesnerioides seeds. *Plant Cell Rep.* **2013,** *32* (6), 829-838.

95. Fridlender, M.; Lace, B.; Wininger, S.; Dam, A.; Kumari, P.; Belausov, E.; Tsemach, H.; Kapulnik, Y.; Prandi, C.; Koltai, H., Influx and Efflux of Strigolactones Are Actively Regulated and Involve the Cell-Trafficking System. *Molecular Plant* **2015,** *8* (12), 1809-1812.

96. Tsuchiya, Y.; Vidaurre, D.; Toh, S.; Hanada, A.; Nambara, E.; Kamiya, Y.; Yamaguchi, S.; McCourt, P., A small-molecule screen identifies new functions for the plant hormone strigolactone. *Nat. Chem. Biol.* **2010,** *6* (10), 741-749.

97. Delacour, Q.; Li, C.; Plamont, M.-A.; Billon-Denis, E.; Aujard, I.; Le Saux, T.; Jullien, L.; Gautier, A., Light-activated proteolysis for the spatiotemporal control of proteins. *ACS Chem. Biol.* **2015,** *10* (7), 1643-1647.

98. Sheldrick, G. M., SHELXT–Integrated space-group and crystal-structure determination. *Acta Crystallographica Section A: Foundations and Advances* **2015,** *71* (1), 3-8.

99. Dolomanov, O. V.; Bourhis, L. J.; Gildea, R. J.; Howard, J. A.; Puschmann, H., OLEX2: a complete structure solution, refinement and analysis program. *J. Appl. Crystallogr.* **2009,** *42* (2), 339-341.

100. Parsons, S.; Flack, H. D.; Wagner, T., Use of intensity quotients and differences in absolute structure refinement. *Acta Crystallographica Section B: Structural Science, Crystal Engineering and Materials* **2013,** *69* (3), 249-259.

101. Evidente, M.; Cimmino, A.; Zonno, M. C.; Masi, M.; Berestetskyi, A.; Santoro, E.; Superchi, S.; Vurro, M.; Evidente, A., Phytotoxins produced by Phoma chenopodiicola, a fungal pathogen of Chenopodium album. *Phytochemistry* **2015,** *117*, 482-488.

102. Gioiello, A.; Rosatelli, E.; Teofrasti, M.; Filipponi, P.; Pellicciari, R., Building a sulfonamide library by eco-friendly flow synthesis. *ACS combinatorial science* **2013,** *15* (5), 235-239.

103. (a) Campos-Toimil, M.; Orallo, F.; Santana, L.; Uriarte, E., Synthesis and vasorelaxant activity of new coumarin and furocoumarin derivatives. *Bioorg. Med. Chem. Lett.* **2002,** *12* (5), 783-786; (b) Akita, S.; Umezawa, N.; Higuchi, T., On-bead fluorescence assay for serine/threonine kinases. *Org. Lett.* **2005,** *7* (25), 5565-5568.

104. TYAGI, Y. K.; TYAGI, S.; RAJ, H. G.; GUPTA, R. K., Synthesis of novel 4-methylcoumarins and comparative specificities of substituted derivatives for acetoxy drug: protein transacetylase. *Sci. Pharm.* **2008,** *76* (3), 395-414.

105. Pollock, C. B.; McDonough, S.; Wang, V. S.; Lee, H.; Ringer, L.; Li, X.; Prandi, C.; Lee, R. J.; Feldman, A. S.; Koltai, H.; Kapulnik, Y.; Rodriguez, O. C.; Schlegel, R.; Albanese, C.; Yarden, R. I., Strigolactone analogues induce apoptosis through activation of p38 and the stress response pathway in cancer cell lines and in conditionally reprogrammed primary prostate cancer cells. *Oncotarget* **2014,** *5* (6), 1683-1698.

106. Daga, M.; Ullio, C.; Argenziano, M.; Dianzani, C.; Cavalli, R.; Trotta, F.; Ferretti, C.; Zara, G. P.; Gigliotti, C. L.; Ciamporcero, E. S., GSH-targeted nanosponges increase doxorubicin-induced toxicity “in vitro” and “in vivo” in cancer cells with high antioxidant defenses. *Free Radical Biol. Med.* **2016,** *97*, 24-37.